CFD MODELLING AND ANALYSIS OF THE MULTIPHASE FLOW AND PERFORMANCE OF DENSE MEDIUM CYCLONE: EFFECTS OF GEOMETRY AND OPERATING CONDITIONS

ZHENG QI

A thesis submitted in fulfilment

of the requirements for the degree of

Master of Science (Research)

Lab for Computer Simulation and Modelling of Particulate Systems

School of Materials Science and Engineering

Faculty of Science

The University of New South Wales

March 2014

To my parents and friends

ABSTRACT

A computational fluid dynamics (CFD) model is proposed to describe the multiphase flow in a dense-medium cyclone (DMC). In this model, the volume of fluid (VOF) multiphase model is first used to determine the initial shape and position of the air core, and then the so called mixture model is employed to describe the flows of the medium, coal particles and air, where the turbulence is described by the Reynolds stress model. The validity of the proposed approach is established by the reasonably good agreement between the measured and calculated results in terms of separation efficiency. This model is then used to quantify the effects of the ratios of spigot to vortex finder diameters (U:O) and medium to coal volumes (M:C) on the standard DMC performance and the effects of M:C ratio and operating Head (given in equivalent diameters of the medium head) on the large diameter DMC performance. The results are shown to be generally comparable to those reported in the literature. The key phenomena predicted are explained by the calculated inner flows.

KEYWORDS: Dense medium cyclone, multiphase flow, separation, modelling and simulation, coal preparation

ACKNOWLEDGMENTS

I would like to express my sincere gratitude to my supervisor, Prof Aibing Yu, for giving me the opportunity to carry out this research project, teaching me about how to do scientific research, and for always keeping my best interest in mind. This work would not be possible without his guidance and inspiration. I also wish to thank Dr Shibo Kuang, my co-supervisor, for much helpful advice and guidance.

I wish to thank University of New South Wales, Australian Research Council (ARC) and Minco Tech Australia Pty Ltd for providing me with postgraduate scholarship, and financial support for this work.

Thanks also to my friends and colleagues in the “Lab for Computer Simulation and Modelling of Particulate Systems” for providing me with much help in my study and fantastic life in Sydney. I am also grateful to the staff in the School of Materials Science and Engineering in UNSW for their various helps during the course of my study. Special thanks to Dr Kaiwei Chu, Dr Ruiping Zou and Mr Jiang Chen for significantly valuable suggestions and discussions.

CONTENTS

LIST OF FIGURES

LIST OF TABLES

NOMENCLATURE

a_k	*Acceleration of phase k, m/s^2*
d	*particle size, m*
D	*diameter, m*
$D_{T,ij}$	*Turbulence diffusion term*
E_p	*Ecart probable*
f_{drag}	*fluid drag force, N*
g	*gravitational acceleration, 9.81 m/s^2*
t	*time, s*
p	*pressure drop, pa*
P_{ij}	*stress production term*
u	*fluid velocity, m/s*
x_i	*Cartesian coordinate*
Re	*Reynolds number*

Greek letters

α	*volume fraction*
ε_{ij}	*dissipation term*
σ_t	*Prandtl-Schmidt number*
ρ	*fluid density, kg/m^3*

$\boldsymbol{\tau}$	*Solid stress tensor, kg/m/s^{-2}*
η_t	*turbulent diffusivity*
$\gamma\Theta$	*collisional dissipation of energy, J*
$\phi_{l,k}$	*energy exchange between the l^{th} solid phase and the k^{th} solid phase, J*
ϕ_{ij}	*Pressure strain term*
Θ	*granular temperature, m^2/s^2*
μ	*fluid viscosity, kg/m/s*

SUBSCRIPTS

c	*corrected*
cut	*cut size*
dr	*drift velocity*
i, j	*tensor directions*
k	*phase k*
l	*phase l*
L	*liquid*
m	*mixture*
mag	*magnetite*
w	*water*
r	*radial*
t	*tangential*

ABBREVIATION

DMC	*dense medium cyclone*
CFD	*computational fluid dynamics*
RSM	*Reynolds stress model*
LDV	*Lase Doppler Velocitometry*
ERT	*Electrical resistance tomography*
GRT	*Gamma gay tomography*
LES	*Large Eddy Simulation*
TFM	*two fluid model*
DEM	*discrete element method*
VOF	*Volume of fluid model*
LPT	*Lagrangian particle tracking*

1. INTRODUCTION

Dense medium cyclones (DMCs) are the work horses in the modern coal industry for upgrading run-of-mine coal in the size range of 0.5 to 50 mm by separating gangue from the product coal. The density of valuable coal particles is generally smaller than 1500 kg/m^3 while those of the rejects or gangue particles are larger than 1500 kg/m^3. Therefore, a fluid of density about 1500 kg/m^3 is needed for effective separation. This is usually achieved by use of a mixture of water and fine magnetite particles, and the mixture is called the "medium" in practice.

Designers/controllers traditionally rely on empirical equations for predicting the DMC performance as a function of variables related to operational, geometrical and materials conditions, and in the past many studies have been made in this direction (Barbee et al., 2005; Davis and Davis, 1987; Ferrara et al., 1999; Honaker et al., 2000; Napier-Munn, 1991; Restarick and Krnic, 1991; Sripriya et al., 2001; Wood, 1990; Zughbi et al., 1991) is, 1987; Ferrara et al., 1999; Honaker et al., 2000; Napier-Munn, 1991; Restarick and Krnic, 1991; Sripriya et al., 2001; Wood, 1990; Zughbi et al., 1991). In the empirical approach however, different sets of experimental data lead to different equations even for the same basic parameters. Moreover, it is difficult to identify, through an empirical approach, small deficiencies related to the DMC design. In principle, these problems can be overcome by numerical simulations.

In the past decades, computational methods had become more preferred to other methods in research. Simulations can not only provide better understanding of the fluid flow in cyclones, but also are capable of predicting performance of large-scale cyclones because of the developments in computers' ability to deal with large calculations making it possible to use a complete numerical solution for modelling and predicting the performance of cyclones. Therefore, there will be always a need for more

convenient and accurate models to be developed to help engineers understand and design the dense medium cyclones.

The aim here is to propose a new model to overcome the problems encountered in previous research and use the model in parametric study.

Chapter 2 reviews previous studies on DMCs, covering an introduction, experimental studies, empirical models and numerical studies. In introduction section, the background on cyclone studies, including operational principles and performance measurements of dense medium cyclones are introduced. Subsequently, the experimental studies on which empirical models are based and numerical studies are briefly introduced. Finally, some important studies on empirical and numerical models are listed in this chapter.

Chapter 3 presents the principle and operation steps of the proposed model.

Chapter 4 validates the proposed model by the comparison between predicted results and experimental results reported by Richard (2007). A simple evaluation of different models, including the proposed model, CFD-LPT and CFD-DEM, is given in this chapter.

Chapter 5 examines the effects of several key factors, including M:C ratio, U:O ratio and Head on performance of standard and large diameter DMCs. The differences of standard and large DMCs are discussed and explained by the calculated inner flows.

Chapter 6 concludes author’s work and discusses some future work.

2. LITERATURE REVIEW

2.1 Introduction

2.1.1 Background

Dense medium cyclones (DMCs), also known as heavy medium cyclones, are widely used in the modern coal preparation industry to upgrade run-of-mine coal in the size range of 0.5 to 50 mm by separating gangue from product coal. The density of valuable coal particles is generally smaller than 1500 kg/m^3 while that of rejects or gangue particles are larger than 1500 kg/m^3. Thus, a fluid of density about 1500 kg/m^3 is needed for effective separation. This is usually achieved by use of a mixture of water and fine magnetite particles, and the mixture is called as “medium” in practice.

The fluid flow in a DMC is complex due to the existence of the medium as well as the dominant turbulence and effect of particle size and density on DMCs’ separation. In the past, studies on DMCs had been mainly based on experimental method. However, these studies always arrived at different conclusions. To solve this problem, a computational fluid dynamics (CFD) model is developed, and such a model has been found to be very useful to achieve a better fundamental understanding and process optimization for DMCs. In particular, researchers have applied the Reynolds stress model (RSM) to describe the turbulence flow in cyclones, and for example, the stochastic Lagrangian model, CFD-DEM model and mixture model have been reported to be reliable to predict the separation performance of DMCs (Chen et al., 2012; Chu et al., 2009a; Kuang et al., 2012; Kuang et al., 2014; Narasimha et al., 2007b; Wang et al., 2009a).

2.1.2 Operational principles

Figure 2.1 shows the conventional design of a dense medium cyclone. It consists of a cylindrical upper body with a central tube which is known as the vortex finder and a conical lower body with a discharge outlet called the apex or spigot. Its geometry is very similar to that of the traditional hydrocyclone and so is the operational principle as shown in Figure 2.2. A mixture of medium and coal particles is fed into the cylindrical part of the cyclone tangentially, thus forming a strong swirling flow. By centrifugal forces, the refuse or high ash particles are thrown towards the wall of the cyclone where the axial velocity is downward and is discharged through the underflow orifice or the spigot. On the other hand, the lighter particles move towards the longitudinal axis of the cyclone, where an air core usually exists. The strong upwards fluid flow around the air core carries light particles to the overflow orifice, or vortex finder.

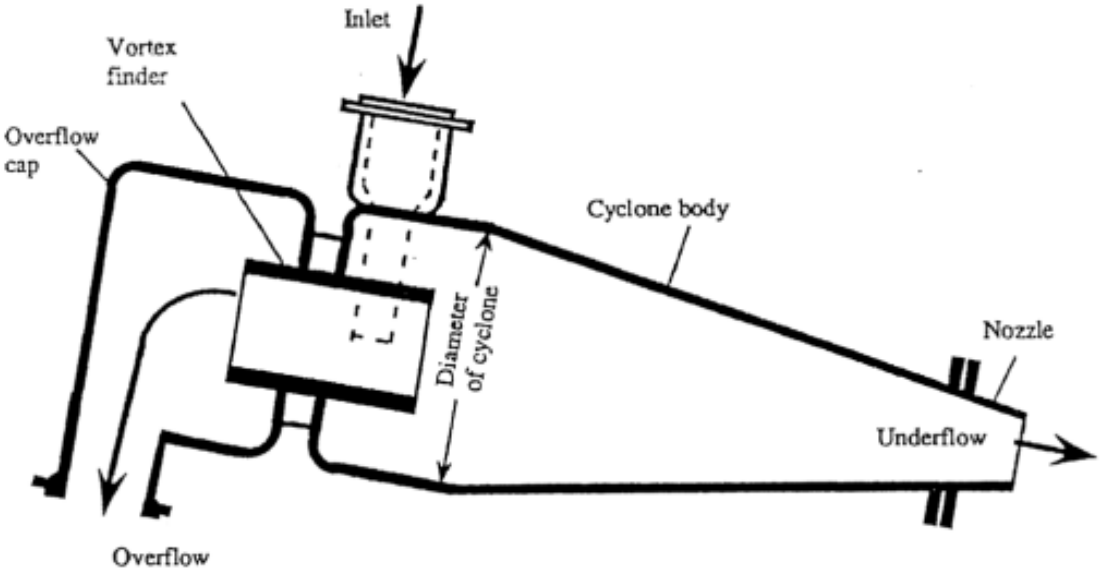

Figure 2.1 Dense medium cyclone configuration (Wood, 1990).

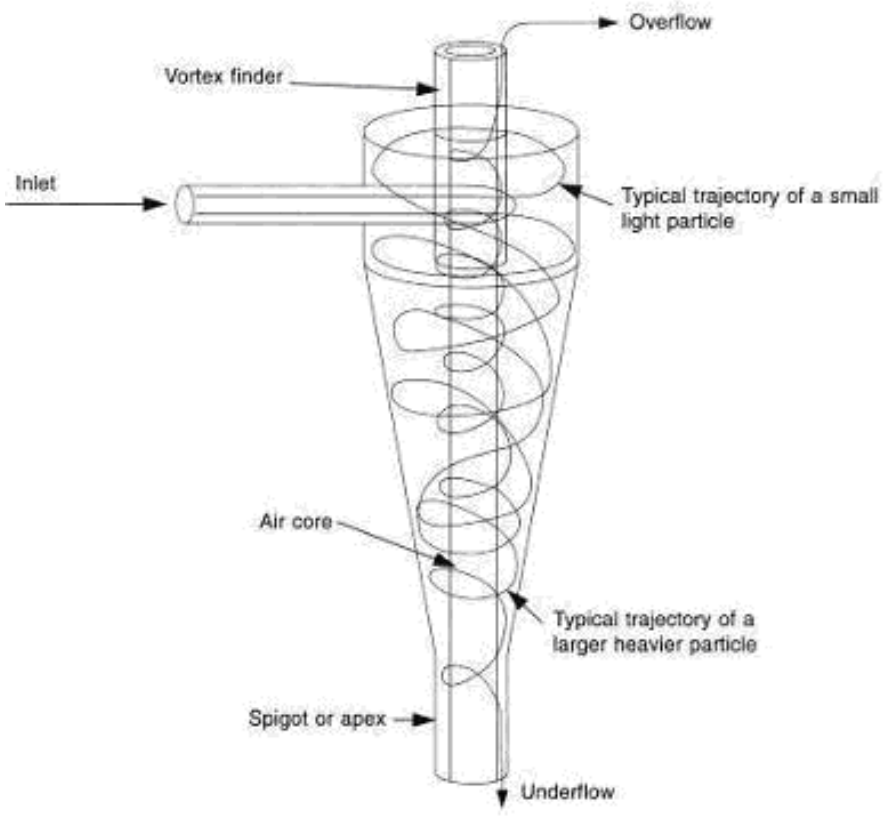

Figure 2.2 Hyrocyclone configuration and working principle (Svarovsky, 1984).

2.1.3 Performance measurements for DMC

A measure of the performance of the operation may obtained by subjecting the overflow and underflow streams to a laboratory procedure called the float-sink analysis, in order to determine the amount of misplaced material (valuables to the underflow and rejects to the overflow in the case of coal). A graph may be plotted between the partition coefficient (number) and the relative density of the feed, where the partition number is the percentage of the feed material of a particular relative density that reports to the underflow. The plot thus obtained is called the partition curve of the tromp curve, the slope of which is a measure of the efficiency of the process (Wills, 1997). Different partition curves are obtained for different size fractions. A typical partition curve and the ideal one are shown in Figure 2.3.

Efficiency of the cyclone is expressed using a term called the "Ecart Probable" (the probable error), E_p, which is half the relative density range between the 25% partition coefficient and the 75% coefficient. From Figure 2.3, this may be written as

$$E_p = \frac{\rho_{75} - \rho_{25}}{2} \tag{2-1}$$

E_p value bears an inverse relationship to the efficiency; a lower E_p implies a higher efficiency. An ideal partition curve is a step curve, with E_p=0, as shown in Figure 2.3. The cut density ρ_{50}, also called the effective density of separation is defined as the density when 50% of the particles are reported to the underflow (Wills, 1997).

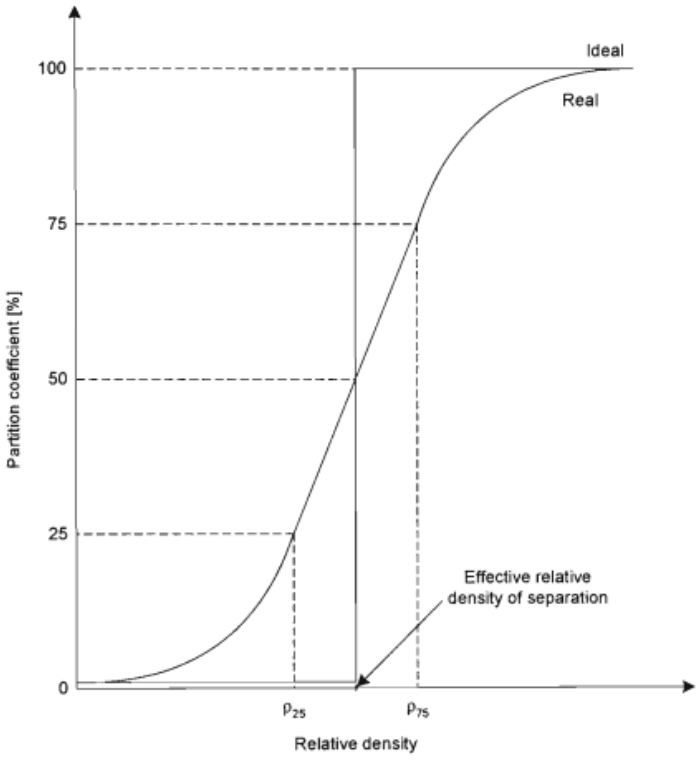

Figure 2.3 Partition or Tromp curve (Wills, 1997).

2.2 Experimental investigation

Much of the work in this area has been carried out to investigate the fluid flow in hydrocyclones, but very little for that in DMCs. However, as mentioned, DMCs and hydrcyclones have a similar geometry and operational principle. Thus, research works on hydrcyclones are likely to be applied to DMCs.

The experimental studies on DMCs mainly fall into five parts, which are related to the velocity field, pressure drop, air core, rheology of magnetite medium and particle motion.

2.2.1 Velocity field

The first comprehensive experiment study on fluid velocity patterns in hydrocyclone was done by Kelsall (1952). He studied small cyclones with dilute feeds by illuminating fine aluminum particles and observing the motion with a microscope having rotating objectives. In his report, tangential and axial velocity components were measured at chosen location. Over years, many developed techniques were introduced to measure velocity profile of cyclone. For instance, Hsieh (1988) used Laser Doppler Velocitometry (LDV) to observe the fluid flow pattern, pressure drop and particle motion in a 75 mm hydrocyclone.

In both the works of Kelsall (1952) and Hsieh (1988), the axial velocity component of fluid was characterized with a motion in two opposite directions. This means a reverse flow is needed. As shown by Fig 2.4, this recirculating flow is around the locus of zero axial velocity, which is between the upward flow to the vortex finder and the downward flow to the apex. It should be noted that near the outer wall of the vortex finder, there exists a short-circulating flow, also known as by-pass way. Some particles are pulled by

this flow to move across the inner roof wall and along the vortex finder wall to join the upward flow. Following Hsieh (1988) work, Monredon (1990) measured the velocity profiles with a Laser Doppler Velocimetry in 75 mm and 150 mm hydrocyclones. This work shed new light on the effect of design variables (vortex finder diameter, spigot diameter and cone angle) on velocity profiles. It showed that the locus of zero axial velocity remained the same in the cylindrical section, but it was shifted inwards in the conical section, when the vortex finder and spigot diameters were increased.

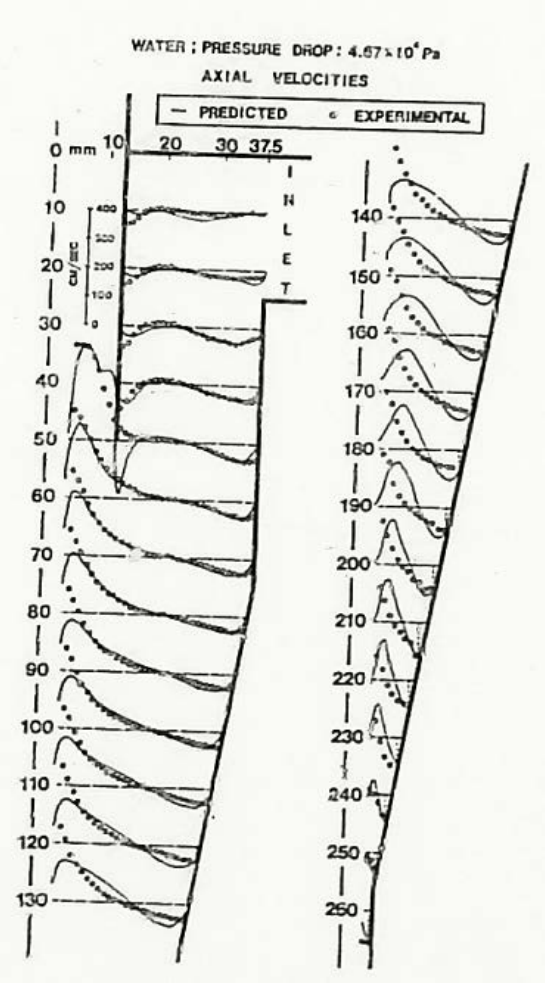

Figure 2.4 Axial velocity profile in a 76 mm hydrocyclone reported by Hsieh (1988).

Kelsall (1952) and Hsieh (1988) also measured tangential velocity profile as shown in Figure 2.5. It can be seen that the tangential velocity increase from the wall as the radius

decreases and reaches a local maximum near the air core. They also found that the position of the tangential velocity peak is within the radius of the vortex finder. This is also mentioned by Svarovsky (1984).

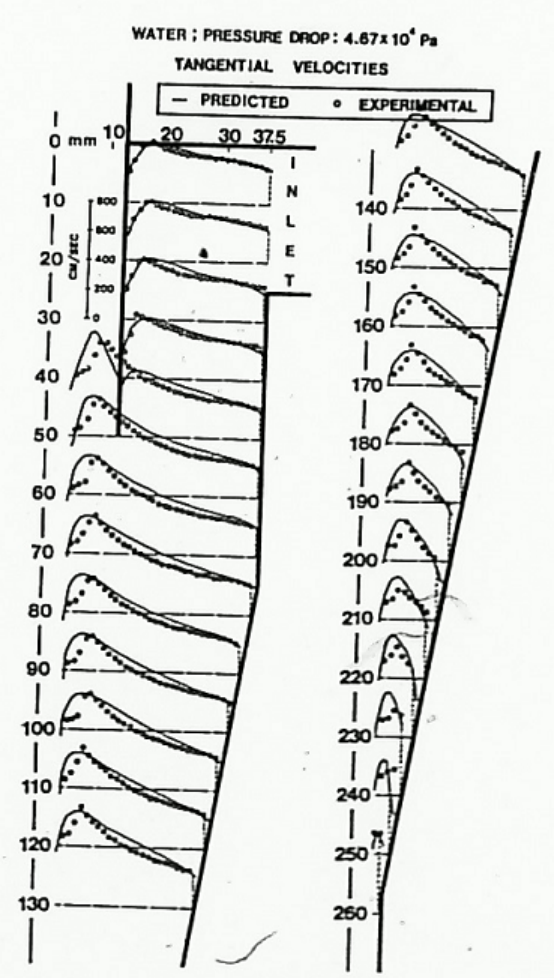

Figure 2.5 Tangential velocity profile in a 76 mm hydrocyclone reported by Hsieh (1988).

2.2.2 Pressure drop

The pressure drop in cyclones is defined as the difference between the feed pressure and outlet orifice pressure. Pressure drop indicates the energy required to operate the cyclones. Many researchers also used the term, “Operation Head” (given in equivalent diameters of the medium head) to express the pressure drop, which relates to the ratio of pressure drop and cyclone size. This parameter can more directly reveal the effect of the radial pressure gradient (dP/dr) on particles.

By studying on a 30 mm DMC, Napier-Munn (1986) gave an expression for the pressure drop:

$$\frac{P}{\rho_m g} = 1.52 \times 10^8 Q_f^{2.30} \left(\frac{\eta}{\rho_m} \right)^{-0.30} \qquad (2\text{-}2)$$

From the expression, it can be seen that the pressure is related to the flow rate and viscosity of the medium. This expression agrees with many experiment results by other researchers. As the flow rate is increased, the pressure drop increased. However, the behavior of the medium used by DMC is like that of a non-Newtonian fluid and the kinematic viscosity η of non-Newtonian fluid has not been well defined.

2.2.3 Air core

It has been well recognized that the air core is an indication of vortex stability and play an important role in DMCs’ performance (Clarkson and Wood, 1993; Dyakowski and Williams, 1993; Sripriya et al., 2013; Williams et al., 1995; Wood, 1990). The air core is formed because the pressure of the cyclone at longitudinal axial region is usually lower than the atmospheric pressure. This pressure difference will let the air into the cyclone.

The first direct air core measurements in DMCs were carried out by Wood (1990) who used a “caliper” introduced into the air core from the vortex finder By this way, he was able to measure the air core diameter. According to his measurements, the air core diameter is influenced strongly by the apex diameter. It should be noted that while medium relative densities are in the range of 1.0 to 1.9, no effect was found on the diameter of the air core. It is also important to point out that the measured air core was almost cylindrical in shape (with a slightly smaller diameter at the apex), except for the vortex finder region, where high turbulence fluctuations are found.

Williams et al. (1995) extended the study of air core by using electrical resistance tomography (ERT). The dynamics of air core were monitored. It was found that if the feed flow rate is reduced below a critical flow, it is hard to form a stable air core. Similar results were also confirmed by Dyakowski and Williams (1996). They used ERT to identify regions of different electrical resistivity inside hydrocyclones. Their results are shown in Figure 2.6, which shows that a more stable core is generated at low concentrations of solids and high flow rates. Besides, the fact that the position of air core was not axially fixed, may have been related to the fluctuating operating conditions at the inlet. More recently, using the gamma ray tomography (GRT), Subramanian (2002) measured the medium density distribution in a 350 mm DMC and found that the air core diameter is uniform in the axial direction.

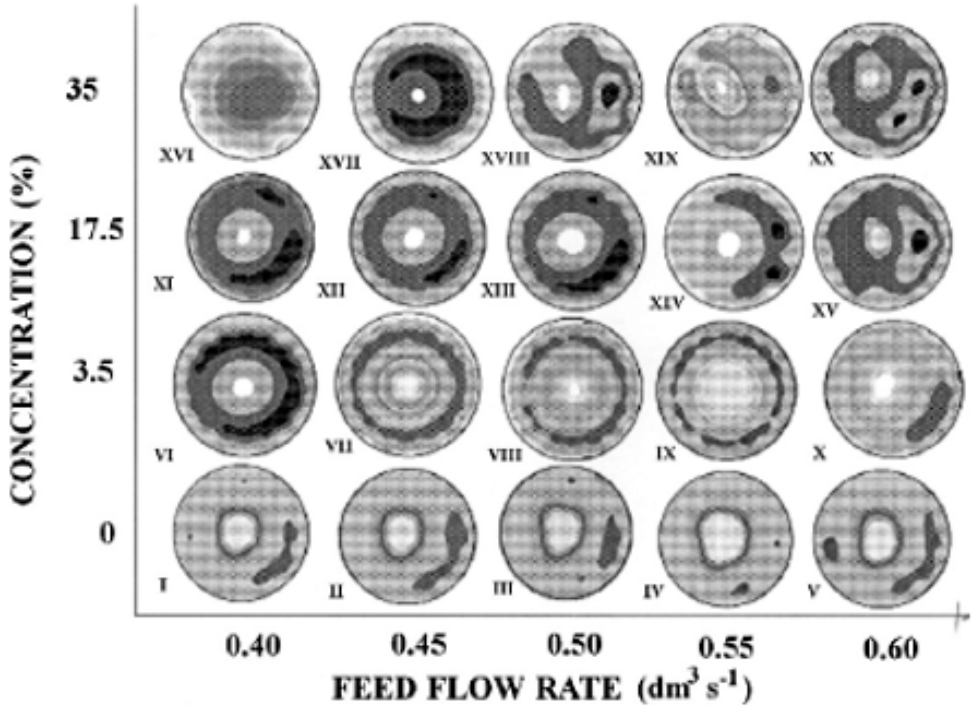

Figure 2.6 Sequence of resistivity images below the feed inlet region in a 44 mm diameter hydrocyclone operating at various feed flow rates (0.4-0.61/s) and different solids concentration (0-35% wt.) (Dyakowski and Williams, 1996).

2.2.4 Rheology of the magnetite medium

The medium used in the coal industry is usually suspension-type media. As the medium flow shows non-Newtonian rheological properties, it is inadequate to use a simple rheological parameter to describe the complex rheological behavior. In coal preparation, the relative medium density typically has a narrow range from 1.2 to 1.6. In this range, the magnetite medium flow can be described by Casson's equation:

$$\tau^{0.5} = \tau_c^{0.5} + \left(\eta_c \cdot S\right)^{0.5} \tag{2-3}$$

where τ is the shear stress for shear rate, S. Thus, the medium rheology over the above range can be defined by two rheological parameters: Casson viscosity, η_c, and the Casson yield stress, τ_c (Narasimha et al., 2006c).

2.2.5 Particle motion

The particle motion in DMC is hard to track experimentally. As such, most researchers have focused on the density or solids concentration distributions to predict the particle behavior.

Galvin and Smitham (1994) used X-ray tomography to measure the density profile in a dense medium cyclone. Their studies show that the highest slurry density part is between the air core and the wall near the apex region. This phenomenon was also found by Subramanian (2002) who measured the slurry density inside a 350 mm dense medium cyclone with gamma ray tomography (GRT). This phenomenon is revealed through the medium density distribution (Figure 2.7) given by him. Subramanian (2002) also found that pressure also had an effect on the medium segregation. With a higher inlet pressure, the medium segregation is better.

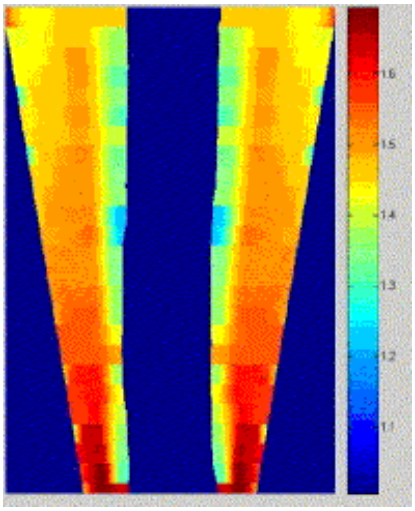

Figure 2.7 Medium density distribution near the apex measured by Subramanian (2002)

2.3 Empirical model

Studies on dense medium cyclones have aimed at developing empirical models that include all practically possible variables, which can affect the operation of a cyclone

plant: namely, cyclone dimensions, medium and coal characteristics, feed medium pressure, and density. Such a model enables the examination of the effects of alternative operating procedures without the need for extensive test work planning. Through a large amount of careful pilot scale test work, many empirical models of DMCs have been developed and applied (Gottfried and Jacobsen, 1977; Wood, 1990).

According to Wang (2009), existing design procedures are based on well-established criteria relating principally to:

- medium to coal ratio
- feed rate
- feed pressure
- magnetite slurry medium RD control
- magnetite medium slurry size distribution
- non-magnetic content of magnetite medium slurry
- DMC dimensions
- wear conditions.

The basic design principle is to ensure that the above parameters are within specified limits such that the best practice separations would be expected to occur. Such conditions allow the expected coal separation performance to be estimated using the empirical approaches mentioned above. With these in place, it is the common practice to simulate coal preparation plant separations to allow resource optimisation to be achieved. Such practices are commonly used to derive yield, recovery and product quality estimates for new and upgraded mines and plants. However, once built a coal preparation plant will almost invariably operate under the conditions which are,

different to varying extents, from those assumed for the design purposes. As a result, yield, recovery and/or quality may be lower than expected.

Davis and Davis (1987), Wood (1990), Clarkson and Wood (1993) and Barbee et al. (2005) have developed the currently available dense medium cyclone models. These models have considered three type of input values which include feed washability characteristics, design variables (e.g., cyclone diameter, inlet size, etc.), and operating variables (e.g., inlet pressure, medium density, etc.). A typical logic flow of the model is shown in Figure 2.8.

According to Barbee et al. (2005), the routines used to simulate the performance of dense medium cyclone can be subdivide in to three categories:

- Medium calculations
- Partition calculations
- Application checks

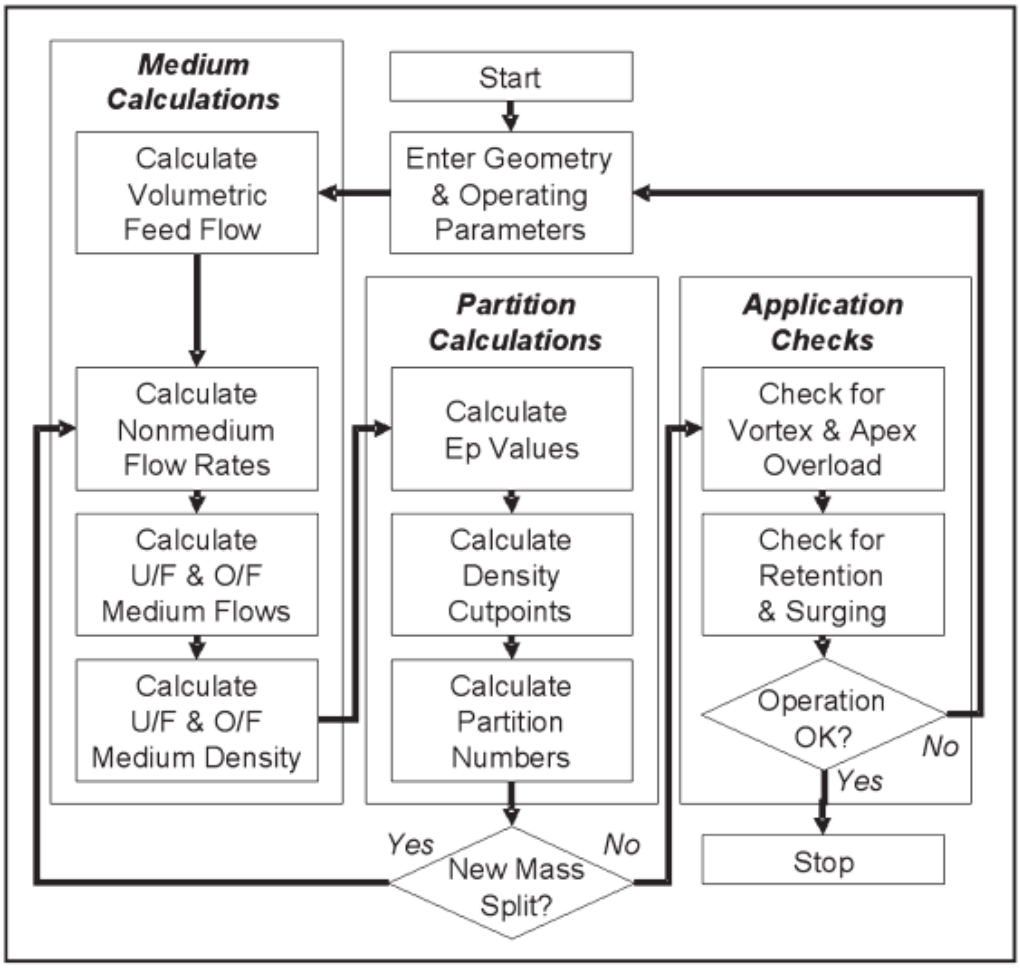

Figure 2.8 Logic flow chart in the application of the dense medium cyclone by Barbee et al. (2005).

In the medium calculation, the first step is to transfer the inlet pressure (P) to the equivalent diameters of the medium head (normally known as the Head):

$$Head = \frac{\frac{P}{\rho_f g} + E}{D_c} \tag{2-4}$$

where ρ_f is the feed slurry density, D_c is the cyclone diameter, and E is the distance between the pressure gauge and the centre line of the cyclone.

The total volumetric feed flow (Q_f) is calculated by:

$$Q_f = KD_c^{1.93} Head^{0.45} \left(\frac{D_u}{D_o} \right)^{0.15} \tag{2-5}$$

where D_u is the apex diameter, D_o is the vortex finder diameter, and K is an empirical fitting and unit conversion coefficient, which is 76 in Clarkson and Wood (1993) model.

The volumetric flow rate of the medium to the underflow without feeding coal (Q_{um}^*) is calculated by:

$$Q_{um}^* = Q_f \left(\frac{0.79}{Head^{0.37}} \right) \left(\frac{D_u}{D_o} \right)^{4.2} \tag{2-6}$$

When feeding coal, the volumetric flow of medium to underflow (Q_{um}) is adjusted to:

$$Q_{um} = 0.97 Q_{un} + \frac{Q_{um}^{*\,2}}{Q_{un} + Q_{um}^*} \tag{2-7}$$

where Q_{un} is the volumetric flow rate of non-medium solids reporting to the underflow.

The medium split to underflow (Q_{um}/Q_{fm}) is calculated by:

$$\frac{Q_{um}}{Q_{fm}} = \frac{Q_{um}}{Q_f - Q_{fn}}$$

where Q_{fn} is the volumetric feed flow rate of non-medium solid, which equals to the ratio of dry coal mass feed rate (M_{fn}) to non-medium solids by the feed coal density (ρ_{fn}).

The density of the underflow medium (ρ_{um}) is calculated by:

$$\rho_{um} = 0.459 \rho_{fm} \left(\frac{Q_{um}}{Q_{fm}} \right)^{0.194(\rho_{fm} - 2.04)} \left(\frac{P_{RR}^{\,0.17} Head^{0.082}}{D_c^{\,0.1}} \right) \tag{2-8}$$

where P_{RR} is the Rosin-Rammler intercept of the feed magnetite size distribution.

Likewise, the density of the overflow medium (ρ_{om}) is calculated by:

$$\rho_{om} = \left(\frac{\rho_{fm}}{1 - \frac{Q_{um}}{Q_{fm}}} \right) \left(1 - \frac{Q_{um}}{Q_{fm}} \frac{\rho_{um}}{\rho_{fm}} \right) \tag{2-9}$$

The next step is the partition calculation.

The Ecart Probables (E_p) is obtained by:

$$E_p = \frac{0.067}{D_p} \left(\frac{D_c}{711} \right)^{0.5} \tag{2-10}$$

where D_p is the mean particle diameter and D_c is the cyclone diameter. It should be noted that in previous models (Wood, 1990), the effect of cyclone diameter on E_p has not been considered.

The pivot point density is given by:

$$\rho_{50}^{*} = 0.360\rho_{fm} + 0.274\rho_{um} + 0.532\rho_{om} - 0.25 \tag{2-11}$$

The separating density (ρ_{50}) for each particle size class is calculated by:

$$\rho_{50} = \rho_{50}^{*} + \frac{E_p}{1.0986} \ln \left(\frac{Q_{fm}}{Q_{um}} - 1 \right) \tag{2-12}$$

Since ρ_{50} and E_p are already known, the partition number for any size fraction can be estimated from the Whiten equation by:

$$P = \frac{1}{1 + \exp \left\{ \frac{1.0986\left(\rho_{50} - \rho \right)}{E_p} \right\}} \tag{2-13}$$

For the final operational check, the simulation will follow the limits of application, product overload and retention and surging issues to identify the accuracy of the predictions.

Although this type of correlations can be used within the operating conditions for what they were derived and for the type of the DMC used, their use at extrapolated conditions of the operating parameters is out of the question. Also due to the complexity of the interaction between the operating and geometrical parameters, general correlations are useless for a particular case, as they need to be adjusted.

Based on this model and some results from CFD-DEM simulation, Cheng (2010) developed a PC-based DMC simulator with a friendly interface which can examine the DMC performance in a fast and easy way as shown in Figure 2.9. Figure 2.10 shows the user friendly interface of the PC-based DMC simulator.

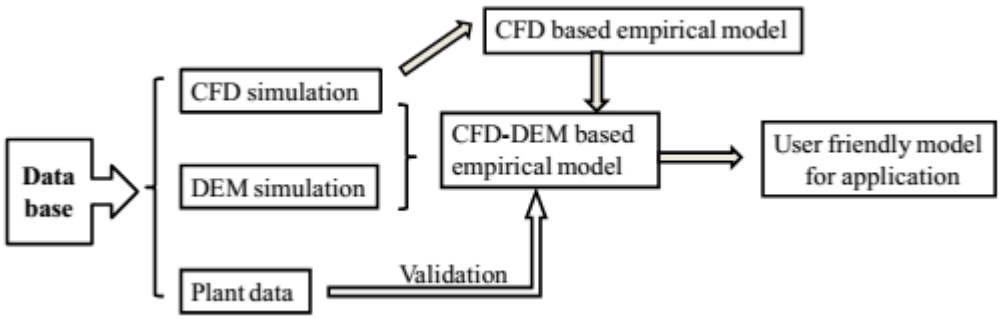

Figure 2.9 A flow chart of the PC based empirical model formulation (Cheng, 2010).

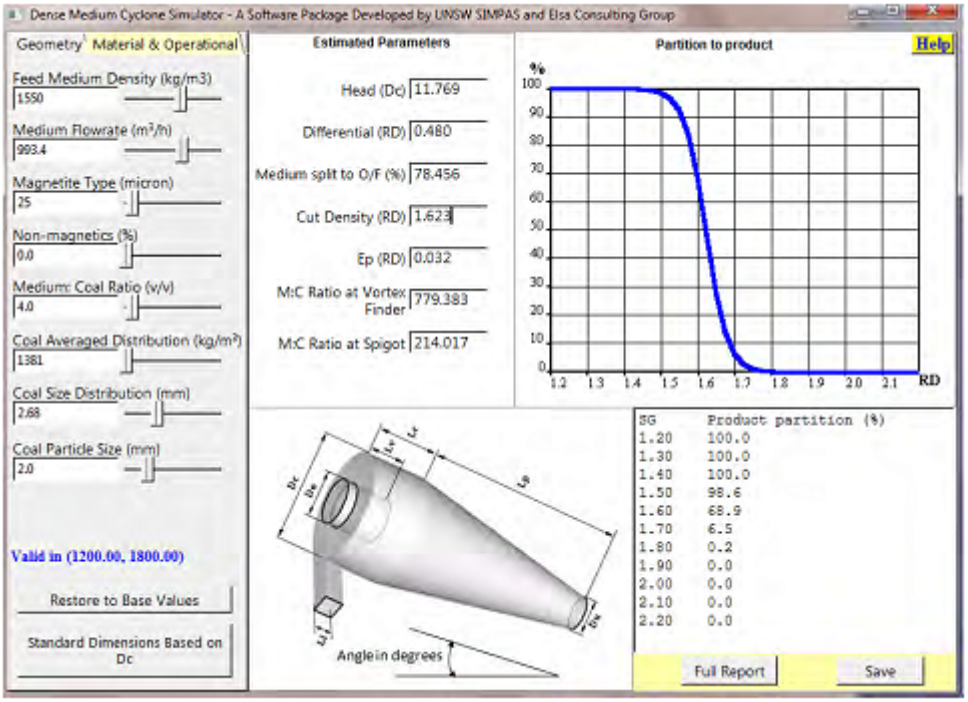

Figure 2.10 The interface of the PC-based DMC simulator (Cheng, 2010).

2.4 Numerical study

In the past decades, computational methods have become more preferred by researchers. Not only because it can provide better understanding of the fluid flow in cyclones, but also because of the developments in computers' ability to deal with large calculations, it makes it possible for researchers to use a complete numerical solution for modelling and predicting the performance of cyclones.

2.4.1 Turbulence modelling

As mentioned previously, the turbulence modelling in DMCs is complex due to the anisotropy and strain caused by the strong swirl and the flow reversal. Also, high computational costs of such simulation adds more difficulties to the modelling. To improve the accuracy of prediction, many research efforts have been made in the above

areas. A summary of numerical studies on the fluid flow in cyclones is given by Narasimha et al. (2006c) and Nowakowski et al. (2004) for the period from 1982 to 2005 as shown in Table 2.1.

2.4.1.1 Plandtl mixing length model

In the past, the computers could not perform large amounts of computations. Therefore, the model had to be simple. In this sense, many researchers preferred the Plandtl mixing-length model rather than the κ-ε model. They also assumed that the DMC is symmetric so that Navier-Stokes equations can be solved in two dimensions. In Planditl mixing-length model, the mixing length varies in helical and axial direction. Hsieh (1988) used the experimental velocity data measured by a laser-Doppler system to verify the predictions. It has been shown that both the axial and tangential components showed a good agreement with the measurements. However, the definitions in different manner for the axial and tangential components make the Prandtl mixing length not an acceptable standard in CFD.

Table 2.1 Summary of published CFD studies on cyclone separators (Narasimha et al., 2006c; Nowakowski et al., 2004).

Authors	Type of cyclone	Assumptions	Numerical method	Results	comments
Boysan et al. (1982)	Gas	An algebraic form of RSM for turbulence with non-vanishing angular component	2D	The velocity and particle distributions.	Model restricted to gas cyclone.
Pericleous and Rhodes (1986) and Pericleous (1987)	Hydrocyclone	Modified Mixing Length model for turbulence, Algebraic slip mixture model for multiphase without particle inertial forces.	2D	The velocity and particle distributions. The recirculation zones.	The effects on aircore obtained without underflow flow influence.
Davidson (1988)	Hydrocyclone	Based on multi-continuum approach without particle inertial forces	2D	The velocity and particle distributions. The recirculation zones.	Model for hydrocyclone without an air core.
Hsieh and Rajamani (1991)	Hydrocyclone	Plandtl mixing model with two turbulence scales. Extended lagrangian approach to calculated particle trajectories.	2D	The velocity and particle distributions. The hydrocyclone performance. An air-core diameter as a function of flow conditions.	Limited to low-solids concentrations.
Zughbi et al. (1991)	Dense medium cyclone	Modified mixing length model. Air core fixed.	2D	The velocity distribution and wear effects.	Model for dense medium cyclones with a fixed air core.
Monredon et al. (1992)	Hydrocyclone	Lagrangian approach to calculate hydrocyclone efficiency. Prantl mixing	2D	The velocity distribution and particle trajectories.	The air core diameter assumed from

		model with two turbulences scales.			experiments.
Dyakowski and Williams (1993)	Hydrocyclone	Anisotropic character of turbulence.	2D	The effect of mean velocity on turbulence. All six components of Reynolds stress.	Only hydrodynamic aspects.
Dyakowski et al. (1994)	Hydrocyclone	Non-Newtonian flow model. A surface-tension force balance.	2D	The velocity distribution.	Model for non-Newtonian flow.
Davidson (1994)	Hydrocyclone	Physics of uniform density and inviscid flow at each outlet.	2D	The air core diameter.	
Malhotra et al. (1994)	Hydrocyclone	Use the κ-ε model with swirl correction.	2D	The new formulation of turbulence energy dissipation.	
Dyakowski and Williams (1995)	Hydrocyclone	Calculation based on the internal pressure distribution.	2D	The air core diameter as the function of various hydrocyclone geometries and operational conditions.	
Fraser et al. (1997)	Gas	Use the κ-ε model with swirl correction	2D	The velocity distribution.	
Averous and Fuentes (1997)	Hydrocyclone	Used the RSM model.	2D	The velocity distributions.	Limited to low solids concentration.
Concha et al. (1996)	Hydrocyclone	Used several turbulence models.	2D-3D	The velocity distributions.	
He et al. (1999)	Hydrocyclone	Used the modified κ-ε model for 3D simulation.	3D	The velocity distributions.	Inaccuracy results caused by retention of

					axial symmetry in the cylindrical curvature grids system.
Meier and Mori (1999)	Gas cyclone	Anisotropic character of turbulence by combining the κ-ε model and the mixing length theory of Prandtl.	2D	The velocity distributions.	
Suasnabar and Fletcher (1999)	Dense medium cyclone	Used the RSM model for turbulence. Combined Eulerian model for medium and langrangian approach for coal particles.	2D	The velocity distributions and separation efficiency curve.	The effect of non-Newtonian rheology was obtained.
Ma et al. (2000)	Gas	Used the RNG model.	3D	The velocity distributions.	Particle tracking technique used for modelling particle motion.
Slack et al. (2000)	Gas	Used RSM and LES model.	3D	The velocity distributions.	Required a very fine mesh and long computational time.
Suasnabar (2000)	Dense medium cyclone	Use RSM model	2D	The velocity distributions	
Statie et al. (2001)	Hydrocyclone	Used the modified κ-ε model for 3D simulation	3D	The influence of hydrocyclone geometry on the separation performance.	Model particle trajectory of fibre/cylindrical rigid.
Petty and Parks (2001)	Hydrocyclone	Used the κ-ε model and the RNG model.	3D	The velocity distributions.	
Cullivan et al.	Hydrocyclone	Used RSM and DPM model.	3D	The velocity and particle	Air core validation with

(2003)				distributions.	ERI tomography.
Brennan (2003)	Dense medium cyclone & Classifying cyclones	Used the RSM and VOF model.	3D	Separation efficiency curve.	Segregation of magnetite and partition curve predicted closely to experiments.
Schuetz et al. (2004)	Hydrocyclone	Used the RSM model.	3D	Simulated separation efficiency curve.	Results limited to very low-solids concentrations.
Noriler et al. (2004)	Gas cyclone	Used the DSM model.			
Narasimha et al. (2005)	Hydrocyclone	Parametrically modified κ-ε, Langrangian frame model for particle tracking.	3D		
Narasimha et al. (2006a)	Hydrocyclone	Used LES model.	3D	Predicted the velocity profile and diameter and shape of air core	
Wang et al. (2009a)	Dense medium cyclone	Used RSM and VOF model.	3D	Predicted the medium segregation and used LPT to predict the partition curves.	The reults were very closed to the experiments.
Stephens and Mohanarangam (2010)	Hydrocyclone	Compared Shear Stress Transport (SST) model with curvature correction and RSM model.	3D	Predicted the velocity profile.	SST-CC model can give pretty good prediction.
Swain and Mohanty (2013)	Hydrocyclone	Compare κ-ε model and RSM model.	3D	Predicted the velocity profile.	

2.4.1.2 κ-ε model

In the κ-ε model, only one scalar velocity fluctuation, which means this model intrinsically assumes that the turbulence is isotropic. Further, the Bousinessq approximation on which the eddy viscosity intrinsically relies upon implies the equilibrium between stress and strain. However, the flow in a cyclone is highly swirling and highly curved, particularly in the conical region. For these reasons, κ-ε model is not suitable to model the turbulence in cyclones.

To overcome this problem, many researchers applied a modification to the standard κ-ε model. Boysan et al. (1982) transformed the exact transport equation for the Reynolds stresses into an algebraic form. Dyakowski and Williams (1993) combined the κ-ε model with equation for the Reynolds stress to include the anisotropic character of the turbulence present in the hydrocyclone flow. Many studies have shown that modified κ-ε model can give very good prediction on cyclones' velocity profile (Stephens and Mohanarangam, 2010; Swain and Mohanty, 2013). However, this model has not been generally applied on predicting the separation of particles.

2.4.1.3 Reynolds stress model (RSM)

It is prevalent thought that Reynolds stress model is more suitable for simulating swirling flows. However, applying this model is computationally expensive due to the six additional transport equations. Stress transport models, in particular the full Differential Reynolds Stress model (DRSM), such as that developed by Launder et al. (1975) solve transport equations for each individual Reynolds stress. This enables stress transport models to model anisotropic turbulence and strained flows where the Bousinessq approximation is known to be flawed. Though the computational cost of

RSM is much more than k-ε model, it is still a good choice to model turbulence in cyclones.

2.4.1.4 Large eddy simulation model (LES)

Recently, Large Eddy Simulation (LES) which has been proven to solve large turbulent structures began to be applied in modelling the turbulence in cyclones. Slack et al. (2000) did an evaluation of the RSM and the large eddy simulation model (LES) for a 205 mm gas cyclone. The study showed that with a relatively coarse mesh the RSM shows good agreement between the predicted and experimental measurements. They point out that the LES results are more expensive but the quality of the results could lead to better performance in the prediction of separation efficiency. Recently, Narasimha et al. (2007b) successfully used LES turbulence model to simulate the slurry flow in dense medium cyclone and the results shows that air core radius predicted by LES model is more accurate and the density distribution had a good agreement with the GRT data.

2.4.2 Particle flow modelling

As mentioned above, the fluid flow within DMCs is complicated. Compared with extensive numerical studies of other cyclone separators such as gas cyclone and hydrocyclone (see, e.g. the reviews by Cortes and Gil (2007) and Narasimha et al. (2007a)), numerical studies of DMCs are few to date. Nonetheless, recent efforts made on DMCs make it possible to study DMC multiphase flow and performance by numerical models, as reviewed below.

The mathematical descriptions required to model DMCs generally need to address two main aspects of the flow: the modelling of the medium flow and the modelling of coal

particle flow, taking into account the mutual interactions of the two flows. Two approaches have been used for such a purpose: namely, the continuum approach and discrete approach. In the continuum approach, the two-fluid Model (TFM) is used to represent the flow at a macroscopic level. On the other hand, in the discrete approach, a combined computational fluid dynamics and discrete element method (CFD-DEM) is used at a microscopic level.

2.4.2.1 Two-fluid model

In the two fluid model (TFM), fluid and particles in a particle-fluid system are treated as continua. The point variables such as the fluid velocity, the fluid pressure, or the velocity of solid matter at a specified point within a particle are replaced by the local mean variables. Note that the mean variables are obtained by averaging the point variables over regions, each with sufficient number of particles, but are smaller than the scale of the "macroscopic" variations from point to point in the system (Anderson and Jackson, 1967). The two fluid models include the full Eulerian multiphase approach and simplified Eulerian approaches, such as the Mixture and Volume of Fluid model (VOF).

The full Eulerian multiphase flow approach, which is featured by a set of continuity, momentum and turbulence equations for each phase is preferred for systems with very high dispersed phase concentrations, where solid/solid interactions carry a significant amount of stress. The disadvantages of the full Eulerian multiphase modelling approach have been its high computational cost, convergence and robustness issues. Further implementations in commercial CFD codes have until recently been limited to using the k-ε model for turbulence. In spite of this Suasnabar (2000) used the full Eulerian approach for granular flow modelling of particulate phases to model a dense medium

cyclone. The technique has also been successfully applied by Nowakowski et al. (2000) and Nowakowski and Dyakowski (2003).

There are models such as the Volume of Fluid model (VOF) (Hirt and Nichols, 1981) and the Mixture model (Manninen et al., 1996), which are simplified Eulerian multiphase approaches where the equations of motion are solved for the mixture and additional transport equations are solved for the volume fractions of additional phases. The VOF model and the mixture model solve significantly less transport equations than the full Eulerian approach and thus numerically more efficient. The VOF and Mixture models are implemented in commercial CFD codes such as Fluent with the option of being used for turbulent flows with the turbulence model enabled for the mixture.

The VOF model is intended for modelling flows where there are two or more continuous phases separated by a phase boundary and this makes it suitable for modelling the air core in both hydrocyclones and dense medium cyclones (Brennan, 2003; Delgadillo and Rajamani, 2005; Suasnabar, 2000).

It has been proved that mixture model can be used to model the slurry flow in DMCs in many studies. Brennan (2003) firstly applied this model on dense medium cyclone simulation. However, the medium segregation was over predicted comparing to the experimental data by Subramanian (2002). Subsequently, viscosity correction was introduced into the model. Wang et al. (2009a) modelled magnetite medium segregation in a dense medium cyclone using the mixture model combined with the Reynolds stress turbulence model and Ishii and Kishima (1984) viscosity correction. The validity of the approach was verified by the reasonably good agreement between the measured and predicted results under different conditions.

2.4.2.2 Lagrangian Model

The Lagrangian approach is intrinsically the combination of CFD and discrete element method without considering the interaction between particles. The paths of individual particles are tracked based on the velocity predicted by a CFD simulation of the fluid. The nature of Lagrangian approach suggests that this model is more suitable for dilute system where the interaction between particles and the influence of particles on the fluid flow are not very significant. By balancing the forces that act on a particle in motion in a carrier fluid, a particle can be tracked along its trajectory. Additionally corrections on the particle trajectory due to the interaction with its surrounding environment can be included. The influence of particles on the fluid can be included by considering a source term in the governing equations of the fluid. Also turbulence dispersion of the particles can be included.(Crowe et al., 1996)

Following the path of a solid particle, the general equation of motion based on the effects treated by Basset, Boussinesq, and Oseen is given by:

$$\frac{4\pi}{3}D_p{}^3\rho_p\frac{du_p}{dt}=\frac{4\pi}{3}D_p{}^3\rho_p F_D\left(u_f-u_p\right)-\frac{4\pi}{3}D_p{}^3\frac{\partial P}{\partial r}+\frac{1}{2}\frac{4\pi}{3}D_p{}^3\rho_f\frac{d\left(u_f-u_p\right)}{dt}$$
$$+6D_p{}^2\sqrt{\pi\rho_f\mu_f}\int_{t_{p0}}^{t_p}d\tau\frac{\left(d/d\tau\right)\left(u_f-u_p\right)}{\sqrt{t_p-\tau}}+F_e \qquad (2\text{-}14)$$

where u_f and u_p are velocities of the fluid and solid particle, ρ_f and ρ_p are the densities of the fluid and solid material, F_e is the external force due to potential field and F_D is the time constant for momentum transfer due to drag force defined by:

$$F_D=\frac{3}{8}C_D\frac{\rho_f}{\rho_p}D_p{}^{-1}\left|u_f-u_p\right| \qquad (2\text{-}15)$$

Where drag coefficient C_D is given by: $C_D = C_D\left(N_{\mathrm{Re}}\right)$. The application of this equation also limited to particle diameters much less than the local turbulence length scale (Crowe et al., 1996).

This model has been successfully applied in both hydrocyclone and dense medium cyclone by Wang (2009). The predicted results showed good agreement with the experimental data. It should be noted that an obvious "Fish-Hook" phenomenon was observed in his study.

2.4.2.3 Combined CFD and DEM model (CFD-DEM)

As mentioned above, the difference between CFD-DEM and CFD-LPT is the consideration about the interaction between particles and the effects of particles on the fluid flow. This means the application of CFD-DEM mainly should address two aspects, the discrete element method and the coupling of CFD and DEM.

For discrete element methods, there are two types that are most common: soft-particle and hard-particle approaches. In the soft-particle method, particles are permitted to have minute overlaps, which represent particle deformations and these deformations are used to calculate restoring elastic, plastic and frictional forces between particles. The motion of particles is described by the well-established Newton's laws of motion. A characteristic feature of the soft-sphere models is that they are capable of handling multiple particle contacts. By contrast, in a hard-particle simulation, a sequence of collisions is processed, one collision at a time and being instantaneous. Therefore, typically, the hard-particle method is most useful in sparse rapid granular flows. Of the two discrete element methods, the soft-sphere method, has been extensively used in the

study of various phenomena, such as particle packing and compaction, particle flow, and particle-fluid flow.

As for the coupling of CFD and DEM, a scheme of coupling and information exchange between continuum (CFD models) and discrete (DEM models) is given in Figure 2.11 by Xu et al. (2001). At each time step, DEM will provide information, such as the position and velocity of individual particles, for the evaluation of the porosity and volumetric fluid drag force in a computational cell. CFD will then use these data to determine the fluid flow field which then produces the fluid drag forces acting on individual particles. Incorporation of the resulting forces into DEM will produce information about the motion of individual particles for the next time step.

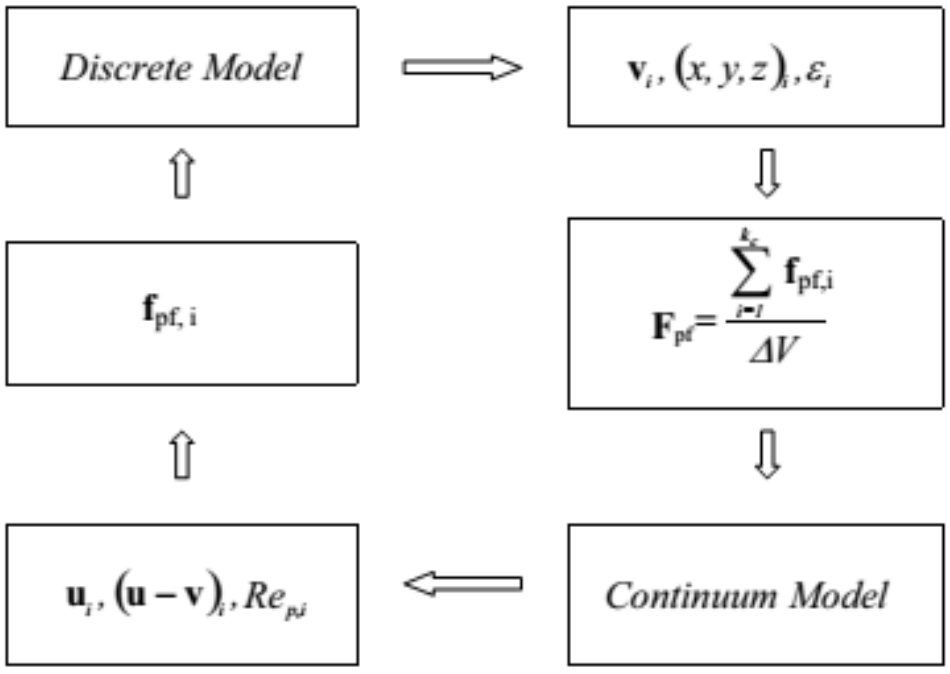

Figure 2.11 Coupling and information exchange between continuum (CFD) and discrete (DEM models) (Xu et al., 2001).

Chu et al. (2009a) developed the first CFD-DEM model for DMCs by combing mixture model for the medium flow and DEM for the coal particle flow, and used it to study various aspects of the DMC process(Chu et al., 2013; Chu et al., 2012a; Chu et al., 2014; Chu et al., 2009a, 2012b, c; Chu et al., 2009b). Although theoretically rational, the CFD-DEM approach is computationally very demanding. It is thus applied mainly to coarse coal particles. Even in this case, each CFD-DEM simulation of DMC needs to be run for a long time to obtain meaningful results. The time required being from a few weeks to a few months depending on applications and computer facilities.

2.5 Proposed research

The aim of this study is to establish a new CFD model, apply it to predicting the performance of a dense medium cyclone and optimize the design or operating conditions. The specific objectives of this study are:

- Model formulation: A new numerical model based on the mixture model will be proposed in this thesis.
- Model validation: Comparisons between predicted results and experimental data will be carried out to validate the proposed model. Also, a simple evaluation of different models (proposed model, CFD-LPT and CFD-DEM) will be made.
- Parametric study: Performance of Standard DMCs and large diameter DMCs will be studied separately. The effect of key parameters will be examined by comparing the performances of DMCs under different conditions. The effects of these variables will be qualitative analysed.

3. MODEL FORMULATION

3.1 Introduction

The mathematic descriptions required to model DMCs generally fall into two main aspects: one is the modelling of the medium flow and another is the modelling of coal particle flow, while allowing for their mutual interaction. The two approaches are used to model the flows as follows: the continuum approach at a macroscopic level is represented by the two-fluid Model (TFM), and the discrete approach at a microscopic level is represented by the combined approach of computational fluid dynamics and discrete element method (CFD-DEM). In the TFM approach, both fluid and solid phases are treated as interpenetrating continuum media in a computational cell that is much larger than individual particles but still small compared to the size of the process equipment. Because of its simple assumption and lower computation costs, the TFM approach is preferred in process modelling and applied research. It was used to model the medium flow in a DMC in terms of the so-called mixture model by different investigators (Brennan, 2003; Narasimha et al., 2006b; Wang et al., 2009a; Zughbi et al., 1991), and as a result, the interface between the air and the medium could also be predicted. On the other hand, in the CFD-DEM approach, the motion of discrete particles is obtained by the DEM, and the flow of continuum fluid is described by the local averaged Navier–Stokes equations that can be solved by the traditional CFD, with the coupling of CFD and DEM through particle–fluid interaction forces. Chu et al. (2009a) developed the first CFD-DEM model for DMCs by combing the mixture model for the medium flow and DEM for the coal particle flow, and used it to study various aspects of the DMC process (Chu et al., 2012a & b & c; 2013; Chu et al., 2009b). Although theoretically rational, the CFD-DEM approach is computationally very demanding. It is thus applied mainly for coarse coal particles. Even in this case, each

CFD-DEM simulation of a DMC needs to be run for a long time to obtain meaningful results, from a few weeks to a few months depending on the applications and computer hardware. This problem does not happen to Lagrangian particle tracking (LPT) method, which only traces the motion of one particle and can be thought of as a simplified DEM model. By combing LPT with the mixture model, different investigators studied the separation behaviours in DMCs (Narasimha et al., 2007b; Wang et al., 2009a & b; 2011; 2013; 2014; Zughbi et al., 1991). Based on the results generated by the CFD-LPT and CFD-DEM simulations, Chen et al. (2012) recently developed a PC-based model for optimizing design and operation of DMCs. However, The CFD-LPT approach should be limited to DMC operations at a large M:C (medium-to-coal) volume ratio, because it ignores the effect of the inter-particle interactions and the reaction of coal particles on the fluid.

In order to overcome the deficiencies associated with the CFD-LPT approach and alleviate the computational load of DMC simulations, a mathematical model, which describes the flows of the medium and coal particles as well as air in DMCs in terms of a continuum mixture model, is proposed in this study.

3.2 Simulation method

3.2.1 Model Strategy

Because of the complexity of the flow in a DMC, the modelling is developed in two steps, similar to the previous CFD-LPT and CFD-DEM modelling procedures (Chu et al., 2009a; Wang et al., 2009a) (see Figure. 3.1). In step 1, only air and slurry with a certain density are considered. The two phases are treated as fluids of homogeneous viscosity and density. The turbulent flow of gas and liquid is modelled using the

Reynolds stress model (RSM), and the interface between the liquid and air core is modelled using the Volume of Fluid (VOF) model (Hirt and Nichols, 1981). The primary air core position and the initial velocity distribution are obtained in this step and used as a part of the initial conditions in the next step.

In step 2, magnetite and coal particles are added to simulate the flows of the medium, air, coal, and magnetite in DMCs and estimate the separation performance. The multiphase model is changed from the VOF model to the mixture model. Also, a correction is needed to estimate the viscosity effect of size distribution of magnetite particles, as suggested by Wang et al. (2009a). In this step, detailed density and velocity distributions of different phases (air, water, magnetite, and coal) are obtained.

Therefore, the whole process involves three linked CFD simulation stages (RSM, VOF, mixture model) and one viscosity correction model, as described below. Note that the VOF model is well documented elsewhere (Nowakowski et al., 2004; Wang and Yu, 2010) and thus, not included in this chapter for brevity.

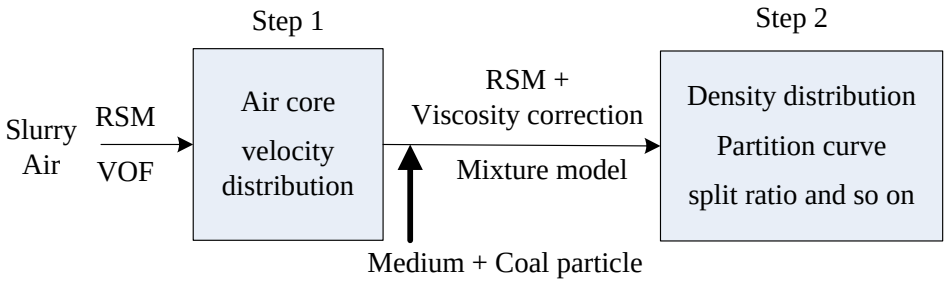

Figure 3.1 Steps used in the present modelling.

3.2.2 Mathematical Model

The mathematical model proposed in this study is a simplified TFM model, also known as the “mixture model”. In the model, both fluid (liquid and air) and solid phases

(magnetite and coal particles) are treated as interpenetrating continua. Particles of different sizes or densities represent different phases. The flow of liquid-gas-solid mixture (as a single phase) is calculated from the continuity and the Navier–Stokes equations based on the local mean variables over a computational cell considering slip velocities between different phases (Manninen et al., 1996), which are given by:

$$\frac{\partial}{\partial t}(\rho_m) + \frac{\partial}{\partial x_i}(\rho_m u_m) = 0 \tag{3-1}$$

and

$$\frac{\partial}{\partial t}(\rho_m u_{mi}) + \frac{\partial}{\partial x_j}(\rho_m u_{mi} u_{mj}) = -\frac{\partial p}{\partial x_i} + \frac{\partial}{\partial x_i}(\sum_{k=3}^{n} p_k) + \frac{\partial}{\partial x_j}[\mu_m(\frac{\partial u_{mi}}{\partial x_j} + \frac{\partial u_{mj}}{\partial x_i})]$$
$$+ \frac{\partial}{\partial x_j}(-\rho_m \overline{u_{mi}^{'} u_{mj}^{'}}) + \frac{\partial}{\partial x_j}(\sum_{k=1}^{n} \rho_k u_{dr,ki} u_{dr,kj}) + g\rho_m \tag{3-2}$$

where g is the gravitational acceleration, p_k is the solid pressure, $u_{dr,ki}$ is the drift velocity, and $-\rho_m \overline{u_{mi}^{'} u_{mj}^{'}}$ is the Reynolds stress term which includes turbulence closure and must be modelled to close Eq. (3-2). RSM, which is necessary to describe the anisotropic turbulence problems as encountered in DMCs, is adopted for such a purpose:

$$\frac{\partial}{\partial t}\left(\rho_m \overline{u_i' u_j'}\right) + \frac{\partial}{\partial x_k}\left(\rho_m u_k \overline{u_i' u_j'}\right) = D_{T,ij} + P_{ij} + \phi_{ij} + \varepsilon_{ij} \tag{3-3}$$

In Equations (3-1) to (3-3), the mass-averaged velocity u_{mi}, mixture density ρ_m and mixture viscosity μ_m of a mixture are respectively defined based on all the phases involved:

$$u_{mi} = \frac{\sum_{k=1}^{n} \alpha_k \rho_k u_{ki}}{\rho_m} \tag{3-4}$$

$$\rho_m = \sum_{k=1}^{n} \alpha_k \rho_k \tag{3-5}$$

$$\mu_m = \sum_{k=1}^{n} \alpha_k \mu_k \tag{3-6}$$

where n is the number of phases, and k represents different phases where k=1 stands for water (the primary phase), and 2 for air, 3−n for the kth type of coal or magnetite particles (the secondary phases).

The volume fraction of phase α_k is obtained according to the continuity equation for phase k:

$$\frac{\partial}{\partial t}(\alpha_k \rho_k) + \frac{\partial}{\partial x_i}(\alpha_k \rho_k u_{mi}) = -\frac{\partial}{\partial x_i}(\alpha_k \rho_k u_{dr,ki}) \tag{3-7}$$

The drift velocity is determined by the algebraic slip mixture model by assuming that the phase velocities should reach equilibrium over a short spatial length (Manninen et al., 1996):

$$u_{dr,ki} = \frac{(\rho_k - \rho_m) d_k^2}{18 \mu_1 f_{drag}} a_{k,i} - \sum_{k=1}^{n} \left(\frac{\alpha_k \rho_k u_{1k,i}}{\rho_m}\right) \tag{3-8}$$

where σ_t is the Prandtl-Schmidt number set to 0.75, η_t is the turbulent diffusivity. $a_{k,i}$ is the acceleration of phase k, and f_{drag} is the drag force on particles or air bubbles, which is determined according to the well-known Ergun & Wen-Yu correlation (1952; 1966) for particles and Schiller and Neumann correlation for air bubbles (1933).

When Equation (3-7) is applied to the air phase to predict the air core, the concept of air bubble is introduced to calculate the interaction force (i.e. drag force) between air and liquid. In this study, the bubble size is set to 10^{-5} m after some tests, so that the mixture model gives almost the same air core as obtained by the VOF under the same condition.

The solid properties such as viscosity and solid pressure are described by the kinetic theory of granular flow (KTGF) model based on the algebraic model of temperature model (Syamlal et al., 1993):

$$-(p_k\mathbf{I}+\boldsymbol{\tau}_k):\nabla\mathbf{u}_k-\gamma\Theta+\phi_{l,k}=0 \tag{3-9}$$

where $-(p_k\mathbf{I}+\boldsymbol{\tau}_s):\nabla\mathbf{u}_k$ is the generation of energy by the solid stress tensor, $\gamma\Theta$ is the collisional dissipation of energy, and $\phi_{l,k}$ is the energy exchange between the *l*th fluid or solid phase and the *k*th solid phase.

The above discussed mixture model is in principle similar to that recently proposed for hydrocyclones (Kuang et al., 2012), the main differences from other models (Narasimha et al., 2006b; Wang et al., 2009a; Zughbi et al., 1991) being in the modelling of solid properties and particle-fluid interaction. Our numerical tests however indicated that this model cannot properly predict the measured performance when directly applied to DMCs. On the other hand, previous modelling efforts of DMCs showed that the medium viscosity is an important parameter for describing the behaviour of the medium and the separation of particles in DMCs (Chu et al., 2009a; Narasimha et al., 2006b; Wang et al., 2009a, b). In those studies, the effect of coal on the rheology of the medium was ignored, and hence the mixture viscosity was approximated by the medium viscosity given by some established correlations. Such a treatment is also adopted in this study. Note that medium viscosity is dependent on many variables, such as magnetite particle size distribution, particle shape, medium density, medium contamination, and so on, and is complicated to determine. For simplicity, it is assumed to be controlled by the solid volume fraction of magnetite, and calculated by a correlation which is due to Ishii

and Mishima (1984) based on experimental studies, but later modified by Wang et al. (2009a):

$$\mu_m = 3.8\mu_w\left(1-\frac{\alpha_{mag}}{0.62}\right) \tag{3-10}$$

where μ_w is the water viscosity, and α_{mag} is the volume fraction of magnetite particles. Now, Eq. (3-10) is used to instead of Eq. (3-6) to determine the mixture viscosity.

4. MODEL VALIDATION

4.1 Introduction

In this chapter, the proposed model will be validated by comparing the predicted results and experimental data. Also, evaluations on partition curves predicting accuracy of different models, including the proposed model, CFD-LPT and CFD-DEM, will be made.

4.2 Simulation conditions

Tables 4.1 and 4.2 list the geometrical and operational conditions considered in this study. Those in the base case are selected according to the experimental work of Richard (2007). Therefore, the validity of the proposed model can be examined by comparing the simulated and measured results. In addition, three variables will be considered in the next chapter of model applications: namely, M:C ratio, U:O ratio and Head. The effect of each variable is studied, while others are kept the same as those in the base case, as listed in Tables 4.1 and 4.2.

Table 4.1 DMC geometric parameters in the present simulation.

Parameter	Symbol	Dimension*
Diameter of the body, mm	D_c	1000 (2000)
Side length of inlet (involute), mm	L_i	266 (532)
Diameter of vortex finder, mm	D_o	450 (240-674/900)
Diameter of spigot, mm	D_u	337 (225-630/674)
Length of cylindrical part, mm	L_c	1200 (2400)
Length of vortex finder, mm	L_v	700(1400)
Length of conical part, mm	L_p	1880(3760)

* base case dimensions and their ranges in the brackets (the single value in brackets is for large diameter dense medium cyclone modelling).

Table 4.2 Operational conditions in the present simulation.

Parameter	Units	Value*
Coal density distribution	kg/m^3	1300 to 2200
Coal particle diameter	mm	0.25-11
Gas density	kg/m^3	1.225
Gas viscosity	kg/m/s	1.8×10^{-5}
Water density	kg/m^3	998.2
Water viscosity	kg/m/s	0.001
Magnetite density	kg/m^3	4945
Magnetite sizes (and volume fractions)	μm	10 (30.5%), 20 (25.6%), 30 (14.6%), 40 (11.5%), 50 (9.9%) and 80 (7.9%)
Medium feed density	kg/m^3	1550
M:C ratio		5.6 (4-50)
Orientation Angle		10º to horizontal
Head	D_c	8.3 (4.15-66.4)
Gauge pressure at the inlet	kPa	158 (78-1264)

* The base case conditions and their ranges in the brackets.

Figure 4.1 shows the geometry and mesh representation of the DMC in the base case. The selection of mesh type, size and arrangement is based on study of Ghodrat et al. (2014). The mesh consisting of 80,318 hexahedral grids is the same as that used in the studies of Chu et al. (2009b) and Wang et al. (2009). In the vicinity of the walls and vortex finder, the grid is more refined in the radial direction than in the remainder of the cyclone. Our tests indicated that the solution is independent of the mesh size used. This also applies to other DMCs simulated.

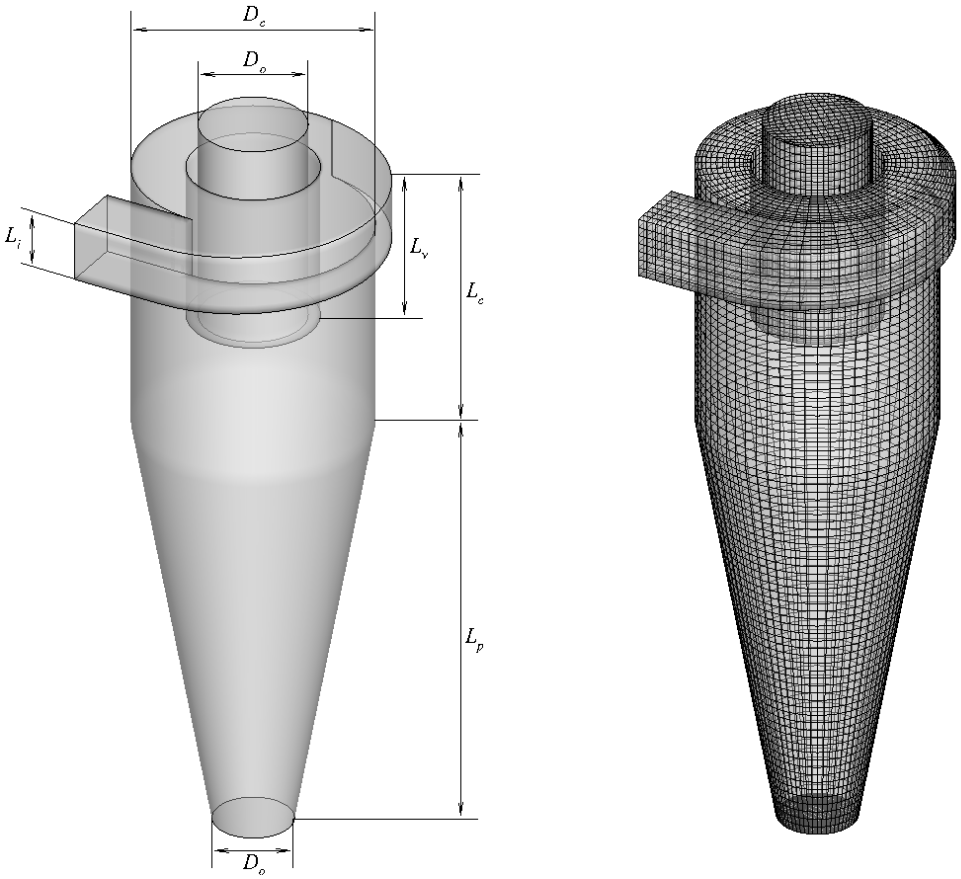

Figure 4.1 Schematic and grid representation of the DMC considered.

A “pressure-inlet” boundary condition is used at the cyclone inlet, and the “pressure-outlet” condition at both the outlets, corresponding to a normal operation in the DMC practice. The gauge pressure at the two outlets (vortex finder and spigot) is zero,

corresponding to the ambient atmospheric pressure, and the gauge pressure at the inlet is 158 kPa.

All the simulations are conducted using the ANSYS Fluent CFD software package (version 14) at the National Computational Infrastructure in Australia. 32 CPUs are assigned to each simulation. Each run of the simulations lasts for about 14 days to ensure that the flow simulated can achieve a steady state at which the macroscopic flow characteristics do not change much with time. Unless otherwise noted, all the results shown are time-averaged.

4.3 Model applicability

As described in Section 2, the proposed modelling involves two steps, because the flow in a DMC is complex. The stepwise approach offers a way to use the existing data to verify the proposed model.

The VOF model for step 1 is the same as previously used in the modelling of the gas-liquid flow in a hydrocyclone. The validity of the model has been established by the good agreement between the measured and calculated results, as reported elsewhere (Kuang et al., 2012; Wang and Yu, 2006). The present model can also reproduce the key phenomena of the medium-only flow in a DMC, as done in the study of Wang et al. (2009a). However, the results are not included in this chapter to avoid the repeatition. Below, we focus on the applicability of the new mixture model of step 2 for describing the DMC performance.

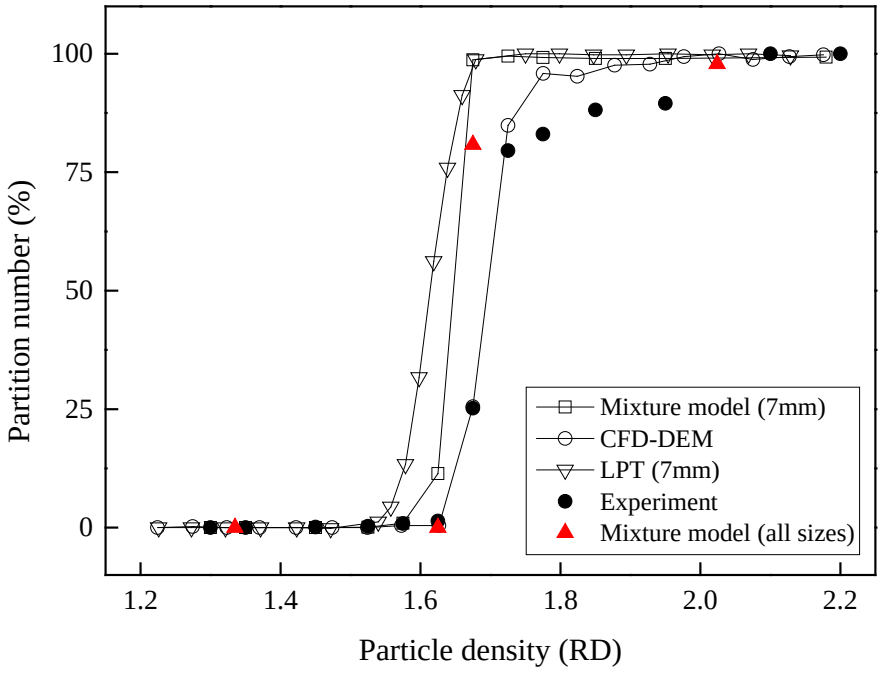
Partition number (%)
100
75
50
25
0
1.2
1.4
1.6
1.8
2.0
2.2
Particle density (RD)
Mixture model (7mm)
CFD-DEM
LPT (7mm)
Experiment
Mixture model (all sizes)

(a)

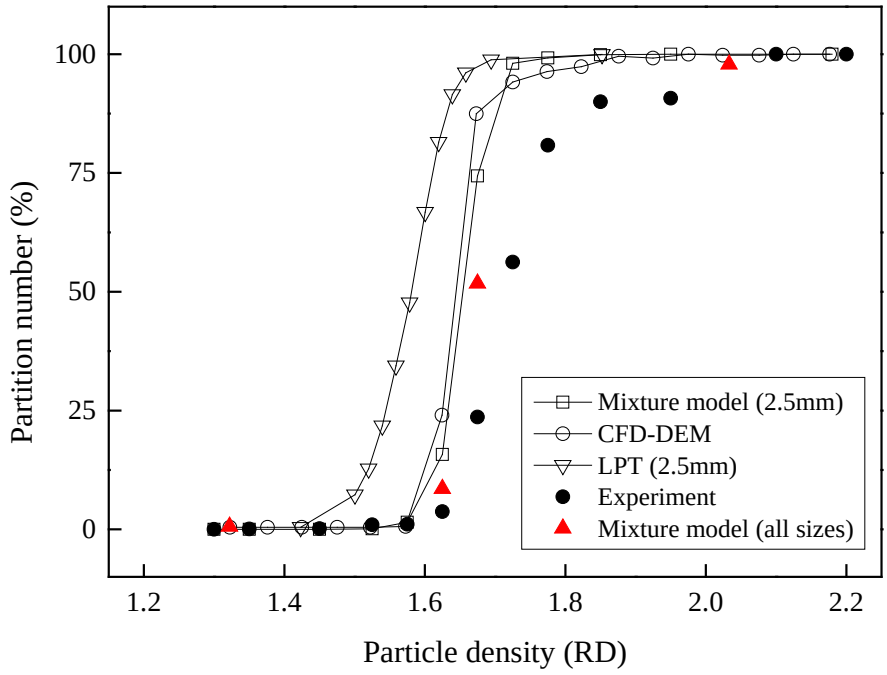
Partition number (%)
100
75
50
25
0
1.2
1.4
1.6
1.8
2.0
2.2
Particle density (RD)
Mixture model (2.5mm)
CFD-DEM
LPT (2.5mm)
Experiment
Mixture model (all sizes)

(b)

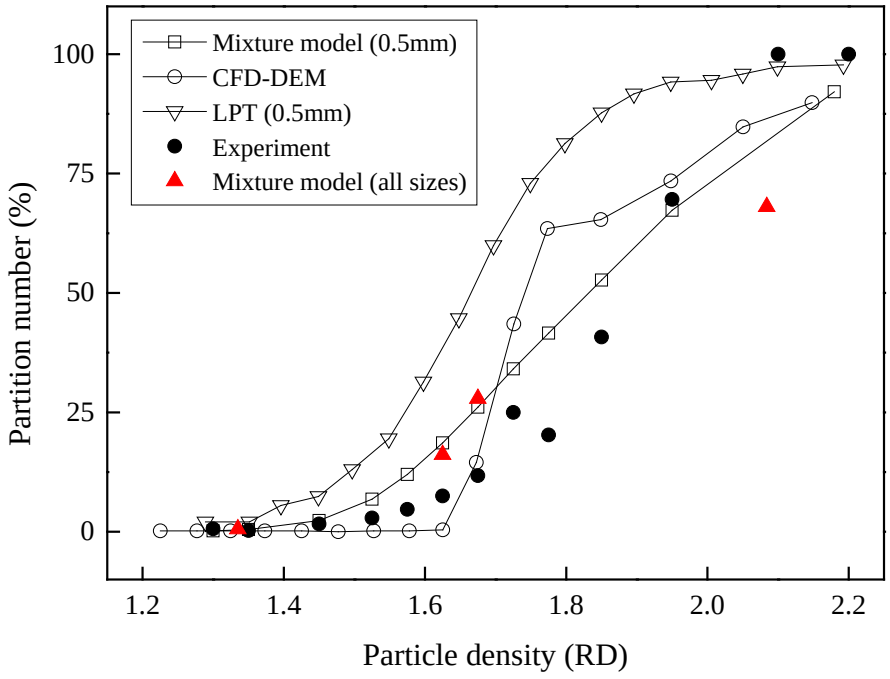

(c)

Figure 4.2 Comparison of the simulated and measured partition curves for different sized particles: (a) 4-11 mm, (b) 1.4-4 mm, and (c) 0.25-1.4 mm.

Figure 4.2 compares the measured and calculated partition curves, obtained based on the mass portions of particle recovery to the underflow. In this figure, the particle density is expressed as the relative density (RD), defined as the density ratio of particles to water. This applies to all the following results. In addition, the calculated results from this study are generated by two methods using the present mixture model. In Method 1, the particles considered are classified into three groups according to particle size, as done in the experimental measurement (Richard, 2007). The size distribution in each group is represented by a mean size, while the density distribution is by 12 mean densities. Three independent simulations are then conducted at the same M:C ratio and different density distributions, ignoring the interplay between particle sizes. In Method 2, only one simulation is carried out, considering both the size and density distributions of particles,

thus the interplay between particle sizes, as in the experiments (Richard, 2007). Note that in the simulations, the size distribution is represented by 3 mean sizes and each of the density distributions by 4 mean densities. For comparison, the results obtained by both CFD-DEM and CFD-LPT simulations in the studies of Wang et al. (2009) and Chu et al. (2009b) are also included in Figure 4.2. As seen from this figure, the mixture, CFD-LPT, CFD-DEM models all give reasonably good predictions of the measured separation efficiencies for the three groups of particle sizes, and reproduce the "breakaway size" phenomenon where the separation efficiency sharply decreases and slows down with decreasing particle size. Notably, the simulations based on the mixture model with and without consideration of the interplay between particle sizes give consistent results. This result, to some degree, supports the CFD-LPT approach, which ignores the interplay between particle densities, between particle sizes, and between particle size and density, however, can reasonably describe DMC performance under a certain condition.

Overall, the results predicted by the mixture model appear in better agreement with the measured results compared to the CFD-LPT model, because the mixture model considers the reaction of particles on the fluid and the particle-particle interaction, which are not considered by the CFD-LPT model. On the other hand, compared to the CFD-DEM model, the mixture model gives a better prediction of separation efficiency for fine particles (Figure 4.2c) but less for the coarse particles (Figure 4.2a). This may be explained as follows. The CFD-DEM approach is theoretically more rational compared to the mixture model (Zhou et al., 2010). However, to simulate fine particles with the current computer capacity, some simplifications are needed to alleviate the computational loading: for example, an assembly of fine particles, whose properties are

assumed to be the same, is represented by a parcel particle of much larger diameter than those of real particles. Nonetheless, the results shown in Figure 4.2 suggest that the proposed model can be used to predict the separation behaviour in DMCs, at least qualitativly.

5. MODEL APPLICATION

5.1 Introduction

In this chapter, standard size DMCs and large size DMCs will be studied based on the proposed model respectively. For the standard size DMCs, the effect of two key factors, M:C ratio and U:O ratio, will be examined and analysed through comparing the separation of particles and the distribution of different parameters in DMCs. On the other hand, the effect of M:C ratio on large diameter DMCs performance is studied separately as large diameter DMCs sometimes show a different performance compared with standard DMCs under the same operating conditions. Subsequently, the effect of Head is studied for the optimisation purpose.

5.2 Standard dense medium cyclone

5.2.1 Effect of M:C ratio

M:C ratio has been known as one of the key factors in DMC operation. Its effect on DMC flow and performance is examined by the present model. Here, relatively fine particles of different densities are focused on, because little attention was paid to such particles in the previous numerical studies of DMC. In addition, considering that the number of phases involved in the mixture model cannot exceed 20 in ANSYS Fluent, although such a limitation is theoretically not necessary, only one size is considered. This allows us to use adequate mean densities in simulations to represent the density distribution involved to generate partition curves that are smooth enough for assessing DMC performance. Figure 5.1 shows the partition curves at different M:C ratios and reveals that the separation efficiency increases with the increase of M:C ratio, in particular, when RD=1.5-1.8 and M:C ratio is relatively small. A similar result was also obtained in the CFD-DEM study of DMC by Chu et al. (2009a) for particles of 5 mm

diameter (2 mm in this study). This again suggests that the CFD-DEM and mixture models can give consistent results, at least qualitatively. The latter is however computationally much more efficient, particularly for fine particles. Note that the CFD-LPT model cannot be used to study the effect of M:C ratio due to its inherent deficiency.

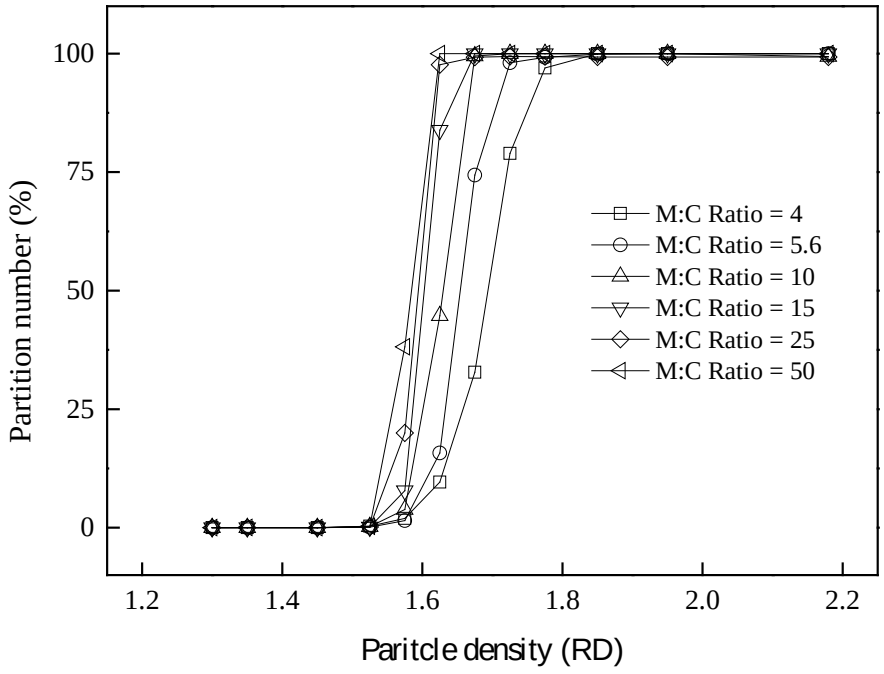

Figure 5.1 Effect of M:C ratio on partition curve when particle size is 2 mm.

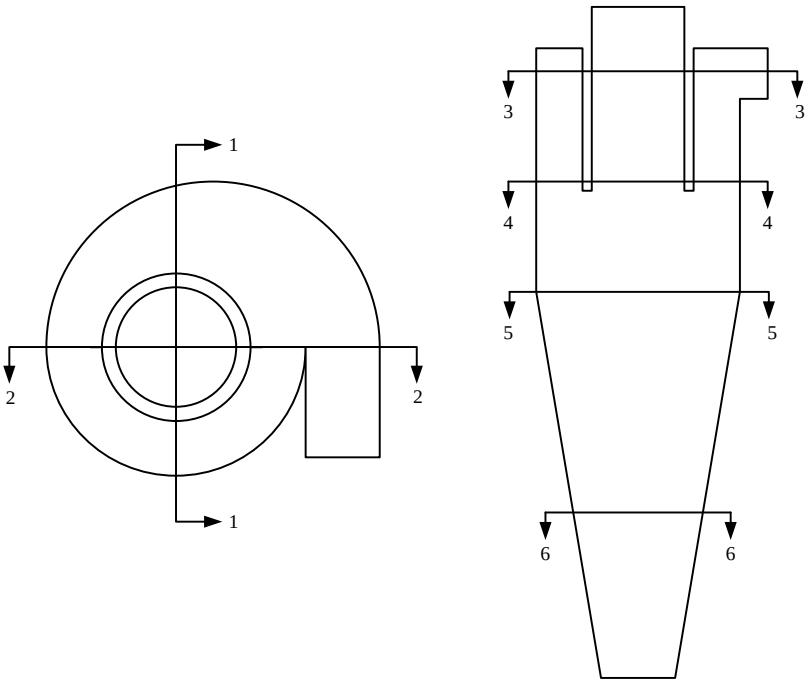

Figure 5.2 Definitions of the sections used in this work.

In order to better understand the particle behaviours at different M:C ratios, we examine representative distributions of particles of different densities on the vertical 2-2 plane defined in Figure 5.2, and the results are given in Figure 5.3. In this figure the white region corresponds to the area occupied by the air core, which is not shown for clarity because the properties of air and liquid phases are fairly different. Three typical particle behaviours generally observed in a DMC can be identified from the coal volume fraction distributions (Figure 5.3a): (a), the light particles (e.g. RD=1.3 and 1.525) flow down along the outside wall of the vortex finder to join the overflow stream within the vortex finder, thus by-passing the separation process; (b), the particles around the cut density (e.g. RD=1.575) is separated around the air core from the vortex finder tip to the spigot; and (c) the heavy particles (e.g. RD=1.675 and 2.179) aggregate at the wall and spiral down to the underflow. Interestingly, the helical path of particles on the wall can be observed for both light and heavy particles under the present condition (see Figure

5.3b), which should account for the “groove” wear pattern, as experimentally observed by Wood (1990). Note that the above discussed particles behaviours can be observed at all the M:C ratios considered. However, the densities corresponding to different particle behaviours vary with M:C ratio. In addition, it should be pointed that the findings from Figure 5.3a can also be obtained based on the particle distributions on the 1-1 vertical plane (Figure 5.2). This case is considered below for the analysis of flow properties.

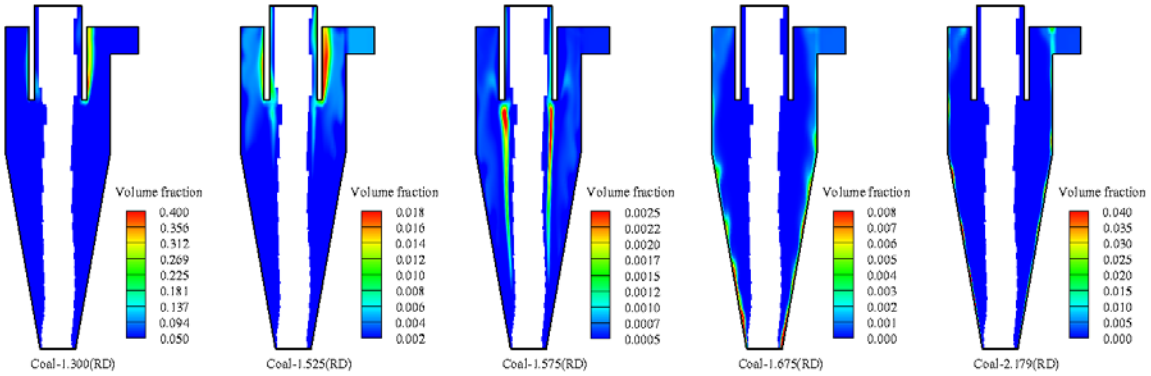

(a)

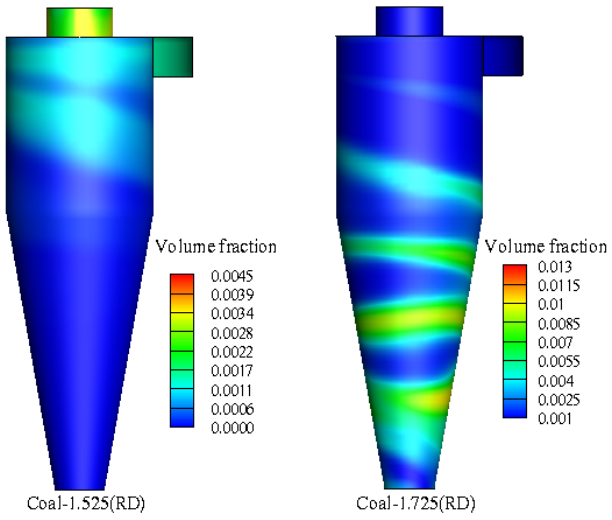

(b)

Figure 5.3 Distributions of coal particles of different densities at t = 30 s: (a) inside the base DMC, and (b) on the wall when M:C ratio=15.

Figure 5.4 shows the effects of M:C ratio on the cut density D_{50} and Ecart probable E_p. Here, D_{50} is the density of the particles reporting to the underflow at a portion of 50%, and E_p is calculated by $(D_{75}-D_{25})/2$, where D_{75} and D_{25} are respectively the densities of the particles reporting to the underflow at portions of 75% and 25%. It is seen that both D_{50} and E_p decrease sharply and then become asymptotic. These results are in line with the experimental observations of Wood (1990) and Sherritt et al. (2010). In addition, a similar trend of D_{50} and E_p is also observed for the coal feed rate at the inlet (Figure 5.5).

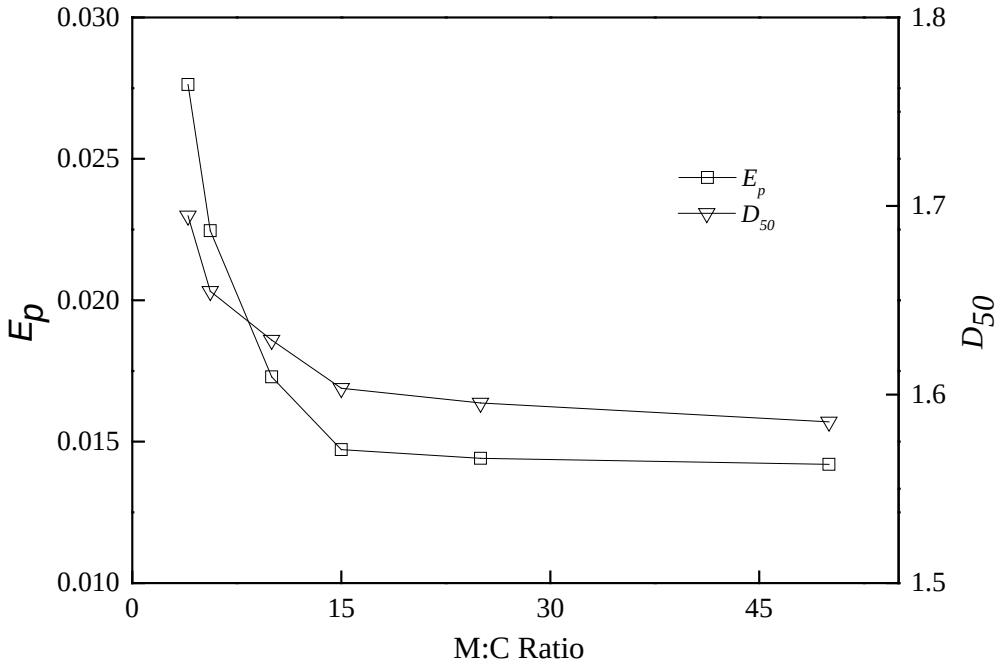

Figure 5.4 DMC performance as a function of M:C ratio.

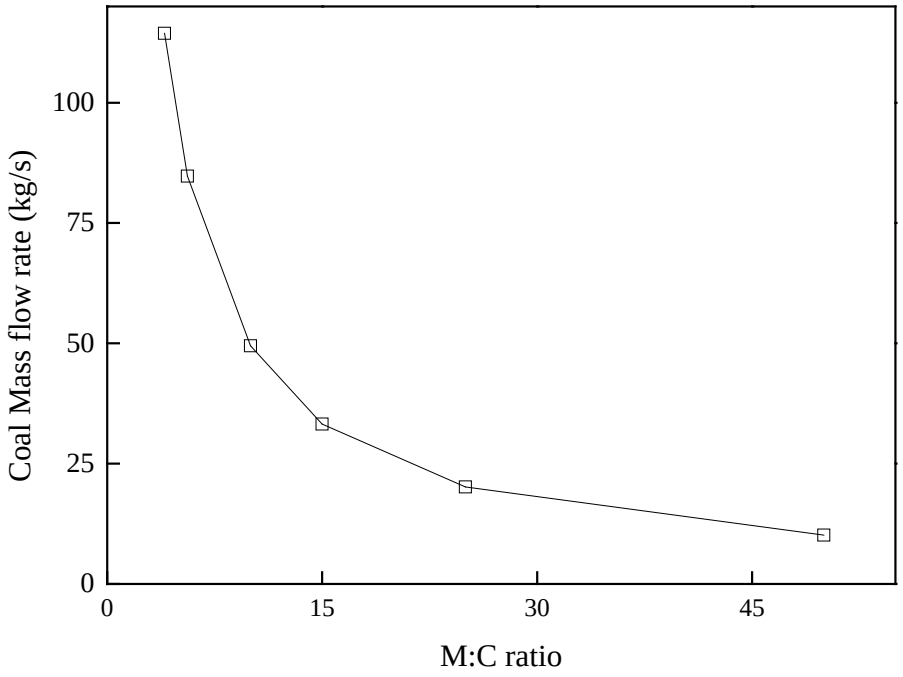

Figure 5.5 Coal feed rate as a function of M:C ratio.

Figure 5.6 shows the representative distributions of pressure drops (defined as the pressure relative to the ambient atmospheric pressure), medium densities, medium tangential and axial velocities, and coal volume fraction on the vertical 2-2 plane at small and large M:C ratios, at which the performance varies significantly. As seen from this figure, when M:C ratio is decreased, the coal volume fraction or amount of coal particles in the cylindrical region increases significantly, similar to those predicted by the CFD-DEM approach (Chu et al., 2009a). However, the medium axial velocities do not change much, particularly for the locus of zero axial velocity (the black line in Figure 5.6), which divides the flow into two parts: the downward (negative) and upward (positive) flows. On the other hand, a smaller M:C ratio leads to increased medium densities, and at the same time, decreased tangential velocities in the entire DMC. Because of the decreased tangential velocities at a smaller M:C ratio, the pressure drops generally decrease, as shown in Figure 5.6. It is known that in a DMC, the separation of

particles is essentially determined by the radial accelerations due to the centrifugal force that throws a particle towards the wall ($= v_t^2 / r$) and the pressure gradient force that moves a particle towards the DMC center ($= \Delta p_r / \rho$). This suggests that smaller tangential velocities and radial pressure drops reduce separation of particles of different densities. It is this case for the operation at a small M:C ratio. On the other hand, when M:C ratio is very large, the variation of M:C ratio leads to negligible variations of medium density, tangential velocity and pressure drop in the DMC. Note that these results are not included in this chapter for brevity. Accordingly, the DMC performance does change significantly when M:C ratio is changed.

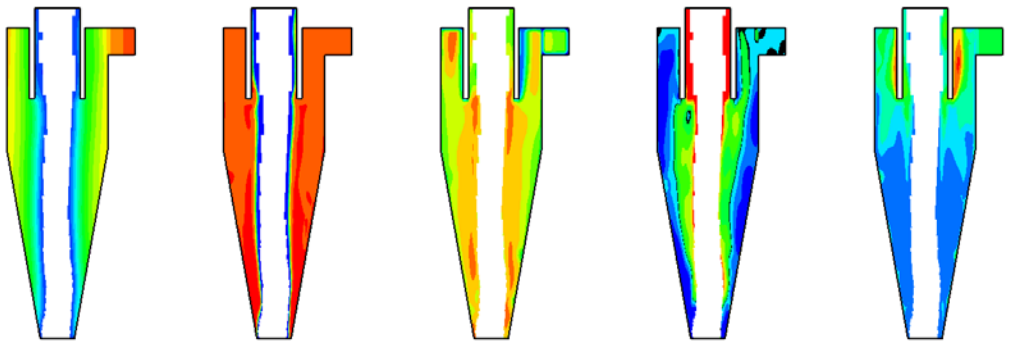

(a)

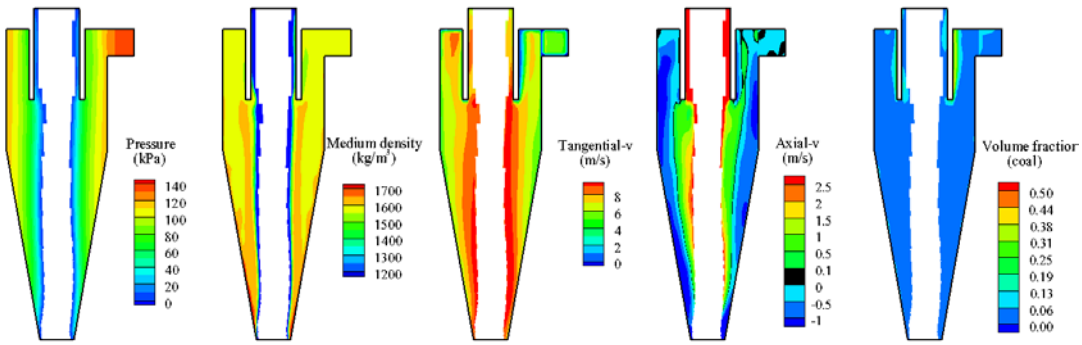

(b)

Figure 5.6 Fluid and solid flow patterns in the base DMC at t = 30 s when: (a) M:C ratio=4, and (b) M:C ratio=15.

5.2.2 Effect of U:O ratio

Diameters of the vortex finder and spigot are interrelated in terms of U:O ratio, however, they are often treated as two individual variables in optimizing cyclone design and operation (Chen et al., 2012; He and Laskowski, 1995). The proposed model is used here to study the relationships among spigot diameter, vortex finder diameter and U:O ratio with respect to DMC flow and performance. For this purpose, within a wide range of U:O ratios, we change one out of the two variables, vortex finder and spigot diameters while the other is fixed at the base case value to achieve the same U:O ratio, when M:C ratio is 5.6 and particle size is 2. 5 mm.

Figure 5.7 shows the predicted partition curves and reveals that the separation efficiency increases with increasing U:O ratio, no matter how the variation of U:O ratio is achieved by changing spigot or vortex finder diameter. Moreover, it is observed that when U:O ratio is larger than 1, the separation efficiencies of relatively light particles, which are supposed to mainly report to the overflow, are fairly large. This is because many of such particles flow with the medium and report to the underflow due to the relatively large spigot diameter. Thus, a large U:O ratio cannot ensure a normal operation, and is not expected in DMC practice. Notably, when U:O ratio is equal to 1 and 1.1, regardless of a fixed vortex finder or spigot diameter, the separation efficiency increases with decreasing particle density beyond a critical particle density. Thus, the partition curve presents a fish-hook shape. It should be pointed out that fish-hook phenomenon is widely observed in hydrocyclones (Majumder et al., 2007; Wang and Yu, 2010), which is however a behaviour in relation to particles of different sizes rather than different densities. Recently, Wang et al. (2010) also observed a fish-hook phenomenon in hydrocyclones similar to that in DMCs.

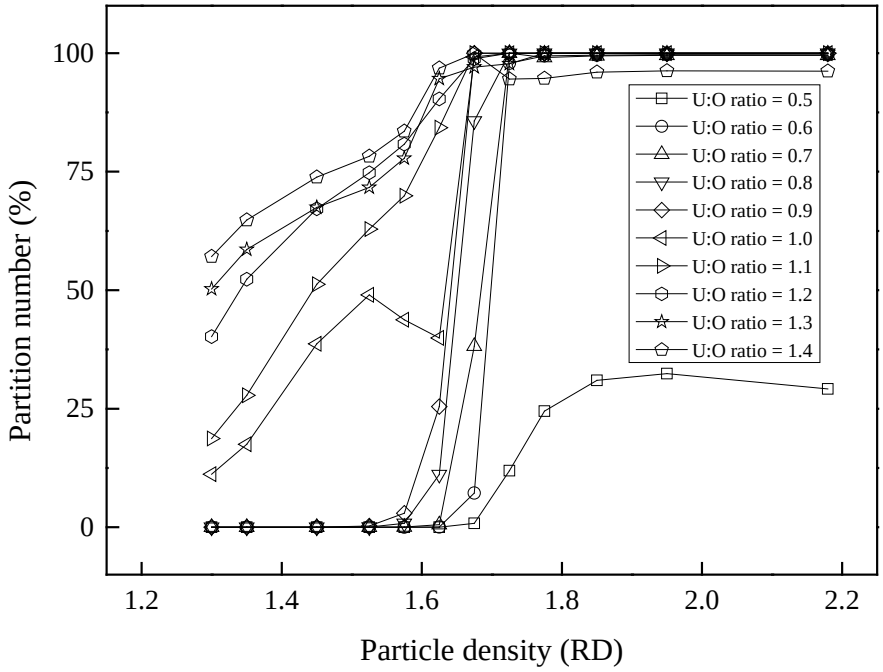

(a)

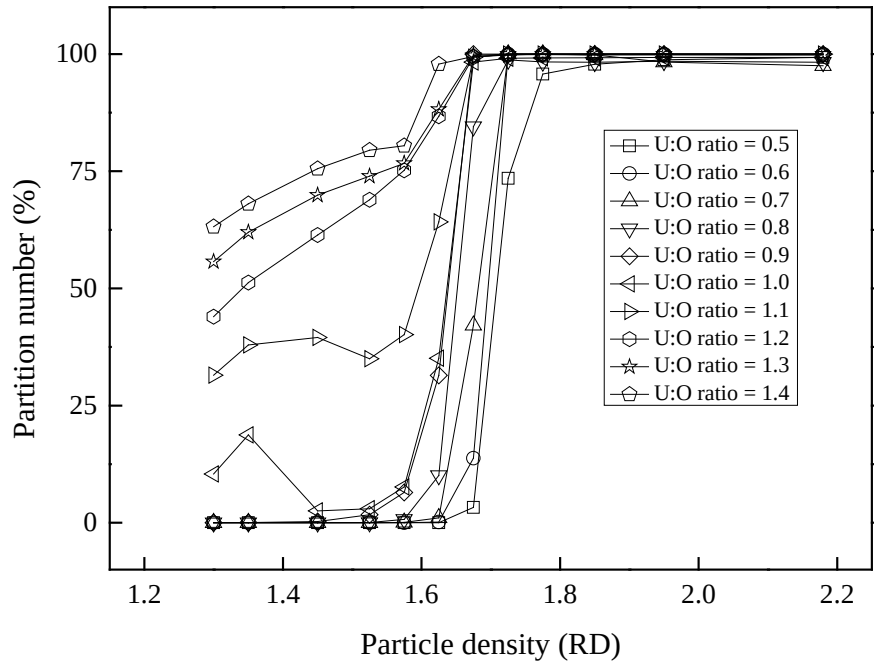

(b)

Figure 5.7 Effect of U:O ratio on partition curve when: (a) D_u=337 mm, and (b) D_o=450 mm.

To explain the fish-hook phenomenon obtained in this study, we examine the details of the flows in the DMCs at different ratios and the key results are given in Figure 5.8. As seen from this figure, under the condition where a fish-hook phenomenon occurs, strongly mixed downward (point A) and upward (point B) flows are developed around the air core in the cylindrical region of the DMC, although an upward flow is supposed to be mainly developed in this region for a normal operation. The downward flow brings light particles to move downwards and report to the underflow, leading to their increased separation efficiencies and thus fish-hook phenomenon. This mechanism is different from that identified for the fish-hook phenomenon in relation to particle size, which is found to be attributed to the significant turbulent dispersion effect of fine particles (Wang and Yu, 2010).

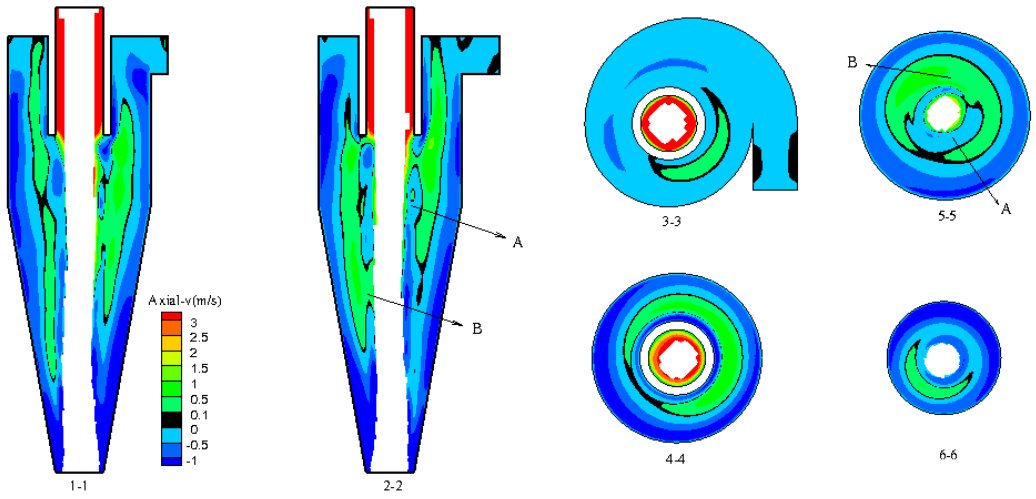

Figure 5.8 Distributions of axial velocities in the DMC at t = 30 s when U:O ratio=1 (D_u=337 mm and D_o=337 mm), corresponding to Figure. 3.5.

Figure 5.9 compares the DMC performance when U:O ratio is varied at a fixed vortex finder or spigot diameter. It is observed that with increasing U:O ratio, E_p increases (Figure 5.9a), and at the same time, the off-set (=D_{50}-ρ_m, where ρ_m is medium density)

and medium split decrease (Figure. 5.9b and 5.9c). This result is in line with the experimental observations of DMC (He and Laskowski, 1995). Moreover, the last two performance parameters are largely the same at both fixed spigot and vortex finder diameters, whereas E_p at a fixed vortex finder diameter is generally larger. On the other hand, when U:O ratio is increased, the coal feed rate increases at a fixed vortex finder diameter but decreases at a fixed spigot diameter (Figure 5.9d). Note that the operations where the separation efficiency of the lightest particles is too large, are not included in Figures 5.9 (a) and (b), because their E_p and/or off-set cannot be determined by definition.

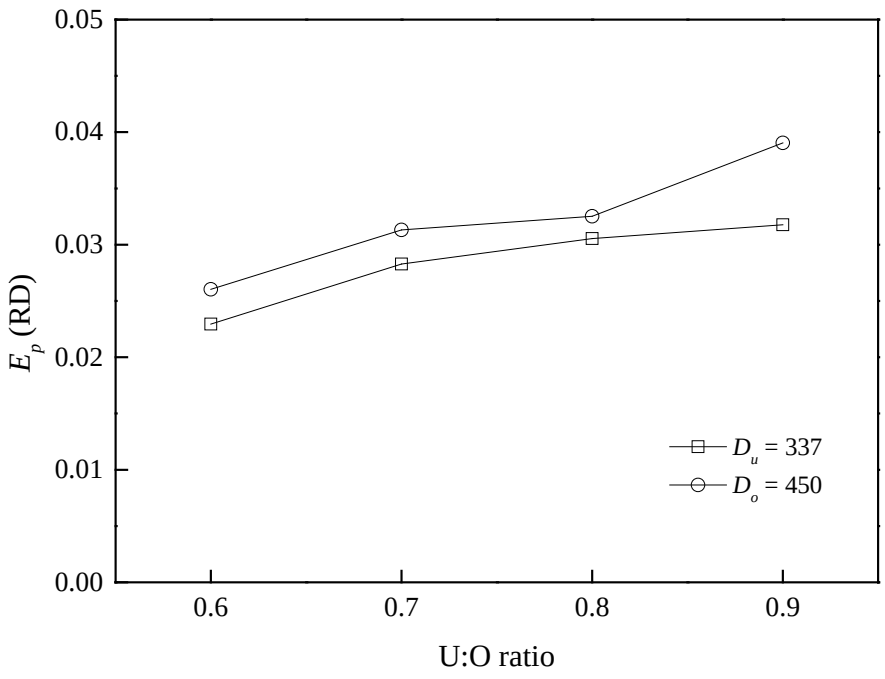

(a)

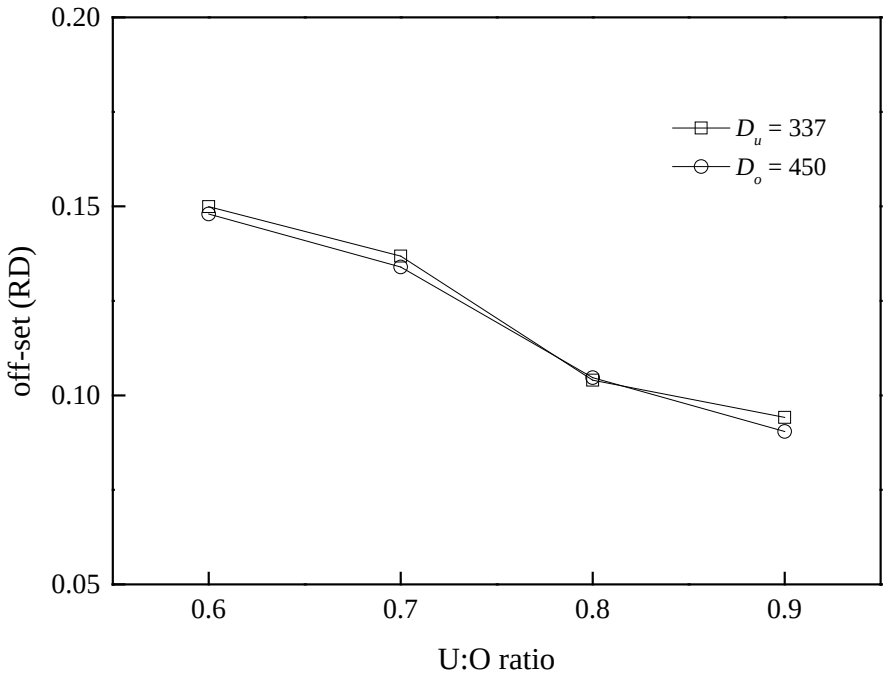
0.20
0.15
0.10
0.05
off-set (RD)
0.6
0.7
0.8
0.9
U:O ratio
D_u = 337
D_o = 450

(b)

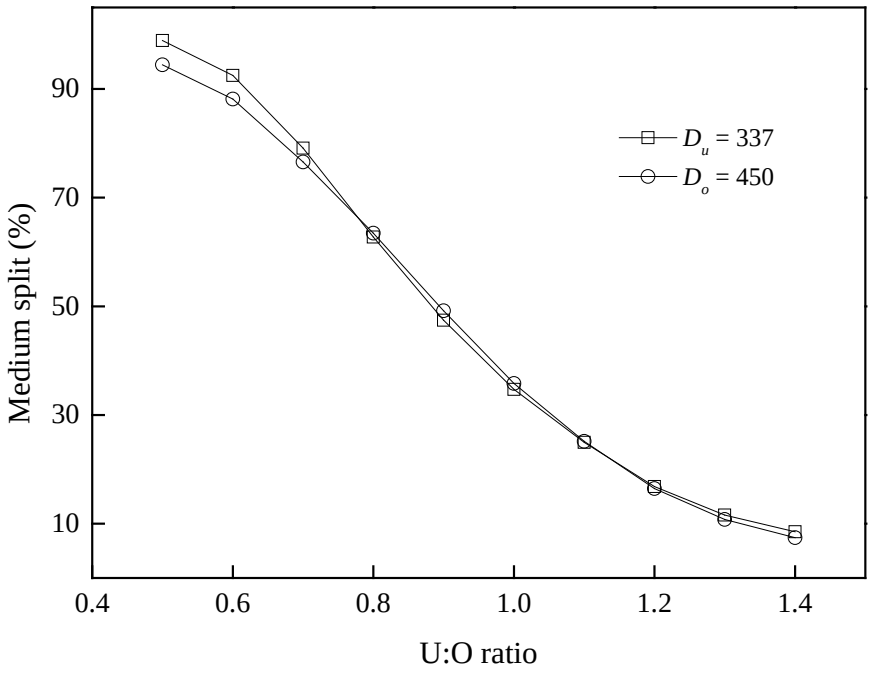
90
70
50
30
10
Medium split (%)
0.4
0.6
0.8
1.0
1.2
1.4
U:O ratio
D_u = 337
D_o = 450

(c)

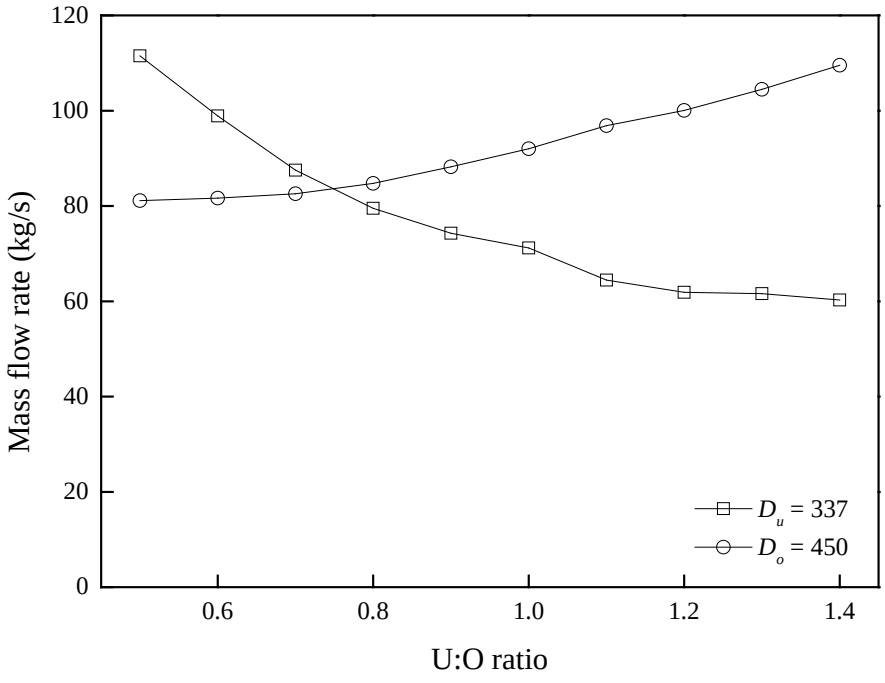

(d)

Figure 5.9 Effect of U:O ratio on DMC performance: (a) E_p, (b) off-set, (c) medium split, and (d) coal feed rate.

Figure 5.10 shows the representative distributions of flow properties on the vertical 2-2 plane at small and large U:O ratios, including pressure drop, medium density, medium tangential and axial velocities, and coal volume fraction. It can be seen from this figure that at a larger U:O ratio, the pressure drops, coal volume fraction, and medium densities in the DMC are generally increased, particularly in the upper region. This increased pressure drop is not expected at high throughputs, but raises the possibility for light (coal) particles to move to the DMC centre. Conversely, the tangential velocities in the upper region are generally smaller at a larger U:O ratio, leading to deteriorated DMC separation performance. Moreover, in the DMC with a larger U:O ratio, a proportion of the feed medium passes directly across the cyclone roof and down the outside wall of the vortex finder to join the overflow stream within the vortex finder,

which represents a short circuit flow (point A in Figure 5.10b). Furthermore the recirculating currents known as eddy flows in the region between the outer wall of vortex finder and wall of body (point B in Figure 5.10b) are also developed. All these features of the tangential and axial velocities explain why a larger U:O ratio leads to an increased E_p.

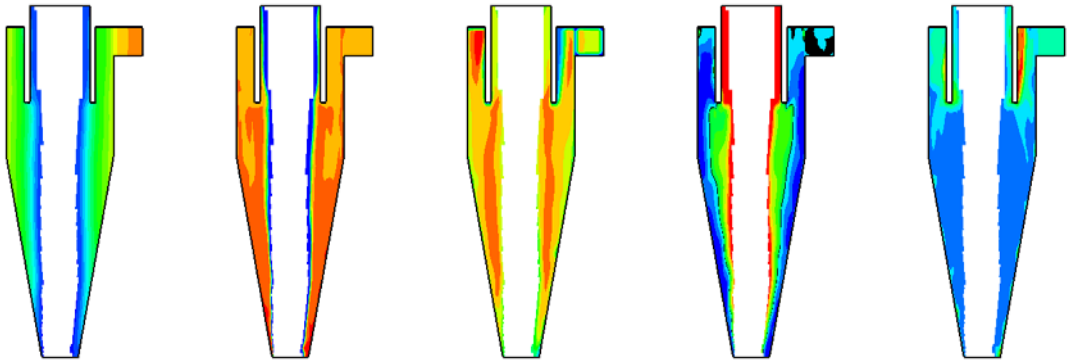

(a)

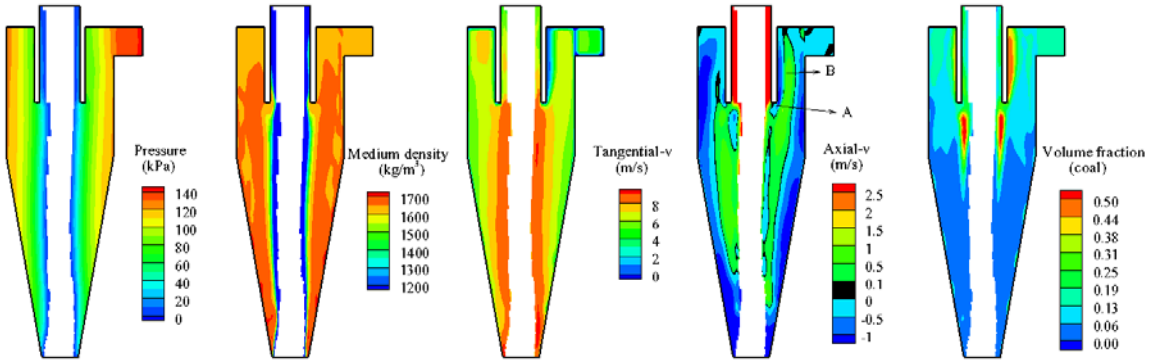

(b)

Figure 5.10 Fluid and solid flow patterns in the DMC at t = 30 s when: (a) U:O ratio=0.6 (D_u=337 mm and D_o=561 mm), and (b) U:O ratio=0.9 (D_u=337 mm and D_o=374 mm).

Figure 5.10 also shows that the upward axial velocities in the spigot region are stronger at a smaller U:O ratio and thus the rejects are more difficult to move out of the spigot.

Consequently, such particles may accumulate in the spigot region, and go down with the help of gravity till a certain amount is reached. This leads to significant fluctuation of mass flow at the underflow, which is reflected in the results shown in Figure 5.11. It can be seen from this figure that the mass flow rate fluctuates more significantly with increasing U:O ratio, even when the operations considered are regarded as normal according to Figure 5.7. This suggests that the operation at a smaller U:O ratio may be more stable. In addition, it is noted that mixed downward and upward flows (see the axial velocity distribution in Figure 5.10) around the air core in the cylindrical region are observed at U:O ratio=0.9. However, in this case, the upward flow dominants, and a fish-hook phenomenon is thus not observed.

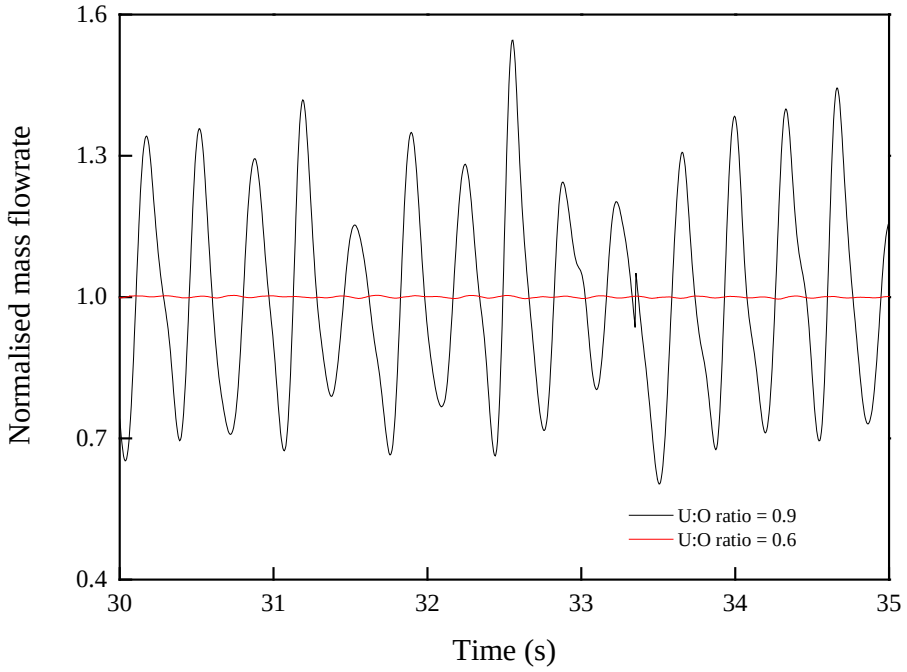

Figure 5.11 Temporal variation of mass flow rate at the underflow when D_u=337 mm.

5.3 Large diameter dense medium cyclone

5.3.1 Comparison between large size DMC and standard DMC

Large diameter dense medium cyclones are known to have the problems of density shift and the cut density of the finer particles being higher than that of the larger particles. To verify these phenomena, a comparison between a 2000 mm and 1000 mm DMCs was done using the present model. In this comparison test, the only variable is the cyclone size, all other operational conditions in two case, like the Head, M:C ratio and density distribution, are the same. It should be noted that to keep the mesh cell same size as standard DMC, the mesh of 2000 mm DMC consists of 169587 hexahedral grids.

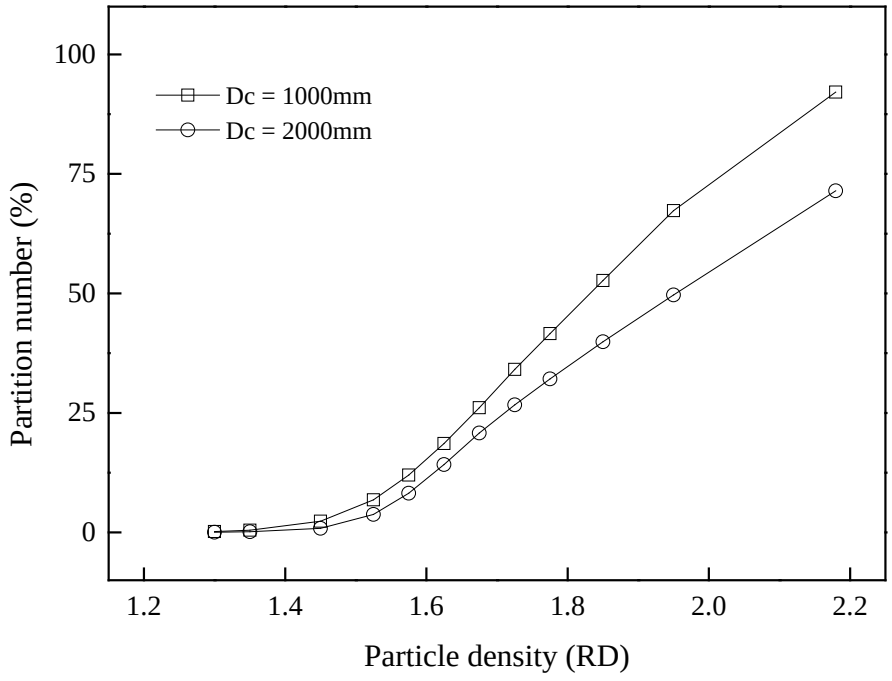

(a)

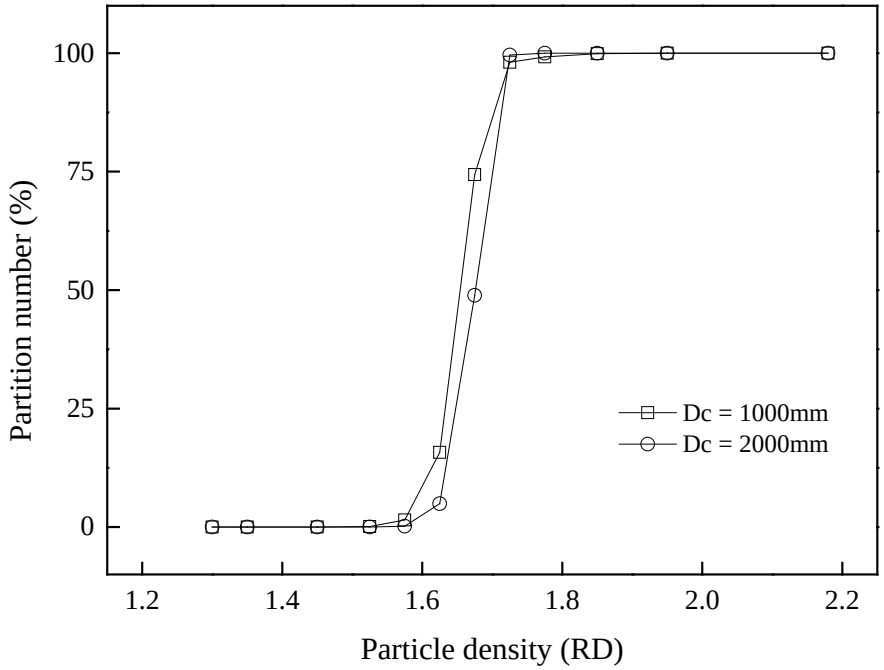

(b)

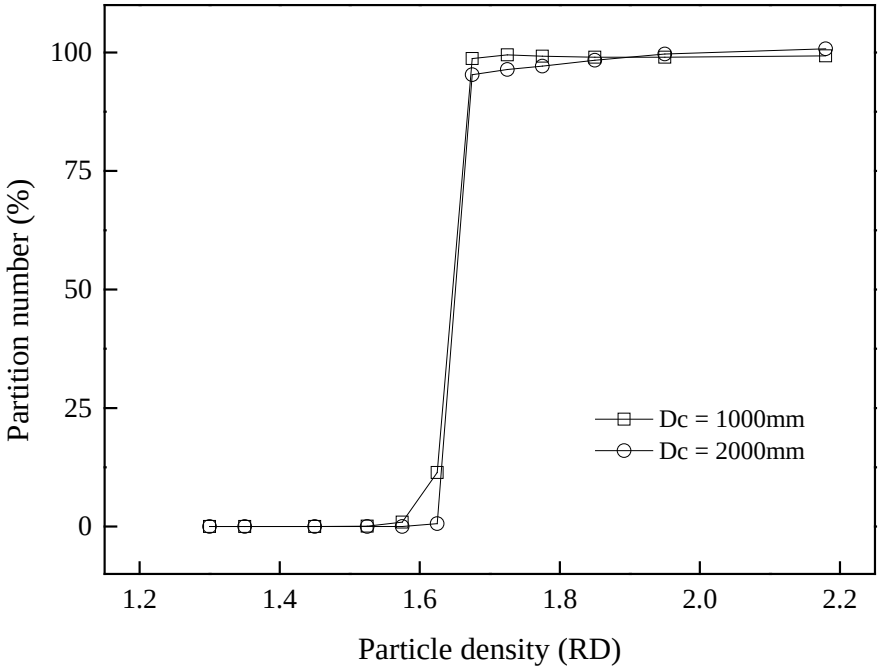

(c)

Figure 5.12 Comparison of the partition curves for different sized particles in 1000 mm and 2000 mm DMCs: (a) 0.5 mm, (b) 2.0 mm, and (c) 7.0 mm.

Figure 5.12 compares the partition curves for different sized particles in 1000 mm and 2000 mm DMCs. It reveals that the cyclone size does affect the separation efficiency of DMCs. In particular for fine particles, the separation is much poorer in DMCs of large diameter. More particles reported to the vortex finder as the particle size decreases. To have a clearer view of the problem of large size DMC, a comparison of the performance of 1000 mm and 2000 mm DMCs with different sized particles is given in Figure 5.13. It can be seen from Figure 5.13(a), for all three sizes of particles, E_p is larger in the 2000 mm DMC and the difference of E_p between 1000 mm and 2000 mm DMCs is the biggest for 0.5 mm particles. In Figure 5.13(b), the phenomenon of the density shift and D_{50} of the finer particles being higher than that of the larger particles can be observed. Specifically, the cut density differential between 0.5 mm and 2.0 particles is around 1.8 in the 1000 mm DMC, while this differential rises to 2.8 in the 2000 mm DMC.

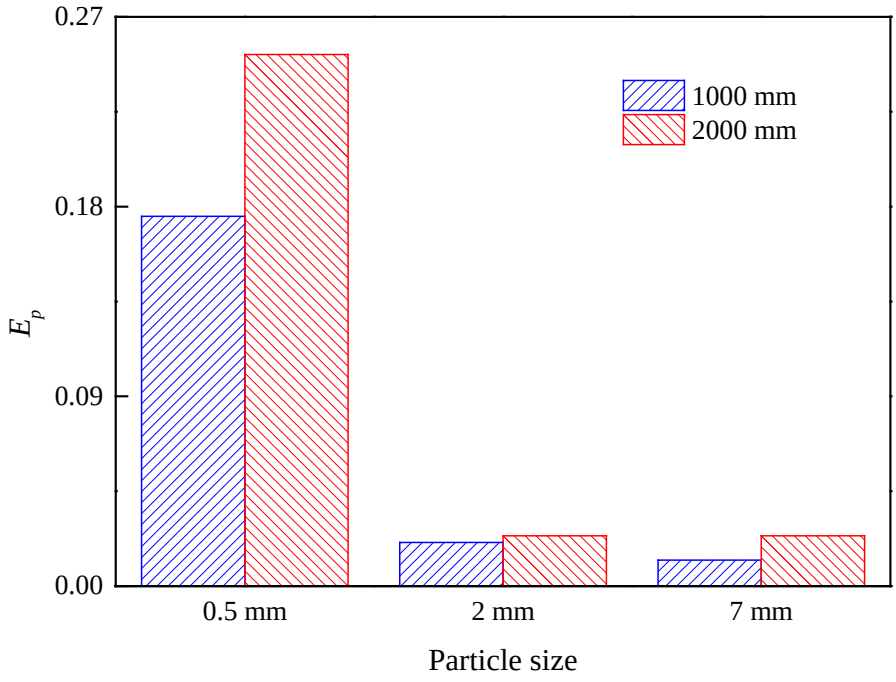

(a)

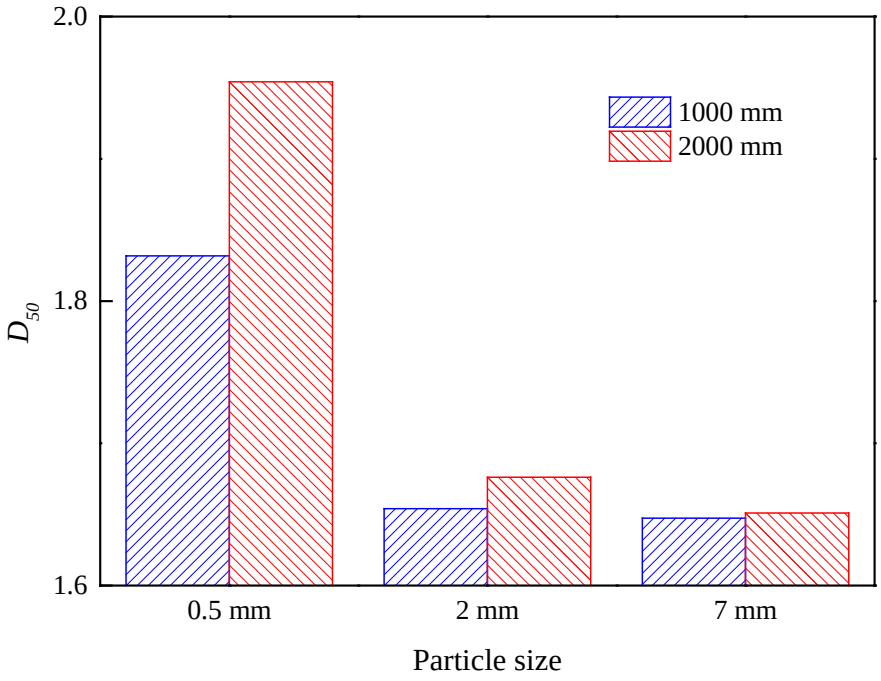

(b)

Figure 5.13 Comparison of the performances of 1000 mm and 2000 mm DMCs using different sized particles: (a) E_p, and (b) D_{50}.

To explain the separation deterioration for fine particles in a large diameter DMC, the details of flow properties are examined (in Figure 5.15) and the key reason of this phenomenon is given in Figure 5.14. As seen from this figure, the upward and downward flows in the large diameter DMC are stronger than that of the standard size DMC. Particularly, at point A, it can be seen that the range of upward flow in the 2000 mm DMC is larger which will lead to a stronger "short-circuit". The upward flow at point A will carry particles to join the short-circuit eddies, which then move particles downward along the outer wall of the vortex finder, finally reporting to the overflow. According to Wang (2009), the formation of a "short-circuit" is due to the presence of the cyclone cover and the outer wall of the vortex finder, which slow down the spin velocity in their immediate vicinity and thus providing areas of lower resistance to flow

from the outer regions where the pressure is high to the inner regions where the pressure is lower. As the Head for both cyclones are the same, the pressure drop of the 2000 mm DMC is about twice that of the 1000 mm DMC. This means the short-circuit is much stronger in large diameter dense medium cyclones and easier to form due to the longer distance between the cyclone cover and the outer wall of the vortex finder.

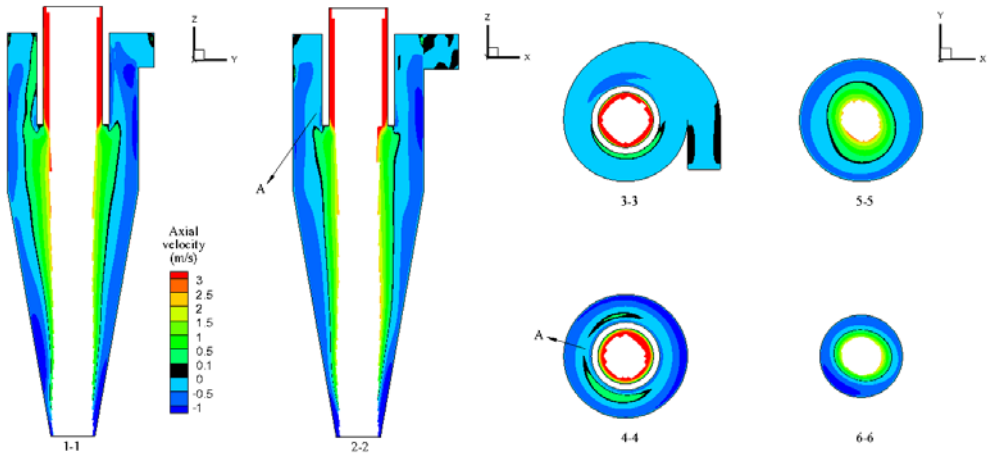

(a)

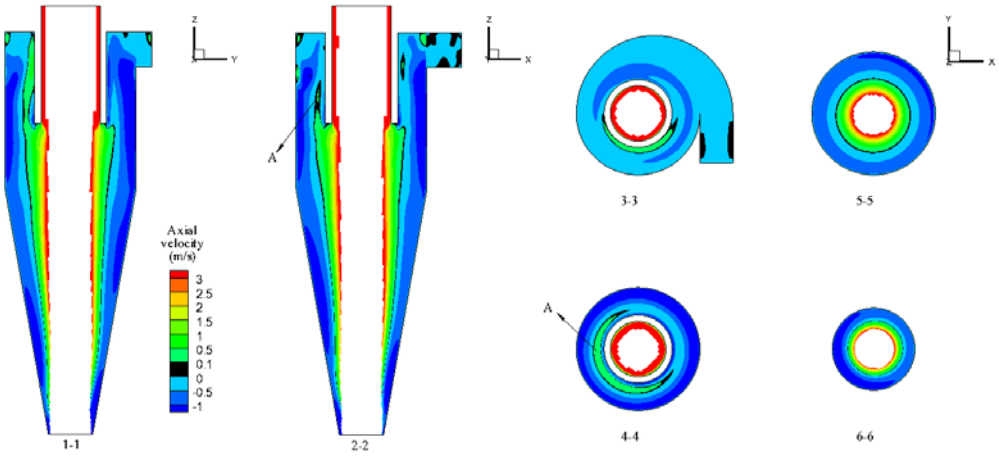

(b)

Figure 5.14 Distribution of axial velocities in DMCs of different sizes at t = 30 s: (a) 1000 mm DMC, and (b) 2000 mm DMC.

Figure 5.15 shows the representative distributions of flow properties on the vertical 1-1 plane, including the pressure gradient, tangential velocity, radial velocity, axial velocity, radial acceleration, the ratio of pressure gradient and radial acceleration, medium density and coal volume fraction in 1000 mm and 2000 mm DMCs. It should be noted that the ratio of pressure gradient and radial acceleration can give a clearer picture of the direction of particles movements. It is known that in a DMC, the separation of particles is essentially determined by the radial accelerations due to the centrifugal force that throws particles towards the wall ($=v_t^2/r$) and the pressure gradient force that moves particles towards the DMC centre ($=\Delta p_r/\rho$). When the ratio of the pressure gradient and centrifugal acceleration ($=\Delta p_r \cdot r/v_t^2$) is higher than the particle density ($=\rho$), the pressure gradient force is larger than the centrifugal force, which will push particles towards the DMC centre. On the contrary, when the ratio is smaller than the particle density, particles will be thrown to the wall. As seen in Figure 5.15, the ratio distribution of pressure gradient and ratio acceleration in the middle part of both DMCs is asymmetric. This means the separation of fine particles is more difficult than coarse particles because fine particles tend to be affected by viscous drag force more easily. This phenomenon is caused by the asymmetry of dense medium cyclone structure design. Despite this, we can also see from Figure 5.15 that the tangential and axial velocities in the large diameter DMC is higher, which increases the capacity of dense medium cyclone. The details of mass flow rate for both DMCs are given in Table 5.1. It can be seen that the mass flow rate of the 2000 mm DMC is more than 4 times that of the 1000 mm DMC.

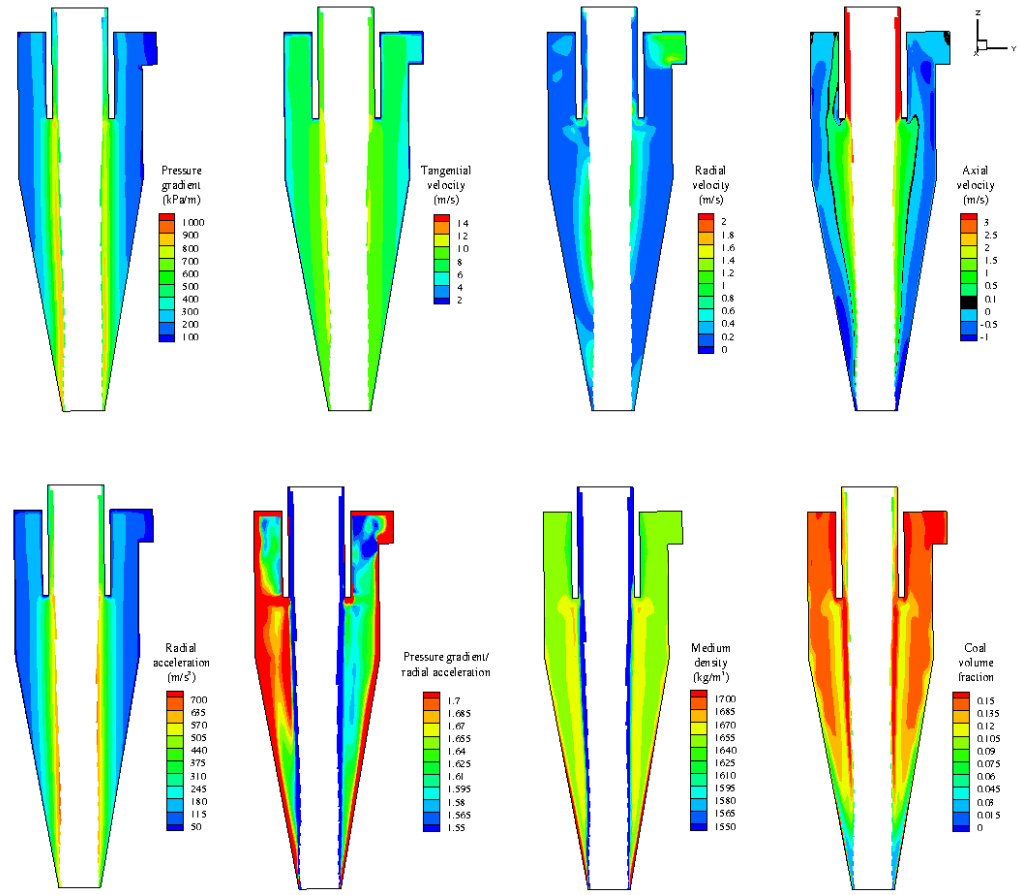
Pressure gradient (kPa/m)
1000
900
800
700
600
500
400
300
200
100
Tangential velocity (m/s)
14
12
10
8
6
4
2
Radial velocity (m/s)
2
1.8
1.6
1.4
1.2
1
0.8
0.6
0.4
0.2
0
Axial velocity (m/s)
3
2.5
2
1.5
1
0.5
0.1
0
-0.5
-1
Radial acceleration (m/s²)
700
685
570
505
440
375
310
245
180
115
50
Pressure gradient/ radial acceleration
1.7
1.685
1.67
1.655
1.64
1.625
1.61
1.595
1.58
1.565
1.55
Medium density (kg/m³)
1700
1685
1670
1655
1640
1625
1610
1595
1580
1565
1550
Coal volume fraction
0.15
0.135
0.12
0.105
0.09
0.075
0.06
0.045
0.03
0.015
0

(a)

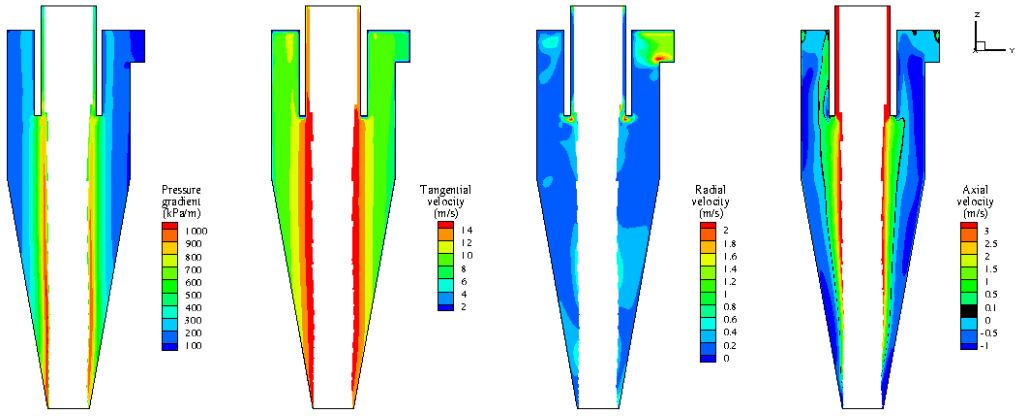
Pressure gradient (kPa/m)
1000
900
800
700
600
500
400
300
200
100
Tangential velocity (m/s)
14
12
10
8
6
4
2
Radial velocity (m/s)
2
1.8
1.6
1.4
1.2
1
0.8
0.6
0.4
0.2
0
Axial velocity (m/s)
3
2.5
2
1.5
1
0.5
0.1
0
-0.5
-1

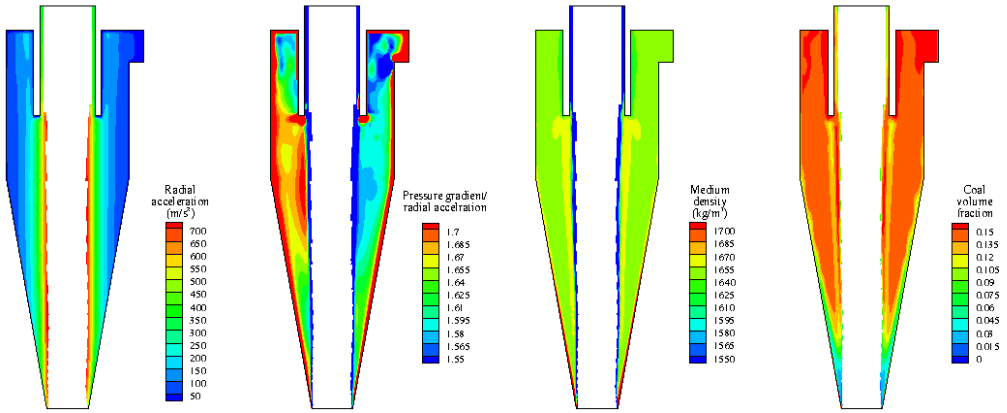

(b)

Figure 5.15 Fluid and solid flows for 0.5 mm particles in different DMCs at = 30 s: (a) 1000 mm DMC, and (b) 2000 mm DMC.

Table 5.1 Comparison of the medium and coal mass flow rates of the 1000 mm and 2000 mm DMCs.

	1000 mm DMC	2000 mm DMC
Medium feed rate (kg/s)	564.564	2484.38
Coal feed rate (kg/s)	84.6079	381.818

5.3.2 Effect of M:C ratio

The effect of M:C ratio on standard DMC's performance has been discussed previously (Kuang et al., 2014). However, this effect is still unclear for large diameter DMCs. This section will examine the extent to which the M:C ratio can improve the performance of a large size DMC, especially for the separation of fine particles.

Figure 5.16 shows the partition curves of different sized particles at different M:C ratio for the 2000 mm DMC. For brevity, the partition curves of coarse particles are not listed here. It can be seen that the trend of effects of particle size on the 2000 mm DMC performance is similar to that of the 1000 mm DMC. To have a clearer view of the effects, the curves of Ecart probable and cut density are given in Figure 5.17. Both D_{50} and E_p decrease sharply and then become asymptotic, and so is the cut density differential (Figure 5.18). The extent of the improvement is also similar for 0.5 mm particles and 2.0 mm particles.

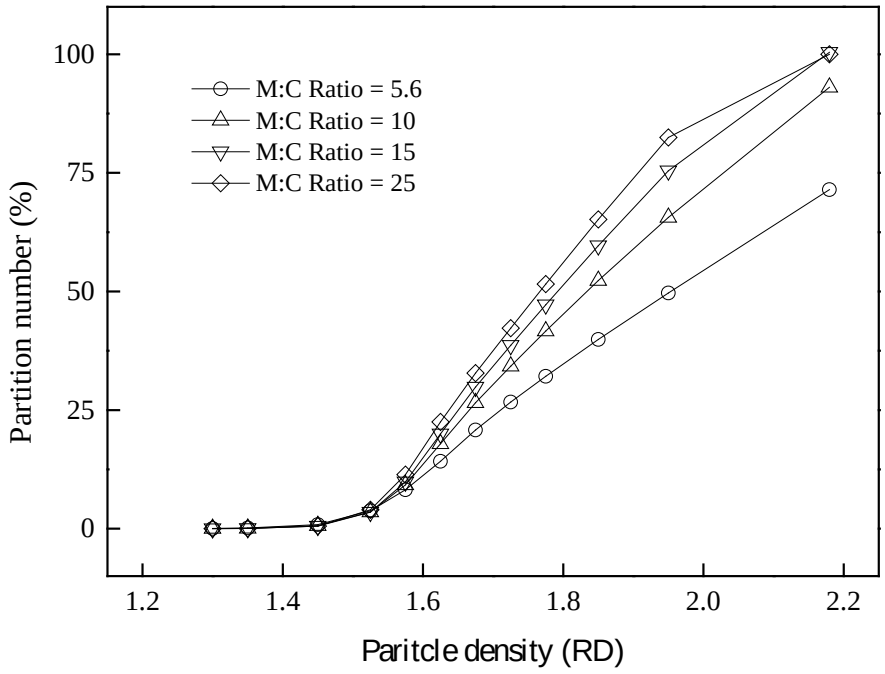

(a)

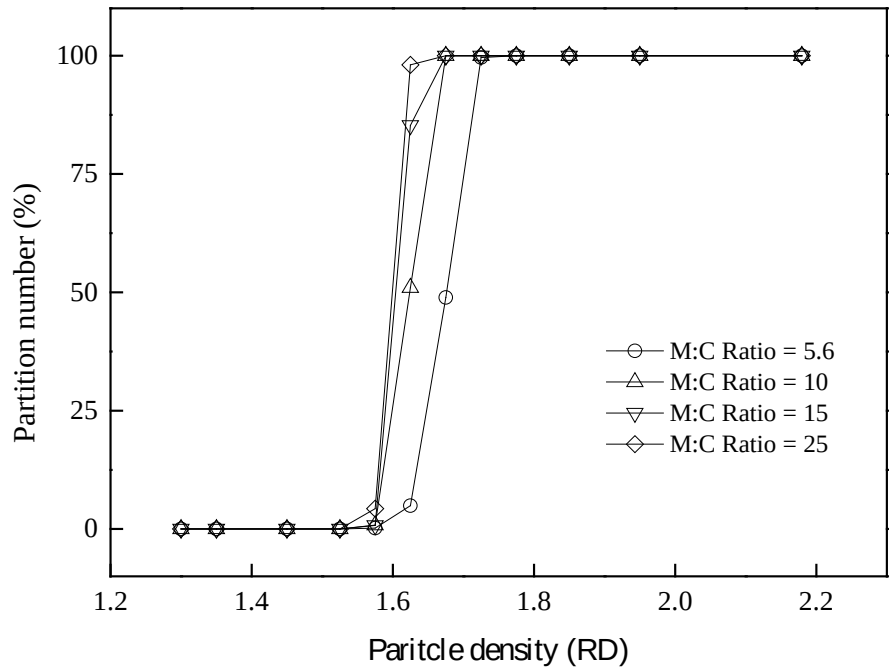

(b)

Figure 5.16 Effect of M:C ratio on partition curves of the 2000 DMC for different sized particles: (a) 0.5 mm, and (b) 2.0 mm.

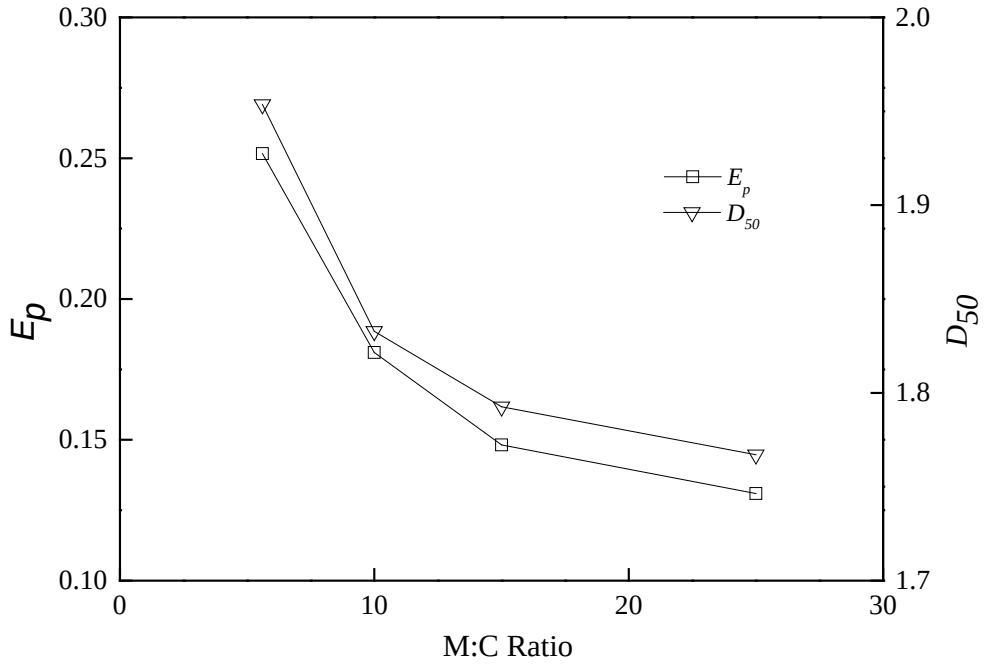

(a)

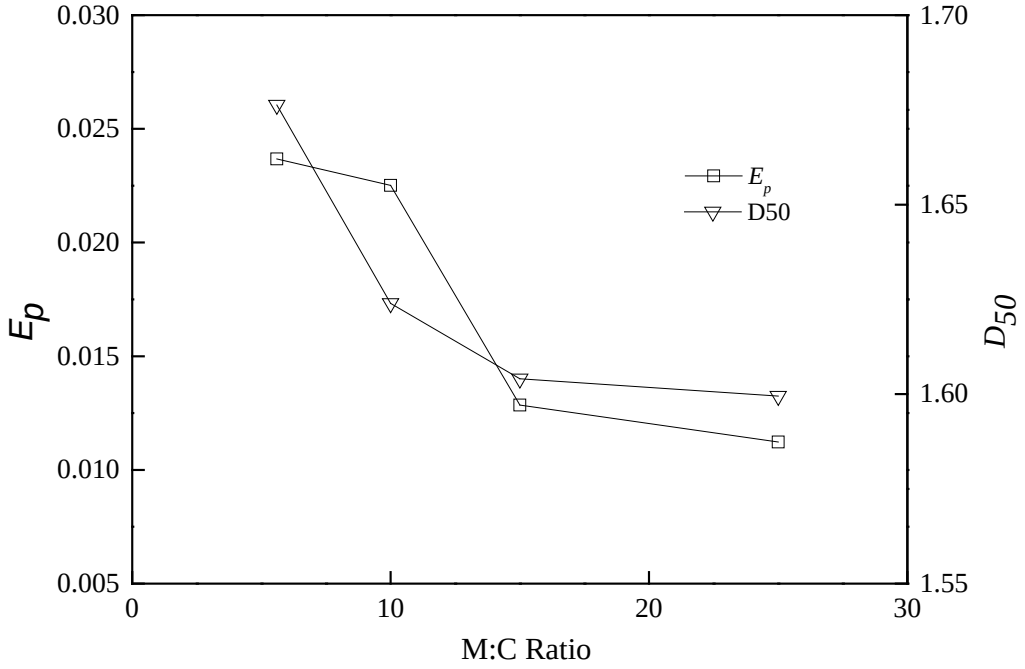

(b)

Figure 5.17 Performance of the 2000 mm DMC as a function of M:C ratio for different sized particles: (a) 0.5 mm, and (b) 2 mm.

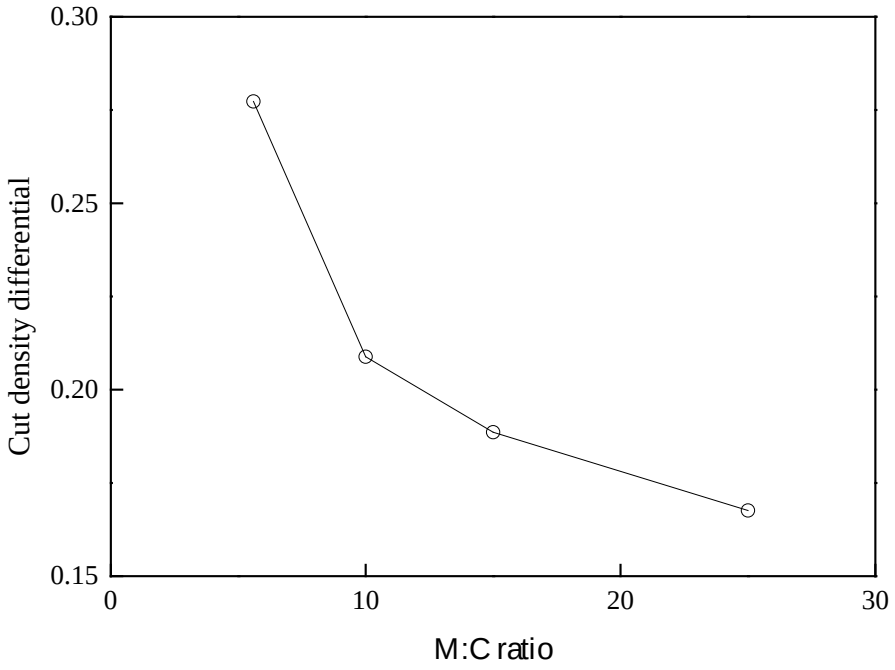

Figure 5.18 Cut density differential between 0.5 mm and 2.0 mm particles as a function of M:C ratio.

Figure 5.19 shows representative distributions of the flow properties on the vertical 1-1 plane for 0.5 mm particles at M:C ratio =15, including pressure gradient, tangential velocity, radial velocity, axial velocity, radial acceleration, the ratio of pressure gradient and radial acceleration, medium density and coal volume fraction. As seen from this figure, the velocity profile of the DMC does not change much compared to Figure 5.15(b). The medium density is lower as the M:C ratio decreases. This will lead to a lower viscous force which contributes to a better separation efficiency, especially for fine particles. In addition, a lower medium density causes the cut density to decrease for both fine and coarse particles.

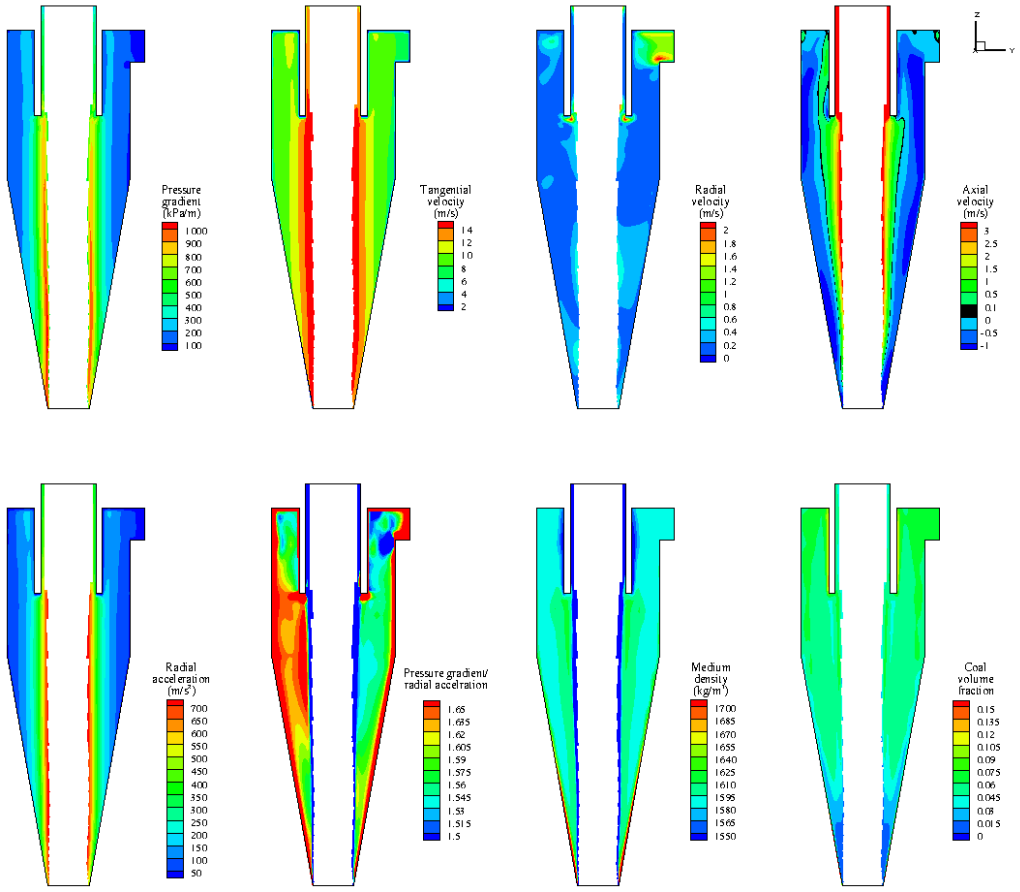

Figure 5.19 Fluid and solid flow patterns in DMC for 0.5 mm particles at t = 30 s when M:C ratio is 15.

5.3.3 Effect of Head

Head is an important factor in DMC operation. This variable is always related to feed flow rate. It has been well known that as the Head increases, the feed flow rate increases. The effect of Head on DMC performance has also been studied by Mukherjee et al. (2003) and Muzenda et al. (2012). Their studies show that Head can improve the performance of small DMCs. However, information on the effect of Head on separation efficiency of different sized particles in large diameter DMCs has been scarce up to now. In this section, we conduct a series of numerical experiments varying the Head in a wide range to study the effect on the separations of different sized particles.

Figure 5.20 shows the predicted partition curves of different sized particles under different values of the Head. For brevity, the partition curves of coarse particles are not shown as they are almost not affected by the Head. It can be seen that the separation efficiency for both 0.5 mm and 2.0 mm particles each is improved as the Head increases. In particular, for 0.5 mm particles, the partition number of coal particles at 2.0 (RD) can reach 100% when Head = 66.4, while this number is only 50% for the base case. Interestingly, the cut density shift shows a different trend for the two particle sizes. Specifically, the partition curve of 0.5 mm particles shifts to left while that of 2.0 mm particles shifts to the right.

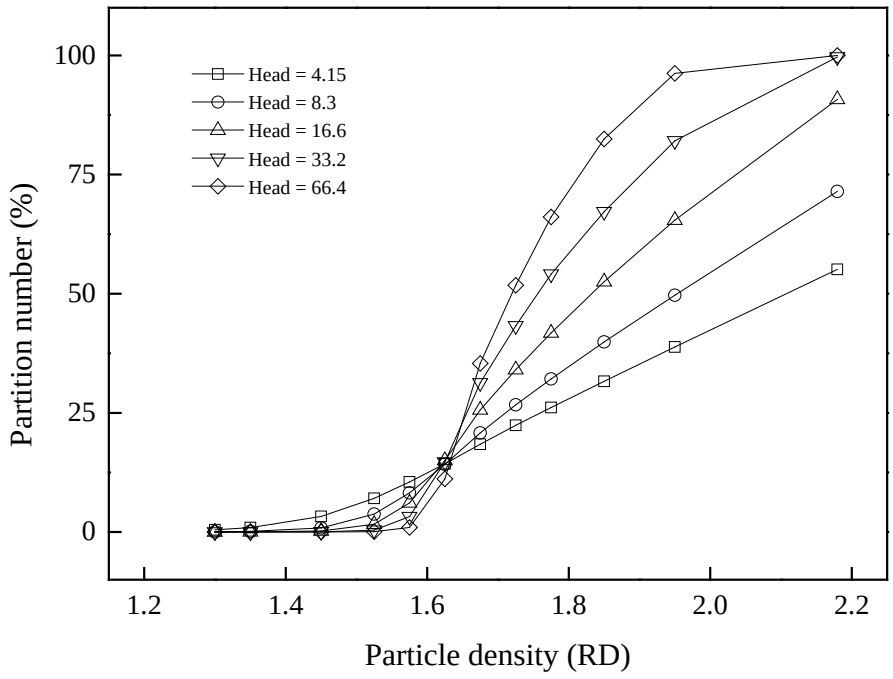

(a)

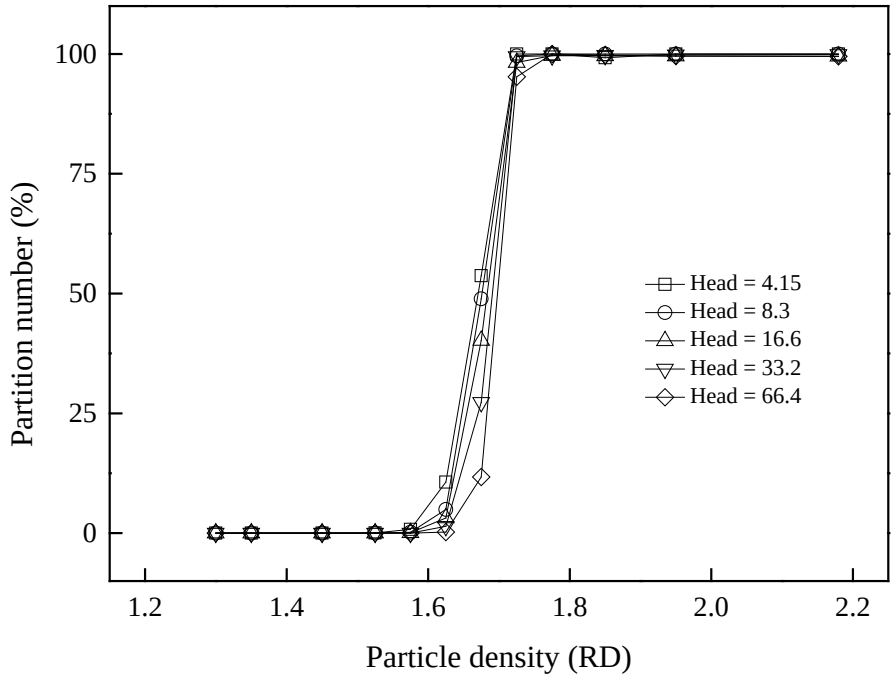

(b)

Figure 5.20 Effect of Head on different partition curves for different sized particles in the 2000 mm DMC; (a) 0.5 mm, and (b) 2.0 mm.

Figure 5.21 presents the effect on DMC performance of different sized particles. For E_p, particles of both sizes show the similar trends: namely, decreasing sharply and then becoming asymptotic. On the other hand, the trend of D_{50} is different. To be specific, the cut density differential between 0.5 mm and 2.0 mm particles decreases as the Head increases (as shown in Figure 5.22). This is a good enhancement for the large diameter DMC, because large cut density differential means more rejects in the product.

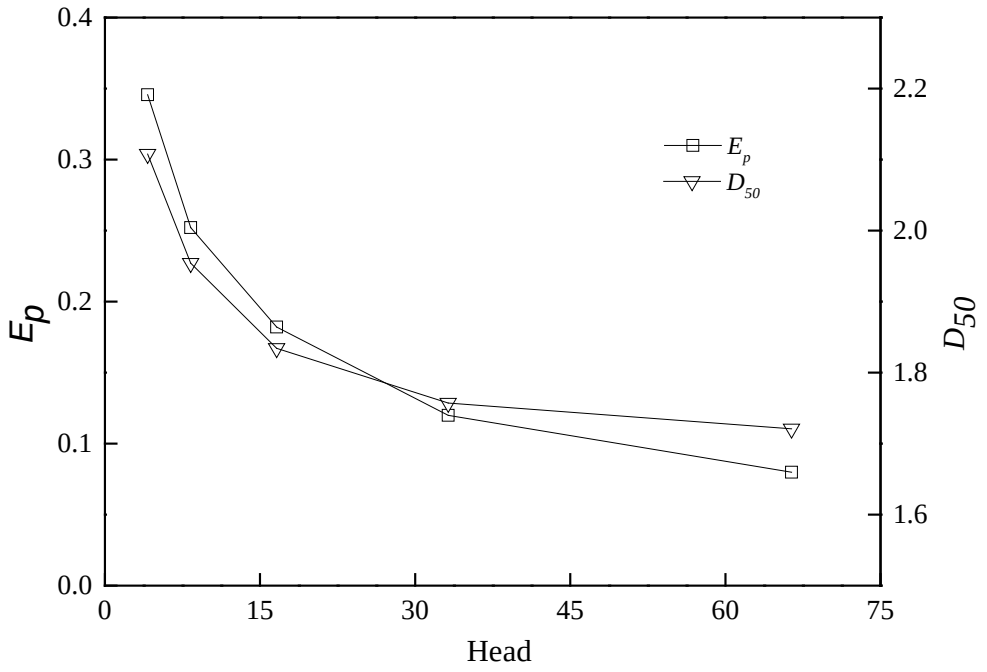

(a)

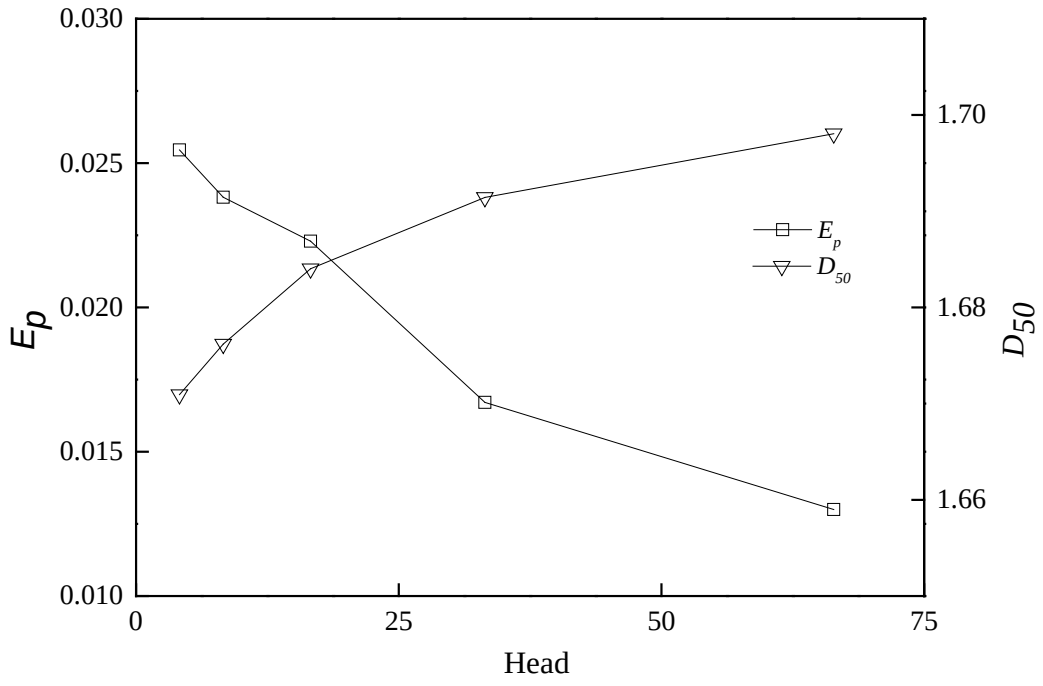

(b)

Figure 5.21 Performance of the 2000 mm DMC as a function of Head for different sized particles: (a) 0.5 mm, and (b) 2 mm.

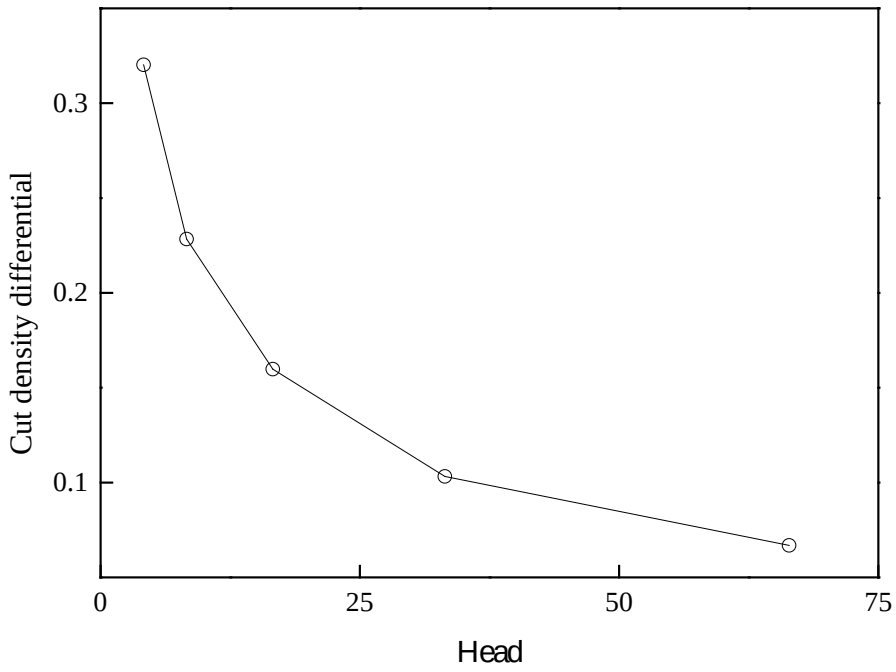

Figure 5.22 Cut density differential between 0.5 mm and 2.0 mm particles as a function of Head.

To explain the effect of Head, distributions of flow properties on the vertical 1-1 plane for 0.5 mm particles at two different Heads are given in Figure 5.23, including pressure gradient, tangential velocity, radial velocity, axial velocity, radial acceleration, the ratio of pressure gradient and radial acceleration, medium density and coal volume fraction. It can be seen that velocity of fluid flow in the DMC is much higher when Head is 66.4. As a result, the problem of DMC asymmetry is alleviated as shown in Figure 5.23 (b) (i.e., the distribution ratio of pressure gradient to radial acceleration is much more symmetrical), which leads to a much better separation efficiency for fine particles. Also, the cut density of fine particles is more close to the medium density due to this improvement. On the other hand, the medium density in Figure 5.23 (b) is higher than that of (a). This difference can explain why the cut density of 2.0 mm particles increases with the Head increasing. Besides, high velocity contributes to a high flow rate as

shown in Figure 5.24. This result is in line with the previous experimental observations on DMCs (Mukherjee et al., 2003; Muzenda et al., 2012; Napier-Munn, 1986).

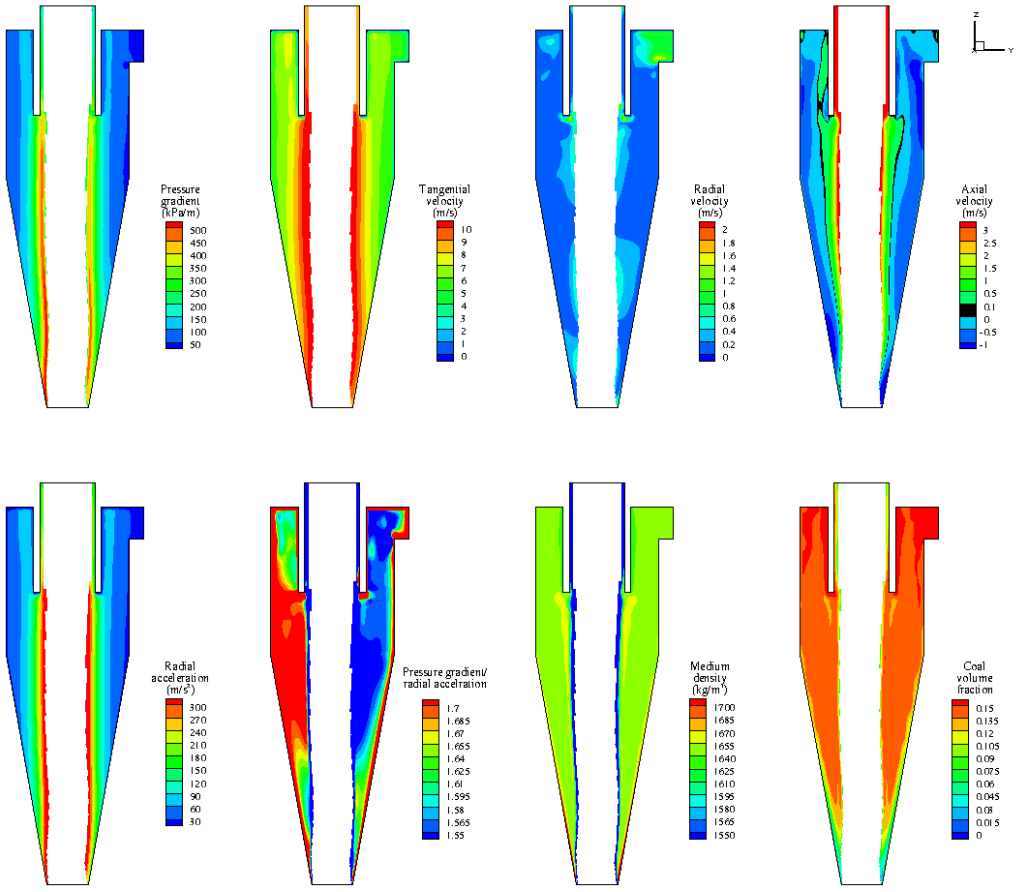

(a)

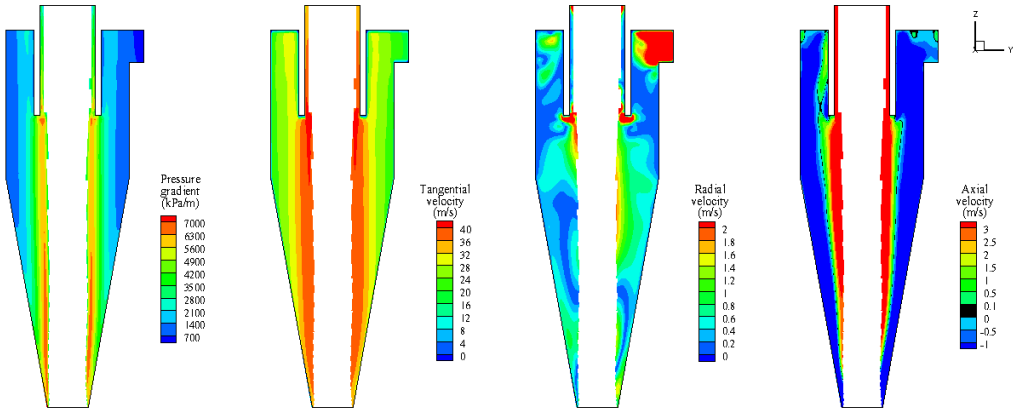

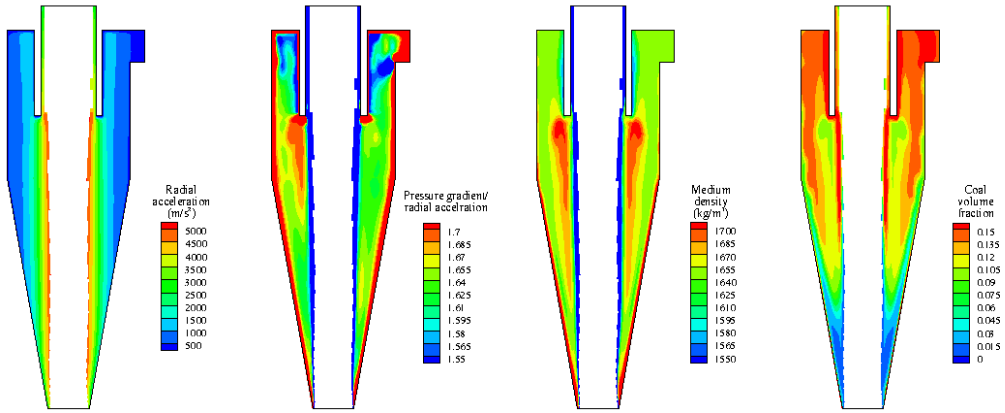

(b)

Figure 5.23 Fluid and solid patterns for 0.5 mm particles in the 2000 mm DMC at t = 30 s when: (a) Head = 4.15 D_c, and (b) Head = 66.4 D_c.

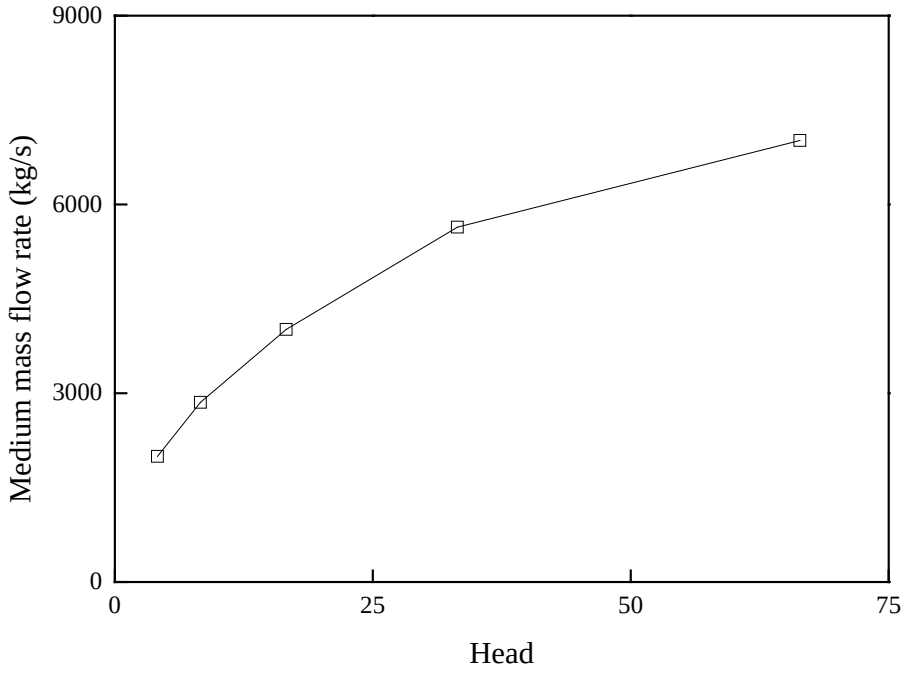

Figure 5.24 Medium mass flow rate as a function of Head in the 2000 mm DMC

While a higher Head improves the general performance of a DMC, some other problems are also observed. Figure 5.25 presents the distribution of 2.00 mm coal particles at 2.179 (RD) on the DMC wall at different Head. As shown in this figure, the distance of

trajectory for heavy particles is longer and clearer when Head = 66.4 D_c. Considering the effect of Head on particles velocity, the wear rate will be high. In addition, it should be noted that rejects tend to accumulate in the spigot region with increasing Head. This is because the upward axial velocities in the spigot region are stronger at high Head, and the rejects are more difficult to move out of the spigot. Consequently, such particles may accumulate in the spigot region, and go down with the help of gravity until a certain amount is reached. This leads to significant fluctuation of mass flow at the underflow, which can be seen from the results shown in Fig. 5.26.

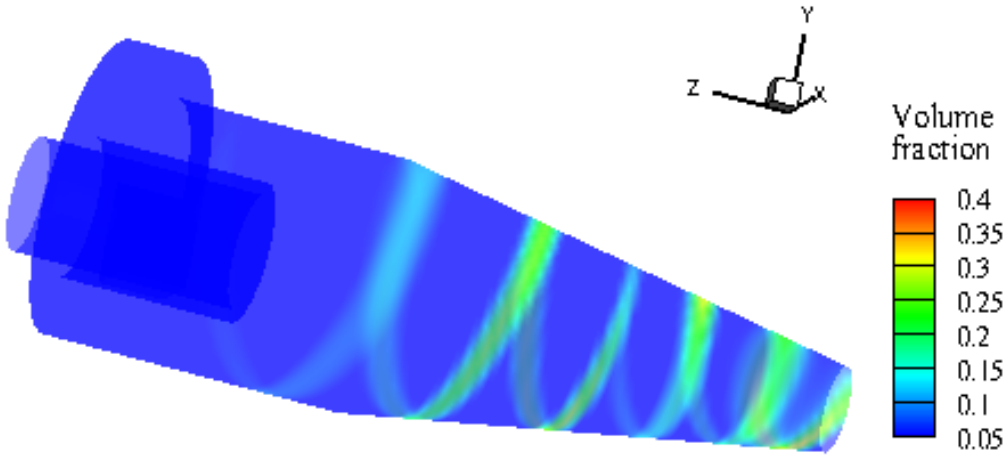

(a)

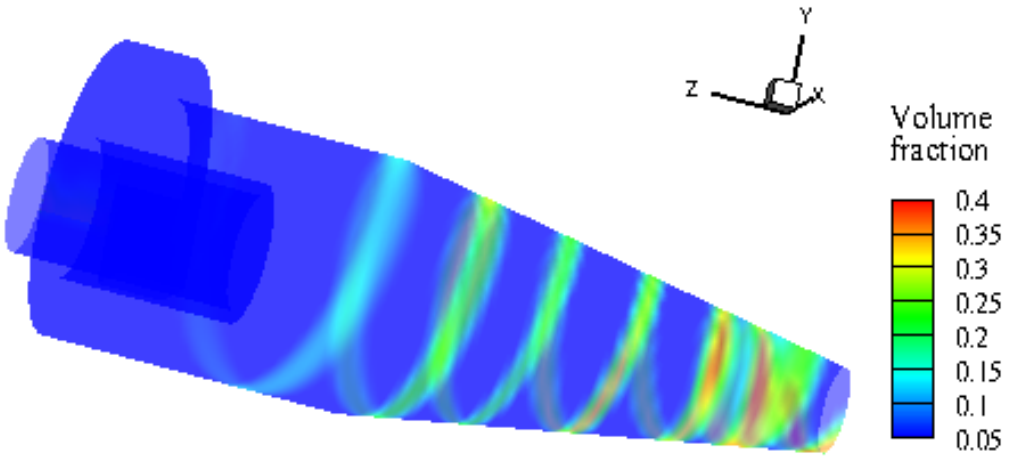

(b)

Figure 5.25 Distribution of 2.00 mm coal particles at 2.179 (RD) on the wall at t = 30 s when (a) Head = 4.15 D_c, and (b) Head = 66.4 D_c.

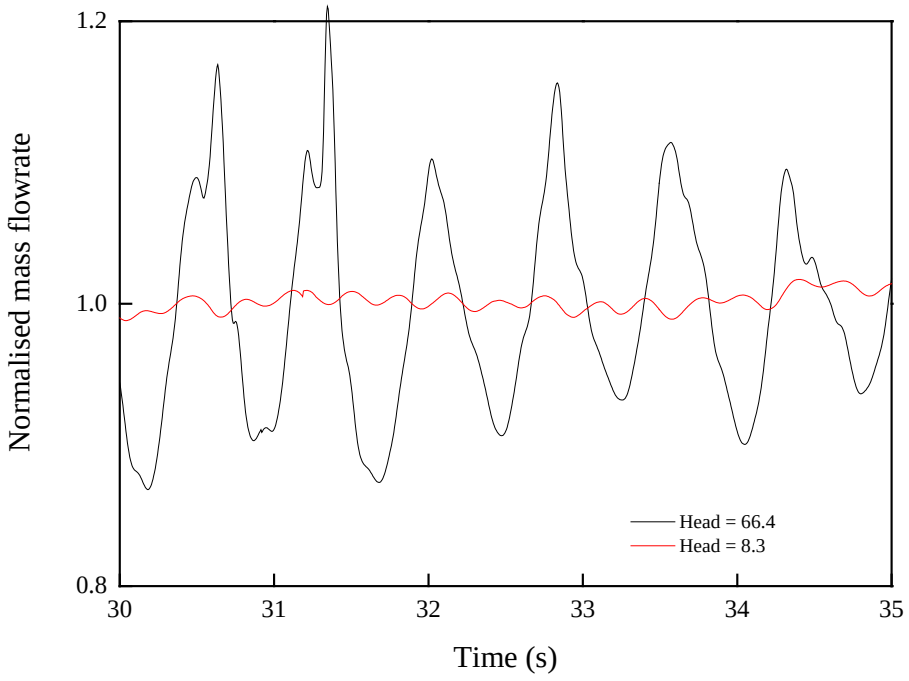

Figure 5.26 Temporal variation of mass flow rate at the underflow

6. CONCLUSIONS AND FUTURE WORK

6.1 Conclusions

A CFD model has been developed to simulate the gas-liquid-solid flow and performance of DMCs, where the mixture model, coupled with the viscosity correction model, is used to determine the interface between air and fluid, and the motion of magnetite and coal particles. The applicability of the proposed model has been established by the reasonably good agreement between the calculated and measured results in terms of separation efficiency.

The calculated results indicate that the current model can describe the effect of M:C ratio on standard DMC performance as observed in the experiments: both the cut density and E_p decrease sharply and then become asymptotic when M:C ratio increases. The deteriorated separation performance at a smaller M:C ratio is attributed to the decreased pressure drops and tangential velocities.

The relationships among spigot diameter, vortex diameter and U:O ratio have been quantified by the proposed model. The numerical results reveal that the deteriorated separation performance at a larger U:O ratio is due to the presence of short circuit in and eddy flows. It is also shown that when vortex finder or spigot diameter is varied at a given U:O ratio, the offset and medium split nearly remain the same; however, the coal feed rate and E_p are different under the conditions considered. A fish-hook phenomenon is observed when U:O ratio is equal to or slightly larger than 1 due to the development of strongly mixed downward and upward flows around the air core in the cylindrical region.

The differences between standard and large diameter DMCs are examined by the current model. Phenomena, including poorer separation for fine particles, density shifts,

and cut density of the finer particles being higher than that of the larger particles are observed. The distribution of ratio of pressure gradient to radial acceleration shows that poorer separation of fine particles is due to the asymmetry of the DMC structure.

As the numerical results show, the effects of the M:C ratio on the performances of different sized DMCs are similar. The separation performance of fine particles is improved as medium density and viscous drag force decrease. However, this improvement is limited as the problem of asymmetry is not solved.

Compared with the effect of M:C ratio, the scope for improvements by increasing the Head is larger. Stronger flow and more symmetric distributions of ratio of pressure gradient to radial acceleration are observed in results. These changes lead to a high flow rate and a decrease of the difference between the cut density and medium density for both fine particles and coarse particles, which result in a significant decrease in the cut density differential. However, a high pressure may cause strong fluctuations in the flow rate at the underflow and a high wear rate of the wall which will result in increased pumping losses.

Overall, both standard and large diameter DMCs can separate coarse particle well under proper operating conditions. Poor separation of fine particles can be improved by adjusting geometries, and M:C ratio of the feed.

6.2 Future work

Based on present works, future studies can be expected in following two aspects.

6.2.1 Model development

As there is a limited number (up to 20) of phases that can be simulated in ANSYS Fluent for numerical stability, combining the CFD-DEM model for coarse coal and the mixture model for fine coal could contribute to the prediction accuracy.

6.2.2 Parameter interaction studies

In this work, parameters are studied separately. The interactions between variables are not considered. Further study should concentrate on the correlation between them, such as the effect of M:C ratio under different geometries and operating Head on DMC performance.

REFERENCES

Anderson, T.B., Jackson, R., A fluid mechanical description of fluidized beds: Equations of motion. Industrial and Engineering Chemistry Fundamentals, 1967, **6(4)**, 527-539.

Averous, J., Fuentes, R., Advances in the numerical simulation of hydrocyclone classification. Can Metall Quart, 1997, **36(5)**, 309-314.

Barbee, C.J., Luttrell, G.H., Wood, C.J., Bethell, P.J., Simulation of heavy medium cyclone performance. Miner Metall Proc, 2005, **22(1)**, 38-42.

Boysan, F., Ayers, W.H., Swithenbank, J., A Fundamental Mathematical-Modeling Approach to Cyclone Design. T I Chem Eng-Lond, 1982, **60(4)**, 222-230.

Brennan, M.S., 2003. Multiphase CFD simulations of dense medium and classifying hydrocyclones, In *Procceedings of the 3rd International Conference on CFD in the Minerals and Process Industries*, ed. CSIRO, Melbourne, Australia.

Chen, J., Chu, K.W., Zou, R.P., Yu, A.B., Vince, A., Prediction of the performance of dense medium cyclones in coal preparation. Minerals Engineering, 2012, **31**, 59-70.

Cheng, J., 2010. PC-based application of dense medium cyclone fundamental simulations. University of New South Wales.

Chu, K.W., Chen, J., Yu, A., Vince, A., 2013. Particle scale modelling of the multiphase flow in a dense medium cyclone: Effect of medium-to-coal ratio, pp. 1182-1185.

Chu, K.W., Kuang, S.B., Yu, A.B., Vince, A., Particle scale modelling of the multiphase flow in a dense medium cyclone: Effect of fluctuation of solids flowrate. Minerals Engineering, 2012a, **33**, 34-45.

Chu, K.W., Kuang, S.B., Yu, A.B., Vince, A., Barnett, G.D., Barnett, P.J., Prediction of wear and its effect on the multiphase flow and separation performance of dense medium cyclone. Minerals Engineering, 2014, **56**, 91-101.

Chu, K.W., Wang, B., Yu, A.B., Vince, A., CFD-DEM modelling of multiphase flow in dense medium cyclones. Powder Technology, 2009a, **193(3)**, 235-247.

Chu, K.W., Wang, B., Yu, A.B., Vince, A., Computational study of the multiphase flow in a dense medium cyclone: Effect of particle density. Chemical Engineering Science, 2012b, **73**, 123-139.

Chu, K.W., Wang, B., Yu, A.B., Vince, A., Particle scale modelling of the multiphase flow in a dense medium cyclone: Effect of vortex finder outlet pressure. Minerals Engineering, 2012c, **31**, 46-58.

Chu, K.W., Wang, B., Yu, A.B., Vince, A., Barnett, G.D., Barnett, P.J., CFD–DEM study of the effect of particle density distribution on the multiphase flow and performance of dense medium cyclone. Minerals Engineering, 2009b, **22(11)**, 893-909.

Clarkson, C.J., Wood, C.J., Model of dense medium cyclone performance. Coal Preparation, 1993, **12(1-4)**, 101-115.

Concha, F., Barrientos, A., Montero, J., Sampaio, R., Air core and roping in hydrocyclones. Int J Miner Process, 1996, **44-5**, 743-749.

Cortes, C., Gil, A., Modeling the gas and particle flow inside cyclone separators. Prog Energ Combust, 2007, **33(5)**, 409-452.

Crowe, C.T., Troutt, T.R., Chung, J.J.N., 1996. Numerical models for two-phase turbulent flows, pp. 11-43.

Cullivan, J.C., Williams, R.A., Cross, C.R., New insights into hydrocyclone operation. Particul Sci Technol, 2003, **21(1)**, 83-103.

Davidson, M.R., Numerical-Calculations of Flow in a Hydrocyclone Operating without an Air Core. Applied Mathematical Modelling, 1988, **12(2)**, 119-128.

Davidson, M.R., A numerical model of liquid-solid flow in a hydrocyclone with high solids fraction. ASME-PUBLICATIONS-FED, 1994, **185**, 29-29.

Davis, J.J., Davis, J.J., 1987. A study of coal washing dense medium cyclones. Thesis (Ph.D.) - University of Queensland, 1987., St. Lucia.

Delgadillo, J.A., Rajamani, R.K., A comparative study of three turbulence-closure models for the hydrocyclone problem. Int J Miner Process, 2005, **77(4)**, 217-230.

Dyakowski, T., Hornung, G., Williams, R.A., Simulation of Non-Newtonian Flow in a Hydrocyclone. Chem Eng Res Des, 1994, **72(A4)**, 513-520.

Dyakowski, T., Williams, R.A., Modeling Turbulent-Flow within a Small-Diameter Hydrocyclone. Chemical Engineering Science, 1993, **48(6)**, 1143-1152.

Dyakowski, T., Williams, R.A., Prediction of Air-Core Size and Shape in a Hydrocyclone. Int J Miner Process, 1995, **43(1-2)**, 1-14.

Dyakowski, T., Williams, R.A., Prediction of high solids concentration regions within a hydrocyclone. Powder Technology, 1996, **87(1)**, 43-47.

Ergun, S., Fluid Flow through Packed Columns. Chem Eng Prog, 1952, **48(2)**, 89-94.

Ferrara, G., Bozzato, P., Chine, B., Performance of conical and cylindrical separatory vessels in dynamic dense-medium separation processes. Miner Metall Proc, 1999, **16(2)**, 8-15.

Fraser, S.M., Razek, A.M.A., Abdullah, M.Z., Computational and experimental investigations in a cyclone dust separator. P I Mech Eng E-J Pro, 1997, **211(E4)**, 247-257.

Galvin, K.P., Smitham, J.B., Use of X-Rays to Determine the Distribution of Particles in an Operating Cyclone. Minerals Engineering, 1994, **7(10)**, 1269-1280.

Ghodrat, M., Kuang, S.B., Yu, A.B., Vince, A., Barnett, G.D., Barnett, P.J., Numerical analysis of hydrocyclones with different vortex finder configurations. Minerals Engineering, 2014, **63(0)**, 125-138.

Gottfried, B.S., Jacobsen, P.S., Generalized Distribution Curve for Characterizing the Performance of Coal-Cleaning Equipment. US Bur Mines Rep Invest, 1977**(8238)**.

He, P., Salcudean, M., Gartshore, I.S., A numerical simulation of hydrocyclones. Chem Eng Res Des, 1999, **77(A5)**, 429-441.

He, Y.B., Laskowski, J.S., Dense Medium Cyclone Separation of Fine Particles Part 1. The Effect of Medium Split Ratio on Dense Medium Cyclone Performance. Coal Preparation, 1995, **16(1)**, 1-25.

Hirt, C.W., Nichols, B.D., Volume of Fluid (Vof) Method for the Dynamics of Free Boundaries. J Comput Phys, 1981, **39(1)**, 201-225.

Honaker, R.Q., Singh, N., Govindarajan, B., Application of dense-medium in an enhanced gravity separator for fine coal cleaning. Minerals Engineering, 2000, **13(4)**, 415-427.

Hsieh, K.T., 1988. Phenomenological model of the hydrocyclone. The University of Utah, Salt Lake City, USA.

Hsieh, K.T., Rajamani, R.K., Mathematical-Model of the Hydrocyclone Based on Physics of Fluid-Flow. Aiche J, 1991, **37(5)**, 735-746.

Ishii, M., Kishima, K., Two-fluid model and hydrodynamic constitutive relations. Nuclear Engineering and Design, 1984, **82**, 107-126.

Kelsall, D.F., A study of the motion of solid particles in a hydraulic cyclone. Chemical Engineering Research and Design, 1952, **30**, 87-108.

Kuang, S.B., Chu, K.W., Yu, A.B., Vince, A., Numerical study of liquid-gas-solid flow in classifying hydrocyclones: Effect of feed solids concentration. Minerals Engineering, 2012, **31**, 17-31.

Kuang, S.B., Qi, Z., Yu, A.B., Vince, A., Barnett, G.D., Barnett, P.J., CFD modeling and analysis of the multiphase flow and performance of dense medium cyclones. Minerals Engineering, 2014, **62(0)**, 43-54.

Launder, B.E., Reece, G.J., Rodi, W., Progress in the Development of a Reynold-Stress Turbulence Closure. J Fluid Mech, 1975, **68(pt 3)**, 537-566.

Ma, L., Ingham, D.B., Wen, X., Numerical modelling of the fluid and particle penetration through small sampling cyclones. J Aerosol Sci, 2000, **31(9)**, 1097-1119.

Majumder, A.K., Shah, H., Shukla, P., Barnwal, J.P., Effect of operating variables on shape of “fish-hook” curves in cyclones. Minerals Engineering, 2007, **20(2)**, 204-206.

Malhotra, A., Branion, R.M.R., Hauptmann, E.G., Modeling the Flow in a Hydrocyclone. Can J Chem Eng, 1994, **72(6)**, 953-960.

Manninen, M., Taivassalo, V., Kallio, S., *On the mixture model for multiphase flow*. 1996, VTT Publications 288, Technical Research Centre of Finland.

Meier, H.F., Mori, M., Anisotropic behavior of the Reynolds stress in gas and gas-solid flows in cyclones. Powder Technology, 1999, **101(2)**, 108-119.

Monredon, T., *Hydrocyclone: Investigation of the Fluid-flow Model*. 1990, Department of Metallurgical Engineering, University of Utah.

Monredon, T.C., Hsieh, K.T., Rajamani, R.K., Fluid-Flow Model of the Hydrocyclone - an Investigation of Device Dimensions. Int J Miner Process, 1992, **35(1-2)**, 65-83.

Mukherjee, A.K., Sripriya, R., Rao, P.V.T., Das, P., Effect of increase in feed inlet pressure on feed rate of dense media cyclone. Int J Miner Process, 2003, **69(1-4)**, 259-274.

Muzenda, E., Abdulkareem, A.S., Afolabi, A.S., Mateescu, C., Effect of Operating Pressure on the Application of Multiple Cyclones in Dense Medium Separation (DMS) Plant. Particul Sci Technol, 2012, **30(1)**, 92-101.

Napier-Munn, T.J., Pressure drop in dense-medium cyclones. Int J Miner Process, 1986, **16(3-4)**, 209-230.

Napier-Munn, T.J., Modelling and simulating dense medium separation processes — A progress report. Minerals Engineering, 1991, **4(3-4)**, 329-346.

Narasimha, M., Brennan, M., Holtham, P.N., Large eddy simulation of hydrocyclone - prediction of air-core diameter and shape. Int J Miner Process, 2006a, **80(1)**, 1-14.

Narasimha, M., Brennan, M., Holtham, P.N., A Review of Cfd Modelling for Performance Predictions of Hydrocyclone. Eng Appl Comp Fluid, 2007a, **1(2)**, 109-125.

Narasimha, M., Brennan, M.S., Holtham, P.N., Numerical simulation of magnetite segregation in a dense medium cyclone. Minerals Engineering, 2006b, **19(10)**, 1034-1047.

Narasimha, M., Brennan, M.S., Holtham, P.N., A review of flow modeling for dense medium cyclones. Coal Preparation, 2006c, **26(2)**, 55-89.

Narasimha, M., Brennan, M.S., Holtham, P.N., Napier-Munn, T.J., A comprehensive CFD model of dense medium cyclone performance. Minerals Engineering, 2007b, **20(4)**, 414-426.

Narasimha, M., Sripriya, R., Banerjee, P.K., CFD modelling of hydrocyclone-prediction of cut size. Int J Miner Process, 2005, **75(1-2)**, 53-68.

Noriler, D., Vegini, A.A., Soares, C., Barros, A.A.C., Meier, H.F., Mori, M., A new role for reduction in pressure drop in cyclones using computational fluid dynamics techniques. Brazilian Journal of Chemical Engineering, 2004, **21(1)**, 93-101.

Nowakowski, A.F., Cullivan, J.C., Williams, R.A., Dyakowski, T., Application of CFD to modelling of the flow in hydrocyclones. Is this a realizable option or still a research challenge? Minerals Engineering, 2004, **17(5)**, 661-669.

Nowakowski, A.F., Dyakowski, T., Investigation of swirling flow structure in hydrocyclones. Chem Eng Res Des, 2003, **81(A8)**, 862-873.

Nowakowski, A.F., Kraipech, W., Williams, R.A., Dyakowski, T., The hydrodynamics of a hydrocyclone based on a three-dimensional multi-continuum model. Chem Eng J, 2000, **80(1-3)**, 275-282.

Pericleous, K.A., Mathematical Simulation of Hydrocyclones. Applied Mathematical Modelling, 1987, **11(4)**, 242-255.

Pericleous, K.A., Rhodes, N., The Hydrocyclone Classifier - a Numerical Approach. Int J Miner Process, 1986, **17(1-2)**, 23-43.

Petty, C.A., Parks, S.M., Flow predictions within hydrocyclones. Filtration & Separation, 2001, **38(6)**, 28-34.

Restarick, C.J., Krnic, Z., The Effect of Underflow Overflow Ratio on Dense Medium Cyclone Operation. Minerals Engineering, 1991, **4(3-4)**, 263-270.

Richard, R., *Industrial trials of novel cyclones : final report. ACARP project C14067*. 2007, Brisbane : Riverside Centre, Qld : Australian Coal Association Research Program ACARP, Brisbane] : Riverside Centre, Qld.

Schiller, L., Naumann, Z., A drag coefficienty correlation. Z. Ver. Deutsch. Ing., 1933, **77**, 318-320.

Schuetz, S., Mayer, G., Bierdel, M., Piesche, M., Investigations on the flow and separation behaviour of hydrocyclones using computational fluid dynamics. Int J Miner Process, 2004, **73(2-4)**, 229-237.

Sherritt, G., Meyers, A., Bennetts, A., Graham, J., 2010. Delineation of large diameter dense medium cyclone performance, In *ACARP Report*.

Slack, M.D., Prasad, R.O., Bakker, A., Boysan, F., Advances in cyclone modelling using unstructured grids. Chem Eng Res Des, 2000, **78(A8)**, 1098-1104.

Sripriya, R., Banerjee, P.K., Rao, P.V.T., Dutta, A., Rao, M.V.S., Critical evaluation of factors affecting the operation of dense medium cyclones treating medium coking coals. Int J Miner Process, 2001, **63(4)**, 191-206.

Sripriya, R., Meikap, B.C., Suresh, N., Chakraborty, S., Bhattacharjee, D., Chandra, S., Role of air core in particle separation in cyclones. Transactions of the Institutions of

Mining and Metallurgy, Section C: Mineral Processing and Extractive Metallurgy, 2013, **122(1)**, 25-35.

Statie, E.C., Salcudean, M.E., Gartshore, I.S., The influence of hydrocyclone geometry on separation and fibre classification. Filtration & Separation, 2001, **38(6)**, 36-41.

Stephens, D.W., Mohanarangam, K., Turbulence model analysis of flow inside a hydrocyclone. Prog Comput Fluid Dy, 2010, **10(5-6)**, 366-373.

Suasnabar, D.J., 2000. Dense medium cyclone performance enhancement via computational modelling of the physical processes. University of New South Wales, p. 284.

Suasnabar, D.J., Fletcher, C.A.J., 1999. A CFD model for dense medium cyclones, In *2nd International Conference on CFD in the Minerals and Process Industries*, ed. CSIRO, Melbourne, Australia.

Subramanian, V.S., 2002. Measuring medium segregation in the dense- medium cyclone using gamma-ray tomography, In *The University of Queensland*, p. 137.

Svarovsky, L., *Hydrocyclones*. 1984, Technomic Publishing Inc.

Swain, S., Mohanty, S., A 3-dimensional Eulerian–Eulerian CFD simulation of a hydrocyclone. Applied Mathematical Modelling, 2013, **37(5)**, 2921-2932.

Syamlal, M., Rogers, W., O'Brien, T.J., 1993. MFIX documentation: theory guide, ed. Service, N.T.I., Springfield, VA.

Wang, B., 2009. Modelling the multiphase flow in cyclones. The University of New South Wales, Sydney, Australia.

Wang, B., Chu, K.W., Yu, A.B., Vince, A., Modeling the Multiphase Flow in a Dense Medium Cyclone. Ind Eng Chem Res, 2009a, **48(7)**, 3628-3639.

Wang, B., Chu, K.W., Yu, A.B., Vince, A., Numerical studies of the effects of medium properties in dense medium cyclone operations. Minerals Engineering, 2009b, **22(11)**, 931-943.

Wang, B., Chu, K.W., Yu, A.B., Vince, A., Computational investigation of the mechanisms of the "breakaway" effect in a dense medium cyclone. Minerals Engineering, 2014, **62(0)**, 111-119.

Wang, B., Chu, K.W., Yu, A.B., Vince, A., Barnett, G.D., Barnett, P.J., Computational study of the multiphase flow and performance of dense medium cyclones: Effect of body dimensions. Minerals Engineering, 2011, **24(1)**, 19-34.

Wang, B., Yu, A.B., Numerical study of particle-fluid flow in hydrocyclones with different body dimensions. Minerals Engineering, 2006, **19(10)**, 1022-1033.

Wang, B., Yu, A.B., Computational Investigation of the Mechanisms of Particle Separation and "Fish-Hook" Phenomenon in Hydrocyclones. Aiche J, 2010, **56(7)**, 1703-1715.

Wen, C.Y., Yu, Y.H., Mechanics of fluidisation. Chem. Eng. Prog. Symp. Series, 1966, **62**, 100-111.

Williams, R.A., Ilyas, O.M., Dyakowski, T., Dickin, F.J., Gutierrez, J.A., Wang, M., Beck, M.S., Shah, C., Rushton, A., Air-Core Imaging in Cyclonic Separators - Implications for Separator Design and Modeling. Chem Eng J Bioch Eng, 1995, **56(3)**, 135-141.

Wills, B.A., *Mineral processing technology : an introduction to the practical aspects of ore treatment and mineral recovery*. 6th edn. 1997, Butterworth-Heinemann, Boston.

Wood, C.J., 1990. A performance model for coal-washing dense medium cyclones. University of Queensland, Brisbane, Australia.

Xu, B.H., Feng, Y.Q., Yu, A.B., Chew, S.J., Zulli, P., A numerical and experimental study of the gas-solid flow in a fluid bed reactor. Powder Handling and Processing, 2001, **13(1)**, 71-76.

Zhou, Z.Y., Kuang, S.B., Chu, K.W., Yu, A.B., Discrete particle simulation of particle-fluid flow: model formulations and their applicability. J Fluid Mech, 2010, **661**, 482-510.

Zughbi, H.D., Schwarz, M.P., Turner, W.J., Hutton, W., Numerical and Experimental Investigations of Wear in Heavy Medium Cyclones. Minerals Engineering, 1991, **4(3-4)**, 245-262.

PUBLICATION

Kuang, S.B., Qi, Z., Yu, A.B., Vince, A., Barnett, G.D., Barnett, P.J., CFD modeling and analysis of the multiphase flow and performance of dense medium cyclones. Minerals Engineering, 2014, **62(0)**, 43-54. http://dx.doi.org/10.1016/j.mineng.2013.10.012